

DESY-08-011

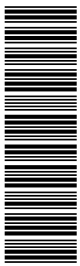
28 January 2008

Deep inelastic inclusive and diffractive scattering at Q^2 values from 25 to 320 GeV² with the ZEUS forward plug calorimeter

ZEUS Collaboration

Abstract

Deep inelastic scattering and its diffractive component, $ep \rightarrow e'\gamma^*p \rightarrow e'XN$, have been studied at HERA with the ZEUS detector using an integrated luminosity of 52.4 pb⁻¹. The M_X method has been used to extract the diffractive contribution. A wide range in the centre-of-mass energy W (37 – 245 GeV), photon virtuality Q^2 (20 – 450 GeV²) and mass M_X (0.28 – 35 GeV) is covered. The diffractive cross section for $2 < M_X < 15$ GeV rises strongly with W , the rise becoming steeper as Q^2 increases. The data are also presented in terms of the diffractive structure function, $F_2^{\text{D}(3)}$, of the proton. For fixed Q^2 and fixed M_X , $x_p F_2^{\text{D}(3)}$ shows a strong rise as $x_p \rightarrow 0$, where x_p is the fraction of the proton momentum carried by the Pomeron. For Bjorken- $x < 1 \cdot 10^{-3}$, $x_p F_2^{\text{D}(3)}$ shows positive $\log Q^2$ scaling violations, while for $x \geq 5 \cdot 10^{-3}$ negative scaling violations are observed. The diffractive structure function is compatible with being leading twist. The data show that Regge factorisation is broken.



The ZEUS Collaboration

S. Chekanov¹, M. Derrick, S. Magill, B. Musgrave, D. Nicholass², J. Repond, R. Yoshida
*Argonne National Laboratory, Argonne, Illinois 60439-4815, USA*ⁿ

M.C.K. Mattingly
Andrews University, Berrien Springs, Michigan 49104-0380, USA

M. Jechow, N. Pavel[†]
Institut für Physik der Humboldt-Universität zu Berlin, Berlin, Germany^b

P. Antonioli, G. Bari, L. Bellagamba, D. Boscherini, A. Bruni, G. Bruni, F. Cindolo,
M. Corradi, G. Iacobucci, A. Margotti, R. Nania, A. Polini
INFN Bologna, Bologna, Italy^e

S. Antonelli, M. Basile, M. Bindi, L. Cifarelli, A. Contin, S. De Pasquale³, G. Sartorelli,
A. Zichichi
University and INFN Bologna, Bologna, Italy^e

D. Bartsch, I. Brock, H. Hartmann, E. Hilger, H.-P. Jakob, M. Jüngst, A.E. Nuncio-Quiroz,
E. Paul⁴, R. Renner⁵, U. Samson, V. Schönberg, R. Shehzadi, M. Wlasenko
Physikalisches Institut der Universität Bonn, Bonn, Germany^b

N.H. Brook, G.P. Heath, J.D. Morris
H.H. Wills Physics Laboratory, University of Bristol, Bristol, United Kingdom^m

M. Capua, S. Fazio, A. Mastroberardino, M. Schioppa, G. Susinno, E. Tassi
Calabria University, Physics Department and INFN, Cosenza, Italy^e

J.Y. Kim⁶
Chonnam National University, Kwangju, South Korea

Z.A. Ibrahim, B. Kamaluddin, W.A.T. Wan Abdullah
Jabatan Fizik, Universiti Malaya, 50603 Kuala Lumpur, Malaysia^r

Y. Ning, Z. Ren, F. Sciulli
Nevis Laboratories, Columbia University, Irvington on Hudson, New York 10027^o

J. Chwastowski, A. Eskreys, J. Figiel, A. Galas, M. Gil, K. Olkiewicz, P. Stopa, L. Zawiejski
*The Henryk Niewodniczanski Institute of Nuclear Physics, Polish Academy of Sciences, Cracow, Poland*ⁱ

L. Adamczyk, T. Bołd, I. Grabowska-Bołd, D. Kisielewska, J. Łukasik, M. Przybycień,
L. Suszycki
Faculty of Physics and Applied Computer Science, AGH-University of Science and Technology, Cracow, Poland^p

A. Kotański⁷, W. Słomiński⁸

Department of Physics, Jagellonian University, Cracow, Poland

U. Behrens, C. Blohm, A. Bonato, K. Borras, R. Ciesielski, N. Coppola, V. Drugakov, S. Fang, J. Fourletova⁹, A. Geiser, P. Göttlicher¹⁰, J. Grebenyuk, I. Gregor, T. Haas, W. Hain, A. Hüttmann, B. Kahle, M. Kasemann, I.I. Katkov, U. Klein¹¹, U. Kötz⁴, H. Kowalski, H. Lim¹², E. Lobodzinska, B. Löhr, R. Mankel, I.-A. Melzer-Pellmann, S. Miglioranza, A. Montanari, T. Namsu, D. Notz¹³, A. Parenti, L. Rinaldi¹⁴, P. Roloff, I. Rubinsky, R. Santamarta¹⁵, U. Schneekloth, A. Spiridonov¹⁶, D. Szuba¹⁷, J. Szuba¹⁷, T. Theedt, G. Wolf, K. Wrona, A.G. Yagües Molina, C. Youngman, W. Zeuner¹³

Deutsches Elektronen-Synchrotron DESY, Hamburg, Germany

W. Lohmann, S. Schlenstedt

Deutsches Elektronen-Synchrotron DESY, Zeuthen, Germany

G. Barbagli, E. Gallo

INFN Florence, Florence, Italy^e

P. G. Pelfer

University and INFN Florence, Florence, Italy^e

A. Bamberger, D. Dobur, F. Karstens, N.N. Vlasov¹⁹

Fakultät für Physik der Universität Freiburg i.Br., Freiburg i.Br., Germany^b

P.J. Bussey²⁰, A.T. Doyle, W. Dunne, M. Forrest, M. Rosin, D.H. Saxon, I.O. Skillicorn
Department of Physics and Astronomy, University of Glasgow, Glasgow, United Kingdom^m

I. Gialas²¹, K. Papageorgiou

Department of Engineering in Management and Finance, Univ. of Aegean, Greece

U. Holm, R. Klanner, E. Lohrmann, P. Schleper, T. Schörner-Sadenius, J. Sztuk, H. Stadie, M. Turcato

Hamburg University, Institute of Exp. Physics, Hamburg, Germany^b

C. Foudas, C. Fry, K.R. Long, A.D. Tapper

Imperial College London, High Energy Nuclear Physics Group, London, United Kingdom^m

T. Matsumoto, K. Nagano, K. Tokushuku²², S. Yamada, Y. Yamazaki²³

Institute of Particle and Nuclear Studies, KEK, Tsukuba, Japan^f

A.N. Barakbaev, E.G. Boos⁴, N.S. Pokrovskiy, B.O. Zhaitykov

Institute of Physics and Technology of Ministry of Education and Science of Kazakhstan, Almaty, Kazakhstan

V. Aushev¹, M. Borodin, A. Kozulia, M. Lisovyi
Institute for Nuclear Research, National Academy of Sciences, Kiev and Kiev National University, Kiev, Ukraine

D. Son
Kyungpook National University, Center for High Energy Physics, Daegu, South Korea ^g

J. de Favereau, K. Piotrkowski
Institut de Physique Nucléaire, Université Catholique de Louvain, Louvain-la-Neuve, Belgium ^q

F. Barreiro, C. Glasman²⁴, M. Jimenez, L. Labarga, J. del Peso, E. Ron, M. Soares, J. Terrón, M. Zambrana
Departamento de Física Teórica, Universidad Autónoma de Madrid, Madrid, Spain ^l

F. Corriveau, C. Liu, J. Schwartz, R. Walsh, C. Zhou
Department of Physics, McGill University, Montréal, Québec, Canada H3A 2T8 ^a

T. Tsurugai
Meiji Gakuin University, Faculty of General Education, Yokohama, Japan ^f

A. Antonov, B.A. Dolgoshein, D. Gladkov, V. Sosnovtsev, A. Stifutkin, S. Suchkov
Moscow Engineering Physics Institute, Moscow, Russia ^j

R.K. Dementiev, P.F. Ermolov, L.K. Gladilin, Yu.A. Golubkov, L.A. Khein, I.A. Korzhavina, V.A. Kuzmin, B.B. Levchenko²⁵, O.Yu. Lukina, A.S. Proskuryakov, L.M. Shcheglova, D.S. Zotkin
Moscow State University, Institute of Nuclear Physics, Moscow, Russia ^k

I. Abt, C. Büttner, A. Caldwell, D. Kollar, B. Reiser, W.B. Schmidke, J. Sutiak
Max-Planck-Institut für Physik, München, Germany

G. Grigorescu, A. Keramidas, E. Koffeman, P. Kooijman, A. Pellegrino, H. Tiecke, M. Vázquez¹³, L. Wiggers
NIKHEF and University of Amsterdam, Amsterdam, Netherlands ^h

N. Brümmer, B. Bylsma, L.S. Durkin, A. Lee, T.Y. Ling
Physics Department, Ohio State University, Columbus, Ohio 43210 ⁿ

P.D. Allfrey, M.A. Bell, A.M. Cooper-Sarkar, R.C.E. Devenish, J. Ferrando, B. Foster, K. Korcsak-Gorzo, K. Oliver, S. Patel, V. Roberfroid²⁶, A. Robertson, P.B. Straub, C. Uribe-Estrada, R. Walczak
Department of Physics, University of Oxford, Oxford United Kingdom ^m

A. Bertolin, F. Dal Corso, S. Dusini, A. Longhin, L. Stanco
INFN Padova, Padova, Italy ^e

P. Bellan, R. Brugnera, R. Carlin, A. Garfagnini, S. Limentani
Dipartimento di Fisica dell' Università and INFN, Padova, Italy^e

B.Y. Oh, A. Raval, J. Ukleja²⁷, J.J. Whitmore²⁸
Department of Physics, Pennsylvania State University, University Park, Pennsylvania 16802^o

Y. Iga
Polytechnic University, Sagamihara, Japan^f

G. D'Agostini, G. Marini, A. Nigro
Dipartimento di Fisica, Università 'La Sapienza' and INFN, Rome, Italy^e

J.E. Cole, J.C. Hart
Rutherford Appleton Laboratory, Chilton, Didcot, Oxon, United Kingdom^m

H. Abramowicz²⁹, A. Gabareen, R. Ingbir, S. Kananov, A. Levy, O. Smith, A. Stern
Raymond and Beverly Sackler Faculty of Exact Sciences, School of Physics, Tel-Aviv University, Tel-Aviv, Israel^d

M. Kuze, J. Maeda
Department of Physics, Tokyo Institute of Technology, Tokyo, Japan^f

R. Hori, S. Kagawa³⁰, N. Okazaki, S. Shimizu, T. Tawara
Department of Physics, University of Tokyo, Tokyo, Japan^f

R. Hamatsu, H. Kaji³¹, S. Kitamura³², O. Ota, Y.D. Ri
Tokyo Metropolitan University, Department of Physics, Tokyo, Japan^f

M. Costa, M.I. Ferrero, V. Monaco, R. Sacchi, A. Solano
Università di Torino and INFN, Torino, Italy^e

M. Arneodo, M. Ruspa
Università del Piemonte Orientale, Novara, and INFN, Torino, Italy^e

S. Fourletov, J.F. Martin, T.P. Stewart
Department of Physics, University of Toronto, Toronto, Ontario, Canada M5S 1A7^a

S.K. Boutle²¹, J.M. Butterworth, C. Gwenlan³³, T.W. Jones, J.H. Loizides, M. Wing³⁴
Physics and Astronomy Department, University College London, London, United Kingdom^m

B. Brzozowska, J. Ciborowski³⁵, G. Grzelak, P. Kulinski, P. Łuźniak³⁶, J. Malka³⁶, R.J. Nowak, J.M. Pawlak, T. Tymieniecka, A. Ukleja, A.F. Żarnecki
Warsaw University, Institute of Experimental Physics, Warsaw, Poland

M. Adamus, P. Plucinski³⁷
Institute for Nuclear Studies, Warsaw, Poland

Y. Eisenberg, D. Hochman, U. Karshon

Department of Particle Physics, Weizmann Institute, Rehovot, Israel ^c

E. Brownson, T. Danielson, A. Everett, D. Kçira, D.D. Reeder⁴, P. Ryan, A.A. Savin,
W.H. Smith, H. Wolfe

Department of Physics, University of Wisconsin, Madison, Wisconsin 53706, USA ⁿ

S. Bhadra, C.D. Catterall, Y. Cui, G. Hartner, S. Menary, U. Noor, J. Standage, J. Whyte

Department of Physics, York University, Ontario, Canada M3J 1P3 ^a

- ¹ supported by DESY, Germany
- ² also affiliated with University College London, UK
- ³ now at University of Salerno, Italy
- ⁴ retired
- ⁵ now at Bruker AXS, Karlsruhe, Germany
- ⁶ supported by Chonnam National University in 2006
- ⁷ supported by the research grant no. 1 P03B 04529 (2005-2008)
- ⁸ This work was supported in part by the Marie Curie Actions Transfer of Knowledge project COCOS (contract MTKD-CT-2004-517186)
- ⁹ now at University of Bonn, Germany
- ¹⁰ now at DESY group FEB, Hamburg, Germany
- ¹¹ now at University of Liverpool, UK
- ¹² now at Argonne National Laboratory, Argonne, USA
- ¹³ now at CERN, Geneva, Switzerland
- ¹⁴ now at Bologna University, Bologna, Italy
- ¹⁵ now at BayesForecast, Madrid, Spain
- ¹⁶ also at Institut of Theoretical and Experimental Physics, Moscow, Russia
- ¹⁷ also at INP, Cracow, Poland
- ¹⁸ also at FPACS, AGH-UST, Cracow, Poland
- ¹⁹ partly supported by Moscow State University, Russia
- ²⁰ Royal Society of Edinburgh, Scottish Executive Support Research Fellow
- ²¹ also affiliated with DESY, Germany
- ²² also at University of Tokyo, Japan
- ²³ now at Kobe University, Japan
- ²⁴ Ramón y Cajal Fellow
- ²⁵ partly supported by Russian Foundation for Basic Research grant no. 05-02-39028-NSFC-a
- ²⁶ EU Marie Curie Fellow
- ²⁷ partially supported by Warsaw University, Poland
- ²⁸ This material was based on work supported by the National Science Foundation, while working at the Foundation.
- ²⁹ also at Max Planck Institute, Munich, Germany, Alexander von Humboldt Research Award
- ³⁰ now at KEK, Tsukuba, Japan
- ³¹ now at Nagoya University, Japan
- ³² Department of Radiological Science, Tokyo Metropolitan University, Japan
- ³³ PPARC Advanced fellow
- ³⁴ partially supported by DESY, Germany
- ³⁵ also at Łódź University, Poland

³⁶ Łódź University, Poland

³⁷ supported by the Polish Ministry for Education and Science grant no. 1 P03B 14129

[†] deceased

- ^a supported by the Natural Sciences and Engineering Research Council of Canada (NSERC)
- ^b supported by the German Federal Ministry for Education and Research (BMBF), under contract numbers 05 HZ6PDA, 05 HZ6GUA, 05 HZ6VFA and 05 HZ4KHA
- ^c supported in part by the MINERVA Gesellschaft für Forschung GmbH, the Israel Science Foundation (grant no. 293/02-11.2) and the U.S.-Israel Binational Science Foundation
- ^d supported by the German-Israeli Foundation and the Israel Science Foundation
- ^e supported by the Italian National Institute for Nuclear Physics (INFN)
- ^f supported by the Japanese Ministry of Education, Culture, Sports, Science and Technology (MEXT) and its grants for Scientific Research
- ^g supported by the Korean Ministry of Education and Korea Science and Engineering Foundation
- ^h supported by the Netherlands Foundation for Research on Matter (FOM)
- ⁱ supported by the Polish State Committee for Scientific Research, grant no. 620/E-77/SPB/DESY/P-03/DZ 117/2003-2005 and grant no. 1P03B07427/2004-2006
- ^j partially supported by the German Federal Ministry for Education and Research (BMBF)
- ^k supported by RF Presidential grant N 8122.2006.2 for the leading scientific schools and by the Russian Ministry of Education and Science through its grant for Scientific Research on High Energy Physics
- ^l supported by the Spanish Ministry of Education and Science through funds provided by CICYT
- ^m supported by the Science and Technology Facilities Council, UK
- ⁿ supported by the US Department of Energy
- ^o supported by the US National Science Foundation. Any opinion, findings and conclusions or recommendations expressed in this material are those of the authors and do not necessarily reflect the views of the National Science Foundation.
- ^p supported by the Polish Ministry of Science and Higher Education as a scientific project (2006-2008)
- ^q supported by FNRS and its associated funds (IISN and FRiA) and by an Inter-University Attraction Poles Programme subsidised by the Belgian Federal Science Policy Office
- ^r supported by the Malaysian Ministry of Science, Technology and Innovation/Akademik Sains Malaysia grant SAGA 66-02-03-0048

1 Introduction

The observation of events with a large rapidity gap in deep inelastic electron (positron) proton scattering (DIS) at HERA by the ZEUS experiment [1] has paved the way for a systematic study of diffraction at large centre-of-mass energies with a variable hard scale provided by the mass squared, $-Q^2$, of the virtual photon. Diffraction is defined by the property that the cross section does not decrease as a power of the centre-of-mass energy. This can be interpreted as the exchange of a colourless system, the Pomeron, which leads to the presence of a large rapidity gap between the proton and the rest of the final state, which is not exponentially suppressed.

Before HERA came into operation, Ingelman and Schlein [2], based on data from UA8 [3, 4], had suggested that the Pomeron may have a partonic structure. Since then, the H1 and ZEUS experiments at HERA have presented results on diffractive scattering in photoproduction and deep inelastic electron-proton scattering for many different final states. In parallel, a number of theoretical ideas and models have been developed in order to understand the data within the framework of Quantum Chromodynamics (QCD) [5].

Several methods have been employed by H1 and ZEUS for isolating diffractive contributions experimentally. In the case of exclusive vector-meson production, resonance signals in the decay mass spectrum combined with the absence of other substantial activity in the detector have been used [?, 6, 8]. The contribution from inclusive diffraction has been extracted using the presence of a large rapidity gap (η_{\max} method [11]), the detection of the leading proton [?, 10] or the hadronic mass spectrum observed in the central detector (M_X method [12, 13]). The selections based on η_{\max} or on a leading proton may include additional contributions from Reggeon exchange. Such contributions are exponentially suppressed when using the M_X method.

In this paper, inclusive processes (Fig. 1),

$$\gamma^* p \rightarrow \text{anything}, \quad (1)$$

and diffractive processes (Fig. 2),

$$\gamma^* p \rightarrow XN, \quad (2)$$

where N is a proton or a low-mass nucleonic state and X is the hadronic system without N , are studied. The contribution from diffractive scattering is extracted with the M_X method. Results on the proton structure function F_2 and on the diffractive cross section and structure function are presented for a wide range of centre-of-mass energies, photon virtualities $-Q^2$ and of mass M_X of the diffractively produced hadronic system, using the data from the ZEUS experiment collected in 1999 and 2000. The results, which will be

referred to as FPC II, are based on integrated luminosities of 11.0 pb^{-1} for $Q^2 = 20 - 40 \text{ GeV}^2$ and 52.4 pb^{-1} for $Q^2 = 40 - 450 \text{ GeV}^2$.

In a previous study, which will be referred to as FPC I [13], results on inclusive and diffractive scattering were presented for the Q^2 values between 2.7 and 55 GeV^2 using an integrated luminosity of 4.2 pb^{-1} . The combined data from the FPC I and FPC II analyses provide a measurement of the Q^2 dependence of diffraction over a range of two orders of magnitude.

2 Experimental set-up and data set

The data used for this measurement were taken with the ZEUS detector in 1999-2000 when positrons of 27.5 GeV collided with protons of 920 GeV . The detector as well as the analysis methods are identical to those used for the FPC I study [13]. A detailed description of the ZEUS detector can be found elsewhere [14, 15]. A brief outline of the components that are most relevant for this analysis is given below.

Charged particles were tracked in the central tracking detector (CTD) [16], which operated in a magnetic field of 1.43 T provided by a thin superconducting solenoid. The CTD consisted of 72 cylindrical drift chamber layers, organised in 9 superlayers covering the polar-angle region $15^\circ < \theta < 164^\circ$. The transverse momentum resolution for full-length tracks was $\sigma(p_T)/p_T = 0.0058 p_T \oplus 0.0065 \oplus 0.0014/p_T$, with p_T in GeV .

The high-resolution uranium-scintillator calorimeter (CAL [17]) consisted of three parts: the forward (FCAL), the barrel (BCAL) and the rear (RCAL) calorimeters. Each part was subdivided transversely into towers and longitudinally into one electromagnetic section (EMC) and either one (in RCAL) or two (in BCAL and FCAL) hadronic sections (HAC). The smallest division of the calorimeter was called a cell. The CAL energy resolutions, as measured under test beam conditions, were $\sigma(E)/E = 0.18/\sqrt{(E)}$ for electrons and $\sigma(E)/E = 0.35/\sqrt{(E)}$ for hadrons, with E in GeV .

The position of electrons scattered at small angles to the electron-beam direction was determined including the information from the SRTD [18, 19] which was attached to the front face of the RCAL and consisted of two planes of scintillator strips. The rear hadron-electron separator (RHES [20]) was inserted in the RCAL.

In 1998, the forward-plug calorimeter (FPC) [21] was installed in the $20 \times 20 \text{ cm}^2$ beam hole of the FCAL. The FPC was used to measure the energy of particles in the pseudorapidity ¹

¹ The ZEUS coordinate system is a right-handed Cartesian system, with the Z axis pointing in the proton direction, referred to as the “forward direction”, and the X axis pointing left towards the centre of HERA. The coordinate origin is at the nominal interaction point.

range $\eta \approx 4.0 - 5.0$. The FPC was a lead-scintillator sandwich calorimeter read out by wavelength-shifter (WLS) fibres and photomultipliers (PMT). A hole of 3.15 cm radius was provided for the passage of the beams. In the FPC, 15 mm thick lead plates alternated with 2.6 mm thick scintillator layers. The scintillator layers consisted of tiles forming towers that were read out individually. The tower cross sections were $24 \times 24 \text{ mm}^2$ in the electromagnetic and $48 \times 48 \text{ mm}^2$ in the hadronic section. The measured energy resolution for positrons was $\sigma_E/E = (0.41 \pm 0.02)/\sqrt{E} \oplus 0.062 \pm 0.002$, with E in GeV. When installed in the FCAL, the energy resolution for pions was $\sigma_E/E = (0.65 \pm 0.02)/\sqrt{E} \oplus 0.06 \pm 0.01$, with E in GeV, and the e/h ratio was close to unity.

The luminosity was measured from the rate of the bremsstrahlung process $ep \rightarrow e\gamma p$. The resulting small-angle energetic photons were measured by the luminosity monitor [22], a lead-scintillator calorimeter placed in the HERA tunnel at $Z = -107 \text{ m}$.

A three-level trigger system was used to select events online [14, 15, 23]. The first- and second-level trigger selections were based on the identification of a scattered positron with impact point on the RCAL surface outside an area of $36 \times 36 \text{ cm}^2$ centred on the beam axis (“set 1”, integrated luminosity 11.0 pb^{-1}), or outside a radius of 30 cm centred on the beam axis (“set 2”, integrated luminosity 41.4 pb^{-1}). In the offline analysis the reconstructed impact point had to lie outside an area of $40 \times 40 \text{ cm}^2$ (set 1) or outside a radius of 32 cm (set 2).

3 Reconstruction of kinematics and event selection

The methods for extracting the inclusive DIS and diffractive data samples are identical to those applied in the FPC I study [13] and will be described only briefly.

The reaction

$$e(k) p(P) \rightarrow e(k') + \text{anything},$$

see Fig. 1, at fixed squared centre-of-mass energy, $s = (k + P)^2$, is described in terms of $Q^2 \equiv -q^2 = -(k - k')^2$, Bjorken- $x = Q^2/(2P \cdot q)$ and $s \approx 4E_e E_p$, where E_e and E_p denote the positron and proton beam energies, respectively. For these data, $\sqrt{s} = 318 \text{ GeV}$. The fractional energy transferred to the proton in its rest system is $y \approx Q^2/(sx)$. The centre-of-mass energy of the hadronic final state, W , is given by $W^2 = [P + q]^2 = m_p^2 + Q^2(1/x - 1) \approx Q^2/x = ys$, where m_p is the mass of the proton.

In diffraction, proceeding via

$$\gamma^* p(P) \rightarrow X + N(N), \tag{3}$$

see Fig. 2, the incoming proton undergoes a small perturbation and emerges either intact ($N = p$), or as a low-mass nucleonic state N , in both cases carrying a large fraction, x_L , of the incoming proton momentum. The virtual photon dissociates into a hadronic system X .

Diffraction is parametrised in terms of the mass M_X of the system X , and the mass M_N of the system N . Since t , the four-momentum transfer squared between the incoming proton and the outgoing system N , $t = (P - N)^2$, was not measured, the results presented are integrated over t . The measurements performed by ZEUS with the leading proton spectrometer [10] show that the diffractive contribution has a steeply falling t distribution with typical $|t|$ values well below 0.5 GeV^2 .

Diffraction was also analysed in terms of the momentum fraction x_p of the proton carried by the Pomeron exchanged in the t -channel, $x_p = [(P - N) \cdot q]/(P \cdot q) \approx (M_X^2 + Q^2)/(W^2 + Q^2)$, and the fraction of the Pomeron momentum carried by the struck quark, $\beta = Q^2/[2(P - N) \cdot q] \approx Q^2/(M_X^2 + Q^2)$. The variables x_p and β are related to the Bjorken scaling variable, x , via $x = \beta x_p$.

The events studied are of the type

$$ep \rightarrow e'X + \text{rest}, \quad (4)$$

where X denotes the hadronic system observed in the detector and ‘rest’ the particle system escaping detection through the forward and/or rear beam holes.

The coordinates of the event vertex were determined with tracks reconstructed in the CTD. Scattered positrons were identified with an algorithm based on a neural network [24]. The direction and energy of the scattered positron were determined from the combined information given by CAL, SRTD, RHES and CTD. Fiducial cuts on the impact point of the reconstructed scattered positron on the CAL surface were imposed to ensure a reliable measurement of the positron energy.

The hadronic system was reconstructed from energy-flow objects (EFO) [25, 26] which combine the information from CAL and FPC clusters and from CTD tracks, and which were not assigned to the scattered positron.

If a scattered-positron candidate was found, the following criteria were imposed to select the DIS events:

- the scattered-positron energy, E'_e , be at least 10 GeV ;
- the total measured energy of the hadronic system be at least 400 MeV ;
- $y_{\text{JB}}^{\text{FB}} > 0.006$, where $y_{\text{JB}}^{\text{FB}} = \sum_h (E_h - P_{Z,h})/(2E_e)$ summed over all hadronic EFOs in FCAL plus BCAL; or at least 400 MeV be deposited in the BCAL or in the RCAL outside of the ring of towers closest to the beamline;

- $-54 < Z_{\text{vtx}} < 50$ cm, where Z_{vtx} is the Z -coordinate of the event vertex;
- $43 < \sum_{i=e,h} (E_i - P_{Z,i}) < 64$ GeV, where the sum runs over both the scattered positron and all hadronic EFOs. This cut reduces the background from photoproduction and beam-gas scattering and removes events with large initial-state QED radiation;
- candidates for QED-Compton (QEDC) events, consisting of a scattered-positron candidate and a photon candidate, with mass $M_{e\gamma}$ less than 0.25 GeV and total transverse momentum less than 1.5 GeV, were removed. A Monte Carlo (MC) study showed that the number of remaining QEDC events was negligible.

The value of Q^2 was reconstructed from the measured energy E'_e and scattering angle θ_e of the positron, $Q^2 = 2E_e E'_e (1 + \cos \theta_e)$.

In the FPC I analysis, which covered lower Q^2 values, the value of W was determined as the weighted average of the values given by the positron and hadron measurement. Here, the value of W was reconstructed with the double-angle algorithm (DA) [27] which relies only on the measurement of the angles of the scattered positron and of the hadronic system.

The mass of the system X was determined by summing over all hadronic EFOs,

$$M_X^2 = \left(\sum E_h \right)^2 - \left(\sum p_{X,h} \right)^2 - \left(\sum p_{Y,h} \right)^2 - \left(\sum p_{Z,h} \right)^2,$$

where $P_h = (p_{X,h}, p_{Y,h}, p_{Z,h}, E_h)$ is the four-momentum vector of a hadronic EFO. All kinematic variables used to describe inclusive and diffractive scattering were derived from M_X , W and Q^2 .

A total of 60 events were found without a vertex, which were due either to cosmic radiation (45) or to an overlay of cosmic radiation with DIS (15); these events were discarded.

About 630k events for data set 1 and 1.4M events for data set 2 passed the selection cuts. The kinematic range for inclusive and diffractive events was chosen taking into account detector resolution and statistics. About 930k events were retained which satisfied $37 < W < 245$ GeV and $20 < Q^2 < 450$ GeV².

The resolutions of the reconstructed kinematic variables were estimated using MC simulation of diffractive events of the type $\gamma^* p \rightarrow XN$ (see Section 4). For the M_X , W and Q^2 bins considered in this analysis, the resolutions are approximately the same as for the FPC I analysis: $\frac{\sigma(W)}{W} = \frac{1}{W^{1/2}}$, $\frac{\sigma(Q^2)}{Q^2} = \frac{0.25}{(Q^2)^{1/3}}$ and $\frac{\sigma(M_X)}{M_X} = \frac{c}{M_X^{1/3}}$, where $c = 0.6$ GeV^{1/3} for $M_X < 1$ GeV and $c = 0.4$ GeV^{1/3} for $M_X \geq 1$ GeV, with M_X, W in units of GeV and Q^2 in GeV².

Results are presented for seven bins in W , nine bins in Q^2 and six bins in M_X , as shown in Table 1.

4 Monte Carlo simulations

The data were corrected for detector acceptance and resolution, and for radiative effects, with suitable combinations of several MC models, following the same procedure and using the same MC models as in the FPC I [13] analysis.

Events from inclusive DIS, including radiative effects, were simulated using the HERACLES 4.6.1 [?] program with the DJANGO 1.1 [29] interface to ARIADNE 4 [30] and using the CTEQ4D next-to-leading-order parton distribution functions [31]. In HERACLES, $O(\alpha)$ electroweak corrections are included. The colour-dipole model of ARIADNE, including boson-gluon fusion, was used to simulate the $O(\alpha_S)$ plus leading-logarithmic corrections to the quark-parton model. The Lund string model as implemented in JETSET 7.4 [32] was used by ARIADNE for hadronisation.

Diffraction DIS in which the proton does not dissociate, $ep \rightarrow eXp$ (including the production of ω and ϕ mesons via $ep \rightarrow eVp$, $V = \omega, \phi$ but excluding ρ^0 production), were simulated with SATRAP, which is based on a saturation model [33] and is interfaced to the RAPGAP 2.08 framework [34]. SATRAP was reweighted as a function of $Q^2/(Q^2 + M_X^2)$ and W . The production of ρ^0 mesons, $ep \rightarrow e\rho^0p$, was simulated with ZEUSVM [35], which uses a parametrisation of the measured ρ^0 cross sections as well as of the production and decay angular distributions [8, 36, 37]. The QED radiative effects were simulated with HERACLES. The QCD parton showers were simulated with LEPTO 6.5 [38].

Diffraction DIS in which the proton dissociates, $ep \rightarrow eXN$, was simulated with SATRAP interfaced to the model called SANG [39], which also includes the production of ρ^0 mesons. Following the previous experience (FPC I), the mass spectrum of the system N was generated according to $d\sigma/dM_N^2 \propto (1/M_N^2) \times 0.89\sqrt{M_N/4}$ for $M_N \leq 4$ GeV, and $d\sigma/dM_N^2 \propto (1/M_N^2) \times (2.5/M_N)^{0.25}$ for $M_N > 4$ GeV. This parametrisation was found to fit the data in the FPC I analysis. The fragmentation of the system N was simulated using JETSET 7.4.

The parameters of SANG, in particular those determining the shape of the M_N spectrum and the overall normalisation, were checked with a subset of the data. Events in this subset were required to have a minimum rapidity gap $\Delta\eta > \eta_{\min}$ between at least one EFO and its nearest neighbours, all with energies greater than 400 MeV. Good sensitivity for double dissociation was obtained with four event samples for the kinematic regions $\eta_{\min} = 3.0$, $W = 55 - 135$ GeV, and $\eta_{\min} = 4.0$, $W = 135 - 245$ GeV, for $Q^2 = 40 - 80$ GeV² and $80 - 450$ GeV². The mass of the hadronic system reconstructed from the energy deposits in FPC+FCAL, M_{FFCAL} , depends approximately linearly on the mass M_N^{gen} of the generated system N . Thus, the M_{FFCAL} distribution is sensitive to those proton dissociative events in which considerable energy of the system N is deposited in FPC and FCAL. The study showed that this is the case, broadly speaking, when the mass

of N taken at the generator level is $M_N > 2.3$ GeV. At large M_{FFCAL} , the distribution is dominated by double dissociation. Figure 3 presents the M_{FFCAL} distributions in four representative (Q^2, W) regions for the data compared to the Monte Carlo expectations for Xp , $\rho^0 p$, XN and non-diffractive processes. The contribution expected from XN as predicted by SANG is dominant. Good agreement between the number of events measured and those predicted is obtained. Since the contribution from diffraction with $M_N > 2.3$ GeV can affect the determination of the slope b for the non-diffractive contribution (see Section 5) it was subtracted statistically from the data as a function of M_X , W and Q^2 . Background from photoproduction, estimated with PYTHIA 5.7 [32], was negligible and was neglected.

The ZEUS detector response was simulated using a program based on GEANT 3.13 [40]. The generated events were passed through the detector and trigger simulations and processed by the same reconstruction and analysis programs as the data.

The measured hadronic energies for data and MC were increased by a factor of 1.065 in order to achieve an average transverse momentum balance between the scattered positron and the hadronic system. The mass M_X reconstructed from the energy-corrected EFOs, in the M_X region analysed, required an additional correction factor of 1.10 as determined from MC simulation ².

Good agreement between data and simulated event distributions was obtained for both the inclusive and the diffractive samples.

5 Determination of the diffractive contribution

The diffractive contribution was extracted from the data using the M_X method, which has been described elsewhere [12] and which has also been used for the FPC I analysis [13].

In the QCD picture of non-peripheral DIS, $\gamma^* p \rightarrow X + \text{rest}$, the hadronic system X measured in the detector is related to the struck quark and ‘rest’ to the proton remnant, both of which are coloured states. The final-state particles are expected to be uniformly emitted in rapidity along the $\gamma^* p$ collision axis and to uniformly populate the rapidity gap between the struck quark and the proton remnant, as described elsewhere [41]. In this case, the mass M_X is distributed as

$$\frac{d\mathcal{N}^{\text{non-diff}}}{d \ln M_X^2} = c \cdot \exp(b \cdot \ln M_X^2), \quad (5)$$

² The hadrons produced in diffractive events, on average, have lower momenta than those for hadrons from non-peripheral events, so that their fractional energy loss in the material in front of the calorimeter is larger.

where b and c are constants³. DJANGO predicts, for non-peripheral DIS, $b \approx 1.9$.

The diffractive reaction, $\gamma^* p \rightarrow XN$, on the other hand, has different characteristics. Diffractive scattering shows up as a peak near $x_L = 1$, the mass of the system X being limited by kinematics to $M_X^2/W^2 \lesssim 1 - x_L$. Moreover, the distance in rapidity between the outgoing nucleon system N and the system X is $\Delta\eta \approx \ln(1/(1 - x_L))$, becoming large when x_L is close to one. Combined with the limited values of M_X and the peaking of the diffractive cross section near $x_L = 1$, this leads to a large separation in rapidity between N and any other hadronic activity in the event. For the vast majority of diffractive events, the decay particles from the system N leave undetected through the forward beam hole. For a wide range of M_X values, the particles of the system X are emitted entirely within the acceptance of the detector. Monte Carlo studies show that X can be reliably reconstructed over the full M_X range of this analysis.

Regge phenomenology predicts the shape of the M_X distribution for peripheral processes. Diffractive production by Pomeron exchange in the t -channel, which dominates x_L values close to unity, leads to an approximately constant $\ln M_X^2$ distribution ($b \approx 0$). Figure 4 shows distributions of $\ln M_X^2$ for the data (from which the contribution from double dissociation with $M_N > 2.3$ GeV, as predicted by SANG, has been subtracted) for low- and high- W bins at low and high Q^2 together with the expectations from MC simulations for non-peripheral DIS (DJANGO) and for diffractive processes (SATRAP + ZEUSVM and SANG for $M_N < 2.3$ GeV). The observed distributions agree well with the expectation for a non-diffractive component giving rise to an exponentially growing $\ln M_X^2$ distribution, and for a diffractive component producing an almost constant distribution in a substantial part of the $\ln M_X^2$ range. At high W there is a clear signal for a contribution from diffraction. At low W the diffractive contribution is seen to be small.

The $\ln M_X^2$ spectra for all (W, Q^2) bins studied in this analysis are displayed in Fig. 5. They are compared with the MC predictions for the contributions from non-peripheral and diffractive production. The MC simulations are in good agreement with the data. It can be seen that the events at low and medium values of $\ln M_X^2$ originate predominantly from diffractive production.

The assumption of an exponential rise of the $\ln M_X^2$ distribution for non-diffractive processes permits the subtraction of this component and, therefore, the extraction of the diffractive contribution without assumptions about its exact M_X dependence. The distribution is of the form:

$$\frac{dN}{d \ln M_X^2} = D + c \cdot \exp(b \ln M_X^2) \quad \text{for } \ln M_X^2 < \ln W^2 - \eta_0, \quad (6)$$

³ Throughout, whenever a logarithm of a quantity with dimensions of energy is used, a normalisation in units of GeV is implied. For example, $\ln M_X^2$ is defined as $\ln(M_X^2/M_0^2)$, where $M_0 = 1$ GeV.

with M_X in GeV, D is the diffractive contribution and the second term represents the non-diffractive contribution. The quantity $(\ln W^2 - \eta_0)$ specifies the maximum value of $\ln M_X^2$ up to which the exponential behaviour of the non-diffractive contribution holds. A value of $\eta_0 = 2.2$ was found from the data. Equation (6) was fitted to the data in the limited range $\ln W^2 - 4.4 < \ln M_X^2 < \ln W^2 - \eta_0$ in order to determine the parameters b and c . The parameter D was assumed to be constant over the fit range, which is suggested by Figs. 4 and 5 where at high W and high Q^2 , $dN/\ln M_X^2$ is a slowly varying function when $M_X^2 > Q^2$ [42, 43]. However, the diffractive contribution was not taken from the fit but was obtained from the observed number of events after subtracting the non-diffractive contribution determined using the fitted values of b and c .

The fit range chosen is smaller than that used for the FPC I analysis (viz. for FPC I: $\ln W^2 - 5.6 < \ln M_X^2 < \ln W^2 - 2.2$). This change takes account of the observation that at high Q^2 and low values of M_X diffraction is suppressed, as seen in Fig. 5.

The non-diffractive contribution in the (W, Q^2) bins was determined by fitting for every (W, Q^2) interval the $\ln M_X^2$ distribution of the data from which the contribution of $\gamma^*p \rightarrow XN$ with $M_N > 2.3$ GeV as given by SANG, has been subtracted (see Appendix A and Tables 2 and 3). A fit of the form of Eq. (6) treating b, c and D as fit variables, was used. Note that this is a difference compared to the FPC I analysis, where for each (W, Q^2) interval, the same value of b , obtained as an average over all W, Q^2 values, was used. Good fits with χ^2 per degree of freedom of about unity were obtained. The value of the slope b varied typically between 1.4 and 1.9. The statistical error of the diffractive contribution includes the uncertainties on b and c .

Only bins of M_X, W, Q^2 , for which the non-diffractive background was less than 50%, were kept for further analysis.

The M_X method used for extracting the diffractive contribution was tested by performing a ‘‘Monte Carlo experiment’’ in which a sample of simulated non-peripheral DIS events (DJANGO) and diffractive events with (SATRAP+ZEUSVM+SANG) and without proton dissociation (SATRAP + ZEUSVM) was analysed as if it were the data. The resulting diffractive structure function (as defined in Section 9 below) is shown in Fig. 6 as a function of x_p for the β and Q^2 values used in the analysis. Only the statistical uncertainties are shown. The extracted structure function agrees with the diffractive structure function used for generating the events which validates the self consistency of the analysis procedure.

The extraction of the diffractive contribution was also studied for the case of a possible contribution from Reggeon exchange interfering with the contribution from diffraction. The amount of Reggeon-Pomeron interference allowed by the data [10] was found to be smaller than the combined statistical and systematic uncertainties in the present mea-

surement, see Appendix B.

6 Evaluation of cross sections and systematic uncertainties

The total and diffractive cross sections for ep scattering in a given (W, Q^2) bin were determined from the integrated luminosity, the number of observed events corrected for background, acceptance and smearing, and corrected to the QED Born level.

The cross sections and structure functions are presented at chosen reference values $M_{X\text{ref}}$, W_{ref} and Q_{ref}^2 . This was achieved as follows: first, the cross sections and structure functions were determined at the weighted average of each (M_X, W, Q^2) bin. They were then transported to the reference position using the ZEUS NLO QCD fit [44] in the case of the proton structure function F_2 , and the result of the BEKW(mod) fit (see Section 9.4) for the diffractive cross sections and structure functions. The resulting changes to the cross section and structure function values from the average to those at the reference positions were at the 5 – 15% level.

6.1 Systematic uncertainties

A study of the main sources contributing to the systematic uncertainties of the measurements was performed. The systematic uncertainties were calculated by varying the cuts or modifying the analysis procedure and repeating the full analysis for every variation. The size of the variations of cuts and the changes of the energy scales were chosen commensurate with the resolutions or the uncertainties of the relevant variables:

- the acceptance depends on the position measurement of the scattered positron. For set 1 the cut was increased from $40 \times 40 \text{ cm}^2$ to $41 \times 41 \text{ cm}^2$ (systematic uncertainty 1a) and decreased to $39 \times 39 \text{ cm}^2$ (systematic uncertainty 1b). For set 2, the radius cut was increased from 32 cm to 33 cm (systematic uncertainty 1a) and decreased to 31 cm (systematic uncertainty 1b). This affected the low- Q^2 region. Changes below 1% were observed;
- the measured energy of the scattered positron was increased (decreased) by 2% in the data, but not in the MC (systematic uncertainties 2a,b). In most cases the changes were smaller than 1%. For a few bins changes up to 3% were observed. For one bin at high Q^2 and high W , a change of 7% was found;
- the lower cut for the energy of the scattered positron was lowered to 8 GeV (raised to 12 GeV) (systematic uncertainties 3a,b). In most cases the changes were smaller than

1%. For a few bins changes up to 3% were found. For one bin at high Q^2 and high W , a change of 7% was found;

- to estimate the systematic uncertainties due to the uncertainty in the hadronic energy, the analysis was repeated after increasing (decreasing) the hadronic energy measured by the CAL by 2% [19] in the data but not in MC (systematic uncertainties 4a,b). The changes were below 3%;
- the energies measured by the FPC were increased (decreased) by 10% in the data but not in MC (systematic uncertainties 5a,b). The changes were below 1%;
- to estimate the uncertainties when the hadronic system h is in one of the transition regions: beam/(FPC+FCAL) (polar angle of the hadronic system $\theta_h < 8^\circ$); FCAL/BCAL ($27^\circ < \theta_h < 40^\circ$) or BCAL/RCAL ($128^\circ < \theta_h < 138^\circ$), the energy of h was increased in the data by 10% but not in MC (systematic uncertainty 6). This led to changes below 1%;
- the minimum hadronic energy cut of 400 MeV as well as the cut $y_{JB} > 0.006$ were increased by 50% (systematic uncertainty 7). In most cases the changes were below 1%. For a few bins at $Q^2 \leq 35 \text{ GeV}^2$, changes up to 3% were found;
- in order to check the simulation of the hadronic final state, the selection on $\sum_{i=e,h} (E_i - P_{Z,i})$ was changed from 43 – 64 GeV to 35 – 64 GeV (systematic uncertainty 8), leading for $Q^2 = 25, 35 \text{ GeV}^2$ to maximum changes at the level of 4%, and to changes up to 6% for $Q^2 = 320 \text{ GeV}^2$.

The above systematic tests apply to the total as well as to the diffractive cross sections. The following systematic tests apply to the diffractive cross section only:

- the reconstructed mass M_X of the system X was increased (decreased) by 5% in the data but not in the MC (systematic uncertainties 9a,b). Changes below 1% were observed except for $Q^2 = 25, 35 \text{ GeV}^2$, where decreasing M_X led to changes up to 5% at high y ;
- the contribution from double dissociation with $M_N > 2.3 \text{ GeV}$ was determined with the reweighted SANG simulation and was subtracted from the data. The diffractive cross section was redetermined by increasing (decreasing) the predicted contribution from SANG by 30% (systematic uncertainties 10a,b). The resulting changes in the diffractive cross section were well below the statistical uncertainty;
- the slope b describing the $\ln M_X^2$ dependence of the non-diffractive contribution (see Eq. (6)) was increased (decreased) by 0.2 units (systematic uncertainties 11a,b); this led to an increase (decrease) of the number of diffractive events for the highest M_X value at a given W, Q^2 by 1 (1.5) times the size of the statistical uncertainty. For the lower M_X values the changes were smaller.

The uncertainty in the luminosity measurement was 2% and was neglected. The major sources of systematic uncertainties for the diffractive cross section, $d\sigma^{\text{diff}}/dM_X$, were found to be the uncertainties 4a,b; 8; 9a,b, 10a,b; and 11a,b for the largest M_X value at a given value of W . The total systematic uncertainty for each bin was determined by adding the individual contributions in quadrature.

7 Proton structure function F_2 and the total γ^*p cross section

The differential cross section for inclusive ep scattering mediated by virtual photon exchange is given in terms of the structure functions F_i of the proton by

$$\frac{d^2\sigma^{e^+p}}{dx dQ^2} = \frac{2\pi\alpha^2}{xQ^4} [Y F_2(x, Q^2) - y^2 F_L(x, Q^2)] (1 + \delta_r(x, Q^2)), \quad (7)$$

where $Y = 1 + (1 - y)^2$, F_2 is the main component of the cross section which in the DIS factorisation scheme corresponds to the sum of the momentum densities of the quarks and antiquarks weighted by the squares of their charges, F_L is the longitudinal structure function and δ_r is a term accounting for radiative corrections.

In the Q^2 range considered in this analysis, $Q^2 \leq 450 \text{ GeV}^2$, the contributions from Z^0 exchange and Z^0 - γ interference are at most of the order of 0.4% and were ignored. The contribution of F_L to the cross section relative to that from F_2 is given by $(y^2/Y) \cdot (F_L/F_2)$. For the determination of F_2 , the F_L contribution was taken from the ZEUS NLO QCD fit [44]. The contribution of F_L to the cross section in the highest y ($=$ lowest x) bin of this analysis was 3.2%, decreasing to 1.3% for the next highest y bin. For the other bins, the F_L contribution is below 1%. The resulting uncertainties on F_2 are below 1%.

The measured F_2 values are listed in Table 4, and are shown in Fig. 7 together with those from the FPC I analysis. Here, the F_2 values of FPC I measured at $Q^2 = 27 \text{ GeV}^2$ were transported to $Q^2 = 25 \text{ GeV}^2$. Good agreement is observed between the measurements done at the same values of Q^2 , namely 25 and 55 GeV^2 . The data are compared to the predictions of the ZEUS NLO QCD fit [44] obtained from previous ZEUS F_2 measurements [19]. The fit describes the data well.

The proton structure function, F_2 , rises rapidly as $x \rightarrow 0$ for all values of Q^2 , the slope increasing as Q^2 increases. The form

$$F_2 = c \cdot x^{-\lambda} \quad (8)$$

was fitted for every Q^2 bin to the F_2 data, requiring $x < 0.01$ to exclude the region where valence quarks may dominate. Since, for fixed Q^2 , the x dependence of F_2 is related to the

W dependence of the total γ^*p cross section, the power λ can be related to the intercept of the Pomeron trajectory, $\lambda = \alpha_P(0) - 1$ (see Section 8.1). For later comparison with the diffractive results, these α_P values will be referred to as α_P^{tot} . The resulting values for c and $\alpha_P^{\text{tot}}(0)$ are listed in Table 5. Figure 8 presents the results from this study together with those from the FPC I analysis. The parameter $\alpha_P^{\text{tot}}(0)$ rises approximately linearly with $\ln Q^2$ from $\alpha_P^{\text{tot}}(0) = 1.155 \pm 0.011(\text{stat.})_{-0.011}^{+0.007}(\text{syst.})$ at $Q^2 = 2.7 \text{ GeV}^2$, to 1.322 ± 0.017 (statistical and systematic uncertainties added in quadrature) at $Q^2 = 70 \text{ GeV}^2$, substantially above the ‘soft Pomeron’ value of $1.096_{-0.009}^{+0.012}$ deduced from hadron-hadron scattering data [45]. This is in agreement with previous observations [13, 46, 47]. Since the Pomeron intercept is changing with Q^2 , the assumption of single Pomeron exchange cannot be sustained.

The total cross section for virtual photon-proton scattering, $\sigma_{\gamma^*p}^{\text{tot}} \equiv \sigma_T(x, Q^2) + \sigma_L(x, Q^2)$, where $T(L)$ stands for transverse (longitudinal) photons, was extracted from the measurement of F_2 using the relation

$$\sigma_{\gamma^*p}^{\text{tot}} = \frac{4\pi^2\alpha}{Q^2(1-x)}F_2(x, Q^2), \quad (9)$$

which is valid for $4m_p^2x^2 \ll Q^2$ [48]. The total cross section values are listed in Table 6 for fixed Q^2 as a function of W .

The total cross section multiplied by Q^2 is shown in Fig. 9 together with the results from the FPC I analysis. For fixed value of Q^2 , $Q^2\sigma_{\gamma^*p}^{\text{tot}}$ rises rapidly with W . For $Q^2 \leq 14 \text{ GeV}^2$, the rise becomes steeper with increasing Q^2 , while for $Q^2 \geq 70 \text{ GeV}^2$ the rise becomes less steep as Q^2 increases. The W behaviour of $\sigma_{\gamma^*p}^{\text{tot}}$ reflects the x dependence of F_2 as $x \rightarrow 0$, viz. $\sigma_{\gamma^*p}^{\text{tot}} \propto W^{2(\alpha_P^{\text{tot}}(0)-1)}$.

8 Diffractive cross section

The cross section for diffractive scattering via $ep \rightarrow eXN$ can be expressed in terms of the transverse (T) and longitudinal (L) cross sections, σ_T^{diff} and σ_L^{diff} , for $\gamma^*p \rightarrow XN$ as

$$\frac{d\sigma_{\gamma^*p \rightarrow XN}^{\text{diff}}(M_X, W, Q^2)}{dM_X} \equiv \frac{d(\sigma_T^{\text{diff}} + \sigma_L^{\text{diff}})}{dM_X} \approx \frac{2\pi}{\alpha} \frac{Q^2}{(1-y)^2 + 1} \frac{d\sigma_{ep \rightarrow eXN}^{\text{diff}}(M_X, W, Q^2)}{dM_X d\ln W^2 dQ^2}. \quad (10)$$

Here, a term $(1 - y^2/[1 + (1 - y)^2])\sigma_L^{\text{diff}}/(\sigma_T^{\text{diff}} + \sigma_L^{\text{diff}})$ multiplying $(\sigma_T^{\text{diff}} + \sigma_L^{\text{diff}})$ has been neglected [13, 48–50]. Since $y = W^2/s$, this approximation reduces the diffractive cross section for $M_X < 2 \text{ GeV}$ by at most 8% at $W < 200 \text{ GeV}$, and by at most 22% in the highest W bin, 200 – 245 GeV, under the assumption that only longitudinal photons contribute. Since the reduction is always smaller than the total uncertainty of the diffractive

cross section given by the statistical and systematic uncertainties added in quadrature: no correction was applied.

8.1 W dependence of the diffractive cross section

The diffractive cross section $d\sigma^{\text{diff}}/dM_X$ for $\gamma^*p \rightarrow XN$, $M_N < 2.3$ GeV, corrected for radiative effects and after transporting the measured values to the reference values (M_X, W, Q^2) using the BEKW(mod) fit (see Section 9.4), is presented in Tables 7 – 12 and Figs. 10 and 11 as a function of W . The results from the FPC I and FPC II analyses are shown. Where measurements at the same values of Q^2 are available, agreement is observed between the two data sets.

The diffractive cross section $d\sigma^{\text{diff}}/dM_X$ varies with M_X , W and Q^2 . For $M_X = 1.2$ GeV, the diffractive cross section shows a moderate increase with increasing W and a steep reduction with Q^2 , approximately proportional to $1/Q^4$. For larger M_X values, the diffractive cross section exhibits a substantial rise with increasing W and a less steep decrease with Q^2 roughly proportional to $1/Q^2$. The diffractive cross section is significant up to $Q^2 = 320$ GeV², provided $M_X = 11 - 30$ GeV.

The W dependence was quantified by fitting the form

$$\frac{d\sigma_{\gamma^*p \rightarrow XN}^{\text{diff}}}{dM_X} = h \cdot (W/W_0)^{a^{\text{diff}}} \quad (11)$$

to the data for each (M_X, Q^2) bin with $M_X < 15$ GeV; here $W_0 = 1$ GeV and h, a^{diff} are free parameters. The a^{diff} values from the FPC I and II analyses are shown in Fig. 12 as a function of Q^2 for different M_X intervals. For $M_X > 4$ GeV they range from 0.3 to 0.8 with a trend for a^{diff} to be larger by about 0.2 – 0.4 units when Q^2 is above 20 GeV².

Under the assumption that the diffractive cross section can be described by the exchange of a single Pomeron, the parameter a^{diff} is related to the Pomeron trajectory averaged over t : $\overline{\alpha_P} = 1 + a^{\text{diff}}/4$. In the present measurement, the diffractive cross section is integrated over t , providing t -averaged values of α_P . In the framework of Regge phenomenology, the cross section for diffractive scattering can be written as [51],

$$d\sigma/dt = f(t) \cdot e^{2(\alpha_P(t)-1) \cdot \ln(W/W_0)^2}, \quad (12)$$

where $f(t)$ characterises the t dependences of the $(\gamma^*IP\gamma^*)$ and $(pIPN)$ vertices. Assuming $d\sigma/dt \propto e^{A \cdot t}$ and $\alpha_P(t) = \alpha_P(0) + \alpha'_P \cdot t$ leads to $\alpha_P(0) = \overline{\alpha_P} + \alpha'_P/A$. Taking $A = 7.9 \pm 0.5(\text{stat.})^{+0.9}_{-0.5}(\text{syst.})$ GeV⁻², as measured by ZEUS with the leading proton spectrometer

(LPS) [10]⁴, and $\alpha'_{\mathbb{P}} = 0.25 \text{ GeV}^{-2}$ [45], gives $\alpha_{\mathbb{P}}(0) \approx \overline{\alpha_{\mathbb{P}}} + 0.03 = 1.03 + a^{\text{diff}}/4$. The $\alpha_{\mathbb{P}}(0)$ values deduced from diffractive cross sections are denoted as $\alpha_{\mathbb{P}}^{\text{diff}}(0)$.

The $\alpha_{\mathbb{P}}^{\text{diff}}(0)$ values for individual M_X bins are given in Table 13. The combined results from FPC I and FPC II for $2 < M_X < 15 \text{ GeV}$ are given in Table 14 and are shown in Fig. 8 as a function of Q^2 for $\alpha'_{\mathbb{P}} = 0.25 \text{ GeV}^{-2}$ and $\alpha'_{\mathbb{P}} = 0$. For $Q^2 < 20 \text{ GeV}^2$, $\alpha_{\mathbb{P}}^{\text{diff}}(0)$ is compatible with the soft-Pomeron value, while a substantial rise with Q^2 above the soft-Pomeron value is observed for $Q^2 > 30 \text{ GeV}^2$. The $\alpha_{\mathbb{P}}^{\text{diff}}(0)$ values lie, however, consistently below those obtained from F_2 , with $[\alpha_{\mathbb{P}}^{\text{diff}}(0) - 1]/[\alpha_{\mathbb{P}}^{\text{tot}}(0) - 1] \approx 0.5 - 0.7$. Since the Pomeron intercept is changing with Q^2 , the Pomeron observed in deep inelastic scattering does not correspond to a simple pole in the angular momentum plane.

8.2 M_X and Q^2 dependences of the diffractive cross section at fixed W

Figure 13 shows the diffractive cross section multiplied by a factor of Q^2 as a function of M_X for $W = 220 \text{ GeV}$. For Q^2 values up to about 55 GeV^2 masses M_X below 5 GeV are prevalent. As Q^2 increases, the maximum shifts to larger values of M_X .

The Q^2 dependence of diffraction was studied in terms of the diffractive cross section multiplied by the factor $Q^2 \cdot (Q^2 + M_X^2)$ since scaling of the diffractive structure function implies that the quantity $Q^2 \cdot (Q^2 + M_X^2) \frac{d\sigma_{\gamma^* p \rightarrow XN}^{\text{diff}}}{dM_X^2}$ (see below) should be independent of Q^2 , up to logarithmic terms. Figure 14 and Tables 15, 16, 17 show $Q^2 \cdot (Q^2 + M_X^2) \frac{d\sigma_{\gamma^* p \rightarrow XN}^{\text{diff}}}{dM_X^2}$ as a function of Q^2 separately for $M_X = 1.2, 3, 6 \text{ GeV}$ and $M_X = 11, 20, 30 \text{ GeV}$. In both cases the data lie within a band of about $\pm 25\%$ width for fixed Q^2 for the M_X values given. For the lower M_X region, $Q^2 \cdot (Q^2 + M_X^2) \frac{d\sigma_{\gamma^* p \rightarrow XN}^{\text{diff}}}{dM_X^2}$ is approximately constant up to $Q^2 \approx 30 - 40 \text{ GeV}^2$, followed by a decrease proportional to $\log Q^2$. For larger M_X values, the data show a weak dependence on $\log Q^2$. A similar behaviour is observed for lower values of W . Thus, the scaling behaviour of $d\sigma_{\gamma^* p \rightarrow XN}^{\text{diff}}/dM_X^2$ is of the form $1/[Q^2(Q^2 + M_X^2)]$.

8.3 Diffractive contribution to the total cross section

The relationship between the total and diffractive cross sections can be derived under certain assumptions. For instance, the imaginary part of the amplitude for elastic scat-

⁴ This value of A has been determined for $x_{\mathbb{P}} < 0.01$, where diffraction is dominant in the ZEUS data. Here it is assumed that A for the diffractive contribution remains the same in the region $0.01 < x_{\mathbb{P}} < 0.03$; $x_{\mathbb{P}} = 0.03$ is the highest value of $x_{\mathbb{P}}$ reached in the FPC I and FPC II analyses.

tering, $A_{\gamma^*p \rightarrow \gamma^*p}(t, W, Q^2)$, at $t = 0$ can be assumed to be linked to the total cross section by a generalisation of the optical theorem to virtual photon scattering. Assuming that $\sigma_{\gamma^*p}^{\text{tot}} \propto W^{2\lambda}$ and that the elastic and inclusive diffractive amplitudes at $t = 0$ are purely imaginary and have the same W and Q^2 dependences, then $A_{\gamma^*p \rightarrow \gamma^*p}(t = 0, W, Q^2)$ is proportional to $W^{2\lambda}$. Neglecting the real part of the scattering amplitudes, the rise of the diffractive cross section with W should then be proportional to $W^{4\lambda}$, so that the ratio of the diffractive cross section to the total γ^*p cross section,

$$r_{\text{tot}}^{\text{diff}} \equiv \frac{\sigma^{\text{diff}}}{\sigma^{\text{tot}}} = \frac{\int_{M_a}^{M_b} dM_X d\sigma_{\gamma^*p \rightarrow XN, M_N < 2.3 \text{ GeV}}^{\text{diff}} / dM_X}{\sigma_{\gamma^*p}^{\text{tot}}}, \quad (13)$$

should behave as $r_{\text{tot}}^{\text{diff}} \propto W^{2\lambda}$.

The ratio $r_{\text{tot}}^{\text{diff}}$ was determined for all $M_a < M_X < M_b$ intervals, with the $\sigma_{\gamma^*p}^{\text{tot}}$ values taken from this analysis. The ratio $r_{\text{tot}}^{\text{diff}}$ is listed in Tables 18 – 23 and is shown in Fig. 15 for the FPC II data, and in Fig. 16 for those from the FPC I analysis. The relative contribution of diffraction to the total cross section is approximately independent of W . It is substantial when $M_X^2 > Q^2$. For $Q^2 = 25 - 320 \text{ GeV}^2$, diffraction with $M_X < 2 \text{ GeV}$ accounts for about 0.1 to 0.4% of the total cross section, while the M_X intervals 15 – 25 GeV and 25 – 35 GeV together account for 3 – 4%.

The ratio $r = \sigma^{\text{diff}}(0.28 < M_X < 35 \text{ GeV}, M_N < 2.3 \text{ GeV}) / \sigma^{\text{tot}}$ was evaluated as a function of Q^2 for the highest W bin ($200 < W < 245 \text{ GeV}$) which provides the best coverage in M_X . Both FPC I and FPC II data are listed in Table 24 and shown in Fig. 17. The ratio r is $15.8_{-1.0}^{+1.1}\%$ at $Q^2 = 4 \text{ GeV}^2$, decreasing to $5.0_{-0.9}^{+0.9}\%$ at $Q^2 = 190 \text{ GeV}^2$. The data are well described by the form $r = a - b \cdot \ln(1 + Q^2)$. Considering both statistical and systematic uncertainties, the fit yielded $a = 0.2069 \pm 0.0075$ and $b = 0.0320 \pm 0.0020$, which is shown by the line in Fig. 17. The figure shows that the ratio r of the diffractive to the total cross section is decreasing logarithmically with Q^2 .

9 Diffractive structure function of the proton

The diffractive structure function of the proton, $F_2^{\text{D}(3)}(\beta, x_p, Q^2)$, is related to the diffractive cross section for $W^2 \gg Q^2$ as follows:

$$\frac{1}{2M_X} \frac{d\sigma_{\gamma^*p \rightarrow XN}^{\text{diff}}(M_X, W, Q^2)}{dM_X} = \frac{4\pi^2\alpha}{Q^2(Q^2 + M_X^2)} x_p F_2^{\text{D}(3)}(\beta, x_p, Q^2). \quad (14)$$

With this definition, $F_2^{\text{D}(3)}$ will include also contributions from longitudinal photons. If $F_2^{\text{D}(3)}$ is interpreted in terms of quark densities, it specifies the probability to find, in a proton undergoing a diffractive reaction, a quark carrying a fraction $x = \beta x_p$ of the proton momentum.

9.1 $x_P F_2^{\text{D}(3)}$ as a function of x_P

Figure 18 shows $x_P F_2^{\text{D}(3)}$ for the FPC II data set as a function of x_P for fixed Q^2 and fixed M_X , or, equivalently fixed β : $x_P F_2^{\text{D}(3)}$ rises approximately proportional to $\ln 1/x_P$ as $x_P \rightarrow 0$. This rise reflects the increase of the diffractive cross section $d\sigma^{\text{diff}}/dM_X$ with W . Figures 19 and 20 show that the combined FPC I and FPC II data exhibit this rise for most Q^2 values from 2.7 to 320 GeV². The data are also provided in Tables 25 – 29.

9.2 $x_P F_2^{\text{D}(3)}$ as a function of Q^2

The Q^2 dependence of $x_P F_2^{\text{D}(3)}$ for fixed β and x_P is provided in Tables 30 – 38 and is presented in Fig. 21 for the FPC I and FPC II data. Fits of the form

$$x_P F_2^{\text{D}(3)} = c + a \cdot \ln(1 + Q^2) \quad (15)$$

yielded the values of c and a given in Table 39 for selected values of x_P , β with six or more data points. Figure 21 and the fit results show that with increasing β the slope a changes from positive values, corresponding to positive logarithmic scaling violations, to constancy or negative logarithmic scaling violations. The data are dominated by positive scaling violations in the region characterised roughly by $x_P \beta = x < 1 \cdot 10^{-3}$, by negative scaling violations for $x \geq 5 \cdot 10^{-3}$, and by constancy in between.

The data contradict the assumption of Regge factorisation [2], that the diffractive structure function $x_P F_2^{\text{D}(3)}(\beta, x_P, Q^2)$ factorises into a term that depends only on x_P and a second term that depends only on β and Q^2 . This can be seen in Table 39 which gives the fit results for fixed $\beta = 0.4$ and $\beta = 0.7$, where the term a shows a strong dependence on x_P .

The Q^2 dependence of $x_P F_2^{\text{D}(3)}$ was also studied for selected values of $x_P = 0.0001, 0.0003, 0.001, 0.003, 0.01$ and of β . These choices of x_P and β values were made for the purpose of comparison with the results from H1 [?]. The values of the diffractive structure function at these values of x_P and β were obtained from those at the measured x_P , β values by using the BEKW(mod) fit to the combined FPC I and FPC II data with a total of 427 measured points (see below). Only points for which the ratio of the transported to the measured value of $x_P F_2^{\text{D}(3)}$ was within 0.75 – 1.33 were retained, corresponding to about half of the data sample. Since the $x_P F_2^{\text{D}(3)}$ data from H1 had been determined for $M_N < 1.6$ GeV while those from this measurement are presented for $M_N < 2.3$ GeV, the H1 data may have to be increased by a factor of 1.1 to 1.2 for an absolute comparison; no correction has been applied.

The measurements of $x_P F_2^{\text{D}(3)}$ by ZEUS and by H1 are compared in Figs. 22 – 24 as a function of Q^2 for fixed values of x_P and β . For $x_P = 0.0003$ the H1 points at $\beta = 0.27$

and 0.43 are lower than those from ZEUS by 10 – 40% while at $\beta = 0.67$ they are in agreement. For $x_p = 0.001$ and $\beta = 0.08 - 0.5$ the H1 points are lower by about 10 - 30 % while at $\beta = 0.8$ and $Q^2 \leq 7 \text{ GeV}^2$ they are higher by about 40%. For $x_p = 0.003$ the H1 points at $\beta = 0.027 - 0.43$ are lower by about 10 - 30%; at $\beta = 0.67$ the H1 results agree within about 15%. For $x_p = 0.01$ there is good agreement between the two measurements for most values of β . For $x_p = 0.03$ and $\beta \leq 0.27$ the H1 points agree with those of ZEUS within the errors, while for $\beta \geq 0.43$ the H1 points are always higher. These differences are not understood.

9.3 $x_p F_2^{\text{D}(3)}$ as a function of β

The β dependence of $x_p F_2^{\text{D}(3)}$ for the FPC I and FPC II data is shown in Figs. 25 – 27 for fixed x_p and Q^2 . The values of $x_p F_2^{\text{D}(3)}$ at the chosen x_p values were obtained from those at the measured x_p values using the BEKW(mod) fit (see below). The diffractive structure function exhibits a fall towards $\beta = 1$ and a broad maximum around $\beta = 0.5$. The broad maximum is approximately of the form $\beta(1 - \beta)$ as expected when the virtual photon turns into a $q\bar{q}$ system. For $x_p \geq 0.005$, $x_p F_2^{\text{D}(3)}$ rises as $\beta \rightarrow 0$ which is suggestive for the formation of $q\bar{q}g$ states via gluon radiation. For $x_p = 0.0025$ and 0.005 there is some excess at high $\beta \geq 0.95$. Since here the $q\bar{q}$ contribution from transverse photons is expected to be small, the excess suggests diffractive contributions from longitudinal photons.

9.4 Comparison with the BEKW parametrisation

Further insight into the $x_p F_2^{\text{D}(3)}$ data can be gained with the help of the BEKW parametrisation [?] which considers the contributions from the transitions: transverse photon $\rightarrow q\bar{q}$, longitudinal photon $\rightarrow q\bar{q}$ and transverse photon $\rightarrow q\bar{q}g$. In the BEKW parametrisation, the incoming virtual photon fluctuates into a $q\bar{q}$ or $q\bar{q}g$ dipole which interacts with the target proton via two-gluon exchange. The β spectrum and the scaling behaviour in Q^2 are derived from the wave functions of the incoming transverse (T) or longitudinal (L) photon on the light cone in the non-perturbative limit. The x_p dependence of the cross section is not predicted by BEKW but is to be determined by experiment. Specifically

$$x_p F_2^{\text{D}(3)}(\beta, x_p, Q^2) = c_T \cdot F_{q\bar{q}}^T + c_L \cdot F_{q\bar{q}}^L + c_g \cdot F_{q\bar{q}g}^T, \quad (16)$$

where

$$F_{q\bar{q}}^T = \left(\frac{x_0}{x_P}\right)^{n_T(Q^2)} \cdot \beta(1 - \beta), \quad (17)$$

$$F_{q\bar{q}}^L = \left(\frac{x_0}{x_P}\right)^{n_L(Q^2)} \cdot \frac{Q_0^2}{Q^2 + Q_0^2} \cdot \left[\ln\left(\frac{7}{4} + \frac{Q^2}{4\beta Q_0^2}\right)\right]^2 \cdot \beta^3(1 - 2\beta)^2, \quad (18)$$

$$F_{q\bar{q}g}^T = \left(\frac{x_0}{x_P}\right)^{n_g(Q^2)} \cdot \ln\left(1 + \frac{Q^2}{Q_0^2}\right) \cdot (1 - \beta)^\gamma. \quad (19)$$

The contribution from longitudinal photons coupling to $q\bar{q}$ is limited to β values close to unity. The $q\bar{q}$ contribution from transverse photons is expected to have a broad maximum around $\beta = 0.5$, while the $q\bar{q}g$ contribution becomes important at small β , provided the power γ is large. The original BEKW parametrisation also includes a higher-twist term for $q\bar{q}$ produced by transverse photons. The present data are insensitive to this term, and it has, therefore, been neglected.

For $F_{q\bar{q}}^L$, the term $(\frac{Q_0^2}{Q^2})$ provided by BEKW was replaced by the factor $(\frac{Q_0^2}{Q^2 + Q_0^2})$ to avoid problems as $Q^2 \rightarrow 0$. The powers $n_{T,L,g}(Q^2)$ were assumed by BEKW to be of the form $n(Q^2) = n_0 + n_1 \cdot \ln[1 + \ln(\frac{Q^2}{Q_0^2})]$. The rise of $\alpha_P(0)$ with $\ln Q^2$ observed in the present data suggested using the form $n(Q^2) = n_0 + n_1 \ln(1 + \frac{Q^2}{Q_0^2})$. This modified BEKW form will be referred to as BEKW(mod). Taking $x_0 = 0.01$ and $Q_0^2 = 0.4 \text{ GeV}^2$, the BEKW(mod) form gives a good description of the data. According to the fit, the coefficients n_0 can be set to zero, and the coefficient n_1 can be assumed to be the same for T , L and g .

The fits of BEKW(mod) to the data from this analysis (FPC II), to the data from the FPC I analysis and to the combined FPC I and FPC II data led to the results shown in Table 40.

Figures 19 and 20 compare the x_P dependence of the $x_P F_2^{D(3)}(\beta, x_P, Q^2)$ data from the FPC I and FPC II analyses with the BEKW(mod) fit. The fit gives a good description of the total of 427 data points.

The measured Q^2 and β dependences of the diffractive structure function are also well reproduced by the BEKW(mod) fit, see Figs. 21, 25 – 27. Based on the BEKW(mod) fit, the data show that the $(q\bar{q})_T$ contribution from transverse photons dominates the diffractive structure function for $0.2 < \beta < 0.9$. In the region $\beta > 0.95$, the contribution from longitudinal photons, $(q\bar{q})_L$, is dominant. This reflects, at least in part, the increase of the contribution from longitudinal compared to transverse photons in the production of ρ^0 mesons [8]. For $\beta \leq 0.15$, the largest contribution is due to gluon emission as described by the term $(q\bar{q}g)_T$. These conclusions hold for all Q^2 values studied.

10 Summary and conclusions

Inclusive and diffractive scattering has been measured with data taken in 1999-2000 with the ZEUS detector augmented by the forward-plug calorimeter (FPC), for Q^2 between 25 and 320 GeV² using an integrated luminosity of 52.4 pb⁻¹. Where appropriate, the results from a previous study (FPC I) using 4.2 pb⁻¹ and covering the region $Q^2 = 2.7 - 55$ GeV², were included.

The proton structure function, $F_2(x, Q^2)$, shows a rapid rise as $x \rightarrow 0$ at all Q^2 values. The rise for the region $x < 0.01$ has been parametrised in terms of the Pomeron trajectory $\alpha_P^{\text{tot}}(0)$, showing a rapid increase of $\alpha_P^{\text{tot}}(0) \propto \ln Q^2$ for Q^2 values between 2.7 and 70 GeV².

The total cross section for virtual-photon proton scattering multiplied by Q^2 , $Q^2 \sigma_{\gamma^* p}^{\text{tot}}$, shows a rapid rise with increasing W , reflecting the rise of F_2 as $x \rightarrow 0$; at lower Q^2 values (2.7 – 55 GeV²), this rise becomes steeper as Q^2 increases. At higher Q^2 values, the trend is reversed.

The diffractive cross section, $d\sigma_{\gamma^* p \rightarrow XN}^{\text{diff}}/dM_X$, $M_N < 2.3$ GeV, was studied as a function of the hadronic centre-of-mass energy W , of the mass M_X of the diffractively produced system X and for different Q^2 values. For $M_X = 1.2$ GeV, the cross section decreases rapidly with increasing Q^2 . For larger M_X values a strong rise with W is observed up to M_X values of 11 GeV. The intercept of the Pomeron trajectory deduced from the data rises with increasing Q^2 but its size is not as large as observed for $F_2(x, Q^2)$, $[\alpha_P^{\text{diff}}(0) - 1]/[\alpha_P^{\text{tot}}(0) - 1] \approx 0.5 - 0.7$. For fixed Q^2 , the ratio of the diffractive cross section for $0.28 < M_X < 35$ GeV to the total cross section is independent of W . For $W = 200 - 245$ GeV this ratio decreases $\propto \ln(1 + Q^2)$ from $15.8 \pm 0.7(\text{stat.})_{-0.7}^{+0.9}(\text{syst.})\%$ at $Q^2 = 4$ GeV² to $5.0 \pm 0.4(\text{stat.})_{-0.8}^{+0.8}(\text{syst.})\%$ at $Q^2 = 190$ GeV².

Diffractive scattering has also been studied in terms of the diffractive structure function of the proton, $F_2^{\text{D}(3)}(\beta, x_p, Q^2)$. For fixed M_X , $x_p F_2^{\text{D}(3)}$ shows a strong rise as $x_p \rightarrow 0$ for all Q^2 between 2.7 and 320 GeV². The x_p dependence of $x_p F_2^{\text{D}(3)}$ varies only modestly with Q^2 . The data show positive scaling violations proportional to $\ln Q^2$ in the region $x_p \beta = x < 2 \cdot 10^{-3}$, and constancy with Q^2 or negative scaling violations proportional to $\ln Q^2$ for $x \geq 2 \cdot 10^{-3}$. Therefore, in the Q^2 region studied, the diffractive structure function is consistent with being of leading twist.

The data contradict Regge factorisation: the diffractive structure function $F_2^{\text{D}(3)}(\beta, x_p, Q^2)$ does not factorise into a term which depends only on x_p and a second term which depends only on β and Q^2 .

A good description of $x_p F_2^{\text{D}(3)}$ as a function of x_p , β and Q^2 has been obtained by fitting the data with the BEKW(mod) parametrisation. This fit implies that the region $0.25 < \beta < 0.9$ is dominated by the $\gamma^* \rightarrow (q\bar{q})_T$ contribution, the region $\beta > 0.95$ is

dominated by the $\gamma^* \rightarrow (q\bar{q})_L$ term, while the rise of $x_{\mathbb{P}} F_2^{D(3)}$ as $\beta \rightarrow 0$ results from gluon emission described by the $\gamma^* \rightarrow (q\bar{q}g)_T$ term.

Acknowledgements

We thank the DESY directorate for their strong support and encouragement. The effort of the HERA machine group is gratefully acknowledged. We thank the DESY computing and network services for their support. The construction, testing and installation of the ZEUS detector has been made possible by the effort of many people not listed as authors. We would like to thank, in particular, J. Hauschildt and K. Löffler (DESY), R. Feller, E. Möller and H. Prause (I. Inst. for Exp. Phys., Univ. Hamburg), A. Maniatis (II. Inst. for Exp. Phys., Univ. Hamburg), N. Wilfert and the members of the mechanical workshop of the Faculty of Physics from Univ. Freiburg for their work on the FPC.

Appendix

A Subtraction of the contribution from proton dissociation with $M_N > 2.3$ GeV

The contribution from proton dissociation with $M_N > 2.3$ GeV to the diffractive data sample was determined with SANG and subtracted from the data sample. Tables 2 and 3 give for every Q^2 , W , M_X bin, for which diffractive cross sections are quoted in Tables 7 – 12, the fraction of events from $M_N > 2.3$ GeV:

$$\frac{\mathcal{N}^{\text{SANG}(M_N > 2.3 \text{ GeV})}}{\mathcal{N}^{\text{event}} - \mathcal{N}^{\text{non-diff}} - \mathcal{N}^{\text{SANG}(M_N > 2.3 \text{ GeV})}}. \quad (20)$$

For 84% of the bins, the fraction of events for proton dissociation with $M_N > 2.3$ GeV that are subtracted, is less than or equal to 20%.

B Extracting the diffractive contribution in the presence of Reggeon exchange

For this analysis the effect of Reggeon exchange interfering with the diffractive component was studied. A positive interference between Pomeron (IP) and Reggeon exchange (IR), which reproduces the rise observed in the LPS data [10] for $x_{IP}F_2^{\text{D}(3)}$ as $x_p > 0.03$, can be achieved by the exchange of the f -meson trajectory. The LPS data were fit to the form

$$x_{IP}F_2^{\text{D}(3)}(\beta, x_{IP}, Q^2) = \left[d_1 \cdot \sqrt{x_{IP}F_2^{\text{D}(3)\text{BEKW}}} + d_2 \cdot \sqrt{x_{IP}/0.01} \right]^2 \quad (21)$$

where $x_{IP}F_2^{\text{D}(3)\text{BEKW}}$ is taken from the fit to the FPC I and FPC II data, see Section 9.5.1, and the second term represents the Reggeon contribution. The fit to the LPS data yielded $d_1 = 0.768 \pm 0.020$ and $d_2 = 0.0177 \pm 0.0019$, with $\chi^2 = 135$ for 78 degrees of freedom.

In order to determine the possible contribution from Reggeon exchange and Reggeon-Pomeron interference ($IR^2 + 2 \cdot IP \cdot IR$) to the diffractive data, Monte Carlo (MC) events were generated according to

$$x_{IP}F_2^{D(3)(2IR+IP)}(\beta, x_{IP}, Q^2) = 2d_1 \cdot d_2 \cdot \sqrt{x_{IP}F_2^{\text{D}(3)\text{BEKW}}} \cdot x_{IP}/0.01 + d_2^2 \cdot \frac{x_{IP}}{0.01} \quad (22)$$

These MC events were subjected to the same analysis procedure as the data. The Reggeon plus Reggeon-Pomeron interference contribution ($IR^2 + 2 \cdot IP \cdot IR$) to the diffractive cross section $d\sigma^{\text{diff}}/dM_X$ was found to be smaller than the combined statistical and systematic uncertainty for all but 3 of the 166 data points. No correction was applied to the data.

References

- [1] ZEUS Coll., M. Derrick et al., Phys. Lett. **B 315**, 481 (1993).
- [2] G. Ingelman and P.E. Schlein, Phys. Lett. **B 152**, 256 (1985).
- [3] UA8 Coll., A. Brandt et al., Phys. Lett. **B 211**, 239 (1988).
- [4] UA8 Coll., A. Brandt et al., Phys. Lett. **B 297**, 417 (1992).
- [5] J.R. Forshaw, Preprint hep-ph/0611275 (2006).
- [6] ZEUS Coll., S. Chekanov et al., Nucl. Phys. **B 695**, 3 (2004).
- [7] ZEUS Coll., S. Chekanov et al., Nucl. Phys. **B 718**, 2 (2005).
- [8] ZEUS Coll., S. Chekanov et al., PMC **A 1**, 6 (2007).
- [9] H1 Coll., C. Aktas et al., Eur. Phys. J. **C 48**, 715 (2006).
- [10] ZEUS Coll., S. Chekanov et al., Eur. Phys. J. **C 38**, 43 (2004).
- [11] H1 Coll., C. Aktas et al., Eur. Phys. J. **C 48**, 749 (2006).
- [12] ZEUS Coll., M. Derrick et al., Z. Phys. **C 70**, 391 (1996);
ZEUS Coll., J. Breitweg et al., Eur. Phys. J. **C 6**, 43 (1999).
- [13] ZEUS Coll., S. Chekanov et al., Nucl. Phys. **B 713**, 3 (2005).
- [14] ZEUS Coll., U. Holm (ed.), *The ZEUS Detector*, Status Report (unpublished), DESY (1993), available on <http://www-zeus.desy.de/bluebook/bluebook.html> .
- [15] ZEUS Coll., M. Derrick et al., Phys. Lett. **B 293**, 465 (1992).
- [16] N. Harnew et al., Nucl. Inst. Meth. **A 279**, 290 (1989);
B. Foster et al., Nucl. Phys. Proc. Suppl. **B 32**, 181 (1993);
B. Foster et al., Nucl. Inst. Meth. **A 338**, 254 (1994).
- [17] M. Derrick et al., Nucl. Inst. Meth. **A 309**, 77 (1991);
A. Andresen et al., Nucl. Inst. Meth. **A 309**, 101 (1991);
A. Caldwell et al., Nucl. Inst. Meth. **A 321**, 356 (1992);
A. Bernstein et al., Nucl. Inst. Meth. **A 336**, 23 (1993).
- [18] A. Bamberger et al., Nucl. Inst. Meth. **A 401**, 63 (1997).
- [19] ZEUS Coll., S. Chekanov et al., Eur. Phys. J. **C 21**, 443 (2001).
- [20] A. Dwurazny et al., Nucl. Inst. Meth. **A 277**, 176 (1989).
- [21] A. Bamberger et al., Nucl. Inst. Meth. **A 450**, 235 (2000).
- [22] ZEUS Coll., M. Derrick et al., Z. Phys. **C 63**, 391 (1994).

- [23] W. H. Smith, K. Tokushuku and L. W. Wiggers, *Proc. Computing in High-Energy Physics (CHEPP), Annecy, France, Sept. 1992*, C. Verkerk and W. Wojcik (eds.), p. 222. CERN, Geneva, Switzerland (1992). Also in preprint DESY 92-150B.
- [24] H. Abramowicz, A. Caldwell and R. Sinkus, Nucl. Inst. Meth. **A 365**, 508 (1995).
- [25] F. Goebel, Ph.D. Thesis, Hamburg University, Hamburg (Germany), DESY-THESIS-2001-049 (2001).
- [26] G. Briskin, Ph.D. Thesis, Tel Aviv University, Tel Aviv (Israel), DESY-THESIS-1998-036 (1998).
- [27] S. Bentvelsen, J. Engelen and P. Kooijman, *Proc. Workshop on Physics at HERA*, W. Buchmüller and G. Ingelman (eds.), Vol. 1, p. 23. Hamburg, Germany, DESY (1992);
K.C. Höger, *ibid.* Vol. 1, p. 43 (1992) .
- [28] A. Kwiatkowski, H. Spiesberger and H.-J. Möhring, Comp. Phys. Comm. **69**, 155 (1992). Also in *Proc. Workshop Physics at HERA*, eds. W. Buchmüller and G. Ingelman, (DESY, Hamburg, 1991).
- [29] K. Charchula, G.A. Schuler and H. Spiesberger, Comp. Phys. Comm. **81**, 381 (1994) .
- [30] L. Lönnblad, Comp. Phys. Comm. **71**, 15 (1992).
- [31] H.L. Lai et al., Phys. Rev. **D 55**, 1280 (1997).
- [32] T. Sjöstrand, Comp. Phys. Comm. **82**, 74 (1994).
- [33] K. Golec-Biernat and M. Wüsthoff, Phys. Rev. **D 59**, 014017 (1999);
K. Golec-Biernat and M. Wüsthoff, Phys. Rev. **D 60**, 114023 (1999).
- [34] H. Jung, Comp. Phys. Comm. **86**, 147 (1995).
- [35] K. Muchorowski, Ph.D. Thesis, Warsaw University, Warsaw (Poland), unpublished (1996).
- [36] ZEUS Coll., J. Breitweg et al., Eur. Phys. J. **C 6**, 603 (1999).
- [37] ZEUS Coll., J. Breitweg et al., Eur. Phys. J. **C 12**, 393 (2000).
- [38] G. Ingelman, A. Edin and J. Rathsman, Comp. Phys. Comm. **101**, 108 (1997).
- [39] H. Lim, Ph.D. Thesis, The Graduate School, Kyungpook National University, Taegu (Republic of Korea), unpublished (2002).
- [40] R. Brun et al., GEANT3, Technical Report CERN-DD/EE/84-1 (1987).
- [41] see R.P. Feynman, *Photon-Hadron Interactions*. Benjamin, New York, (1972).
- [42] M. Genovese, N.N. Nikolaev and B.G. Zakharov, Sov. Phys. JETP **81**, 625 (1995).

- [43] A. Donnachie and P.V. Landshoff, Nucl. Phys. **B 303**, 634 (1988).
- [44] ZEUS Coll., S. Chekanov et al., Phys. Rev. **D 67**, 12007 (2003).
- [45] A. Donnachie and P.V. Landshoff, Nucl. Phys. **B 244**, 322 (1984);
A. Donnachie and P.V. Landshoff, Phys. Lett. **B 296**, 227 (1992);
J.R. Cudell, K. Kang and S.K. Kim, Phys. Lett. **B 395**, 311 (1997).
- [46] ZEUS Coll., J. Breitweg et al., Eur. Phys. J. **C 7**, 609 (1999).
- [47] H1 Coll., C. Adloff et al., Phys. Lett. **B 520**, 183 (2001).
- [48] L.N. Hand, Phys. Rev. **129**, 1834 (1963).
- [49] S.D. Drell and J.D. Walecka, Ann. Phys. **28**, 18 (1964).
- [50] F.J. Gilman, Phys. Rev. **167**, 1365 (1968).
- [51] See e.g. P.D.B. Collins, *An Introduction to Regge Theory and High Energy Physics*.
University Press, Cambridge (1977).
- [52] J. Bartels et al., Eur. Phys. J. **C7**, 443 (1999).

Q^2 (GeV ²)	20 - 30	30 - 40	40 - 50	50 - 60	60 - 80	80 - 100	100 - 150	150 - 250	250 - 450
Q_{ref}^2 (GeV ²)	25	35	45	55	70	90	120	190	320
W (GeV)	37 - 55	55 - 74	74 - 99	99 - 134	134 - 164	164 - 200	200 - 245		
W_{ref} (GeV)	45	65	85	115	150	180	220		
M_X (GeV)	0.28 - 2	2 - 4	4 - 8	8 - 15	15 - 25	25 - 35			
$M_{X\text{ref}}$ (GeV)	1.2	3	6	11	20	30			

Table 1: *Binning and reference values for Q^2 , W and M_X .*

Q^2 (GeV ²)	W (GeV)	$M_X = 1.2$ (GeV)	$M_X = 3$ (GeV)	$M_X = 6$ (GeV)	$M_X = 11$ (GeV)	$M_X = 20$ (GeV)	$M_X = 30$ (GeV)
25	45	0.06	0.09				
25	65	0.08	0.06	0.11			
25	85	0.06	0.06	0.08	0.20		
25	115	0.08	0.06	0.08	0.20		
25	150	0.09	0.05	0.07	0.17		
25	180	0.05	0.05	0.05	0.11	0.23	
25	220	0.07	0.04	0.06	0.10	0.20	0.47
35	45	0.04	0.05				
35	65	0.02	0.07	0.12			
35	85	0.08	0.09	0.09			
35	115	0.05	0.07	0.10	0.15		
35	150	0.13	0.06	0.07	0.12	0.25	
35	180	0.06	0.07	0.06	0.13	0.29	
35	220	0.05	0.07	0.06	0.11	0.23	0.36
45	45	0.20					
45	65	0.11	0.08	0.13			
45	85	0.03	0.06	0.09			
45	115	0.06	0.06	0.10	0.17		
45	150	0.07	0.08	0.08	0.13	0.33	
45	180	0.07	0.03	0.08	0.12	0.24	
45	220	0.07	0.05	0.05	0.09	0.15	0.30
55	45	0.09	0.07				
55	65	0.20	0.09				
55	85	0.08	0.12	0.08			
55	115	0.03	0.05	0.09	0.18		
55	150	0.10	0.07	0.07	0.11	0.26	
55	180	0.11	0.06	0.09	0.12	0.26	
55	220	0.07	0.09	0.06	0.08	0.22	0.29

Table 2: Fraction of events from proton dissociation with $M_N > 2.3$ GeV in the diffractive data sample, as determined with SANG in bins of Q^2, W, M_X , for $Q^2 = 25 - 55$ GeV².

Q^2 (GeV ²)	W (GeV)	$M_X = 1.2$ (GeV)	$M_X = 3$ (GeV)	$M_X = 6$ (GeV)	$M_X = 11$ (GeV)	$M_X = 20$ (GeV)	$M_X = 30$ (GeV)
70	65	0.00	0.06				
70	85	0.06	0.08	0.10			
70	115	0.00	0.04	0.08	0.16		
70	150	0.13	0.04	0.09	0.11		
70	180	0.24	0.03	0.09	0.12	0.22	
70	220	0.12	0.07	0.08	0.11	0.17	0.40
90	45	0.00					
90	65	0.00	0.04				
90	85	0.00	0.13	0.08			
90	115	0.03	0.04	0.17	0.18		
90	150	0.07	0.07	0.09	0.10	0.27	
90	180	0.05	0.12	0.08	0.12	0.25	0.31
90	220	0.08	0.06	0.10	0.09	0.23	0.25
120	65		0.12				
120	85	0.00	0.20	0.14			
120	115	0.08	0.08	0.06	0.13		
120	150	0.00	0.15	0.09	0.18		
120	180	0.06	0.10	0.08	0.10	0.21	
120	220	0.00	0.05	0.11	0.11	0.23	
190	45	0.00	0.00				
190	65	0.00	0.00				
190	85	0.00	0.29				
190	115		0.08	0.11	0.10		
190	150		0.00	0.14	0.15	0.17	
190	180	0.00	0.18	0.05	0.21	0.18	0.23
190	220	0.00	0.1	0.12	0.09	0.24	0.34
320	45	0.00					
320	85		0.00				
320	115		0.00	0.00	0.04		
320	150		1.34	0.00	0.05	0.17	
320	180	0.00	0.00	0.07	0.03	0.54	
320	220	0.00	0.00	0.34	0.10	0.15	

Table 3: Fraction of events from proton dissociation with $M_N > 2.3$ GeV in the diffractive data sample, as determined with SANG in bins of Q^2, W, M_X , for $Q^2 = 70 - 320$ GeV².

Q^2 (GeV ²)	x	$F_2 \pm \text{stat.} \pm \text{syst.}$	Q^2 (GeV ²)	x	$F_2 \pm \text{stat.} \pm \text{syst.}$
25	0.012200	$0.609 \pm 0.005^{+0.026}_{-0.013}$	90	0.042570	$0.514 \pm 0.006^{+0.011}_{-0.012}$
25	0.005884	$0.768 \pm 0.007^{+0.017}_{-0.016}$	90	0.020860	$0.639 \pm 0.008^{+0.013}_{-0.013}$
25	0.003449	$0.895 \pm 0.007^{+0.018}_{-0.019}$	90	0.012300	$0.756 \pm 0.009^{+0.015}_{-0.016}$
25	0.001887	$1.054 \pm 0.008^{+0.022}_{-0.022}$	90	0.006760	$0.919 \pm 0.010^{+0.019}_{-0.019}$
25	0.001110	$1.259 \pm 0.012^{+0.026}_{-0.027}$	90	0.003984	$1.104 \pm 0.014^{+0.023}_{-0.023}$
25	0.000771	$1.360 \pm 0.014^{+0.032}_{-0.030}$	90	0.002770	$1.229 \pm 0.018^{+0.025}_{-0.026}$
25	0.000516	$1.464 \pm 0.017^{+0.056}_{-0.053}$	90	0.001856	$1.359 \pm 0.022^{+0.043}_{-0.037}$
35	0.017000	$0.575 \pm 0.007^{+0.029}_{-0.013}$	120	0.055970	$0.491 \pm 0.006^{+0.011}_{-0.011}$
35	0.008218	$0.734 \pm 0.009^{+0.016}_{-0.015}$	120	0.027620	$0.590 \pm 0.007^{+0.012}_{-0.013}$
35	0.004821	$0.891 \pm 0.010^{+0.018}_{-0.018}$	120	0.016340	$0.717 \pm 0.008^{+0.015}_{-0.015}$
35	0.002640	$1.022 \pm 0.011^{+0.021}_{-0.021}$	120	0.008993	$0.884 \pm 0.009^{+0.018}_{-0.018}$
35	0.001553	$1.165 \pm 0.016^{+0.024}_{-0.024}$	120	0.005305	$1.046 \pm 0.013^{+0.022}_{-0.022}$
35	0.001079	$1.303 \pm 0.017^{+0.029}_{-0.028}$	120	0.003690	$1.150 \pm 0.014^{+0.024}_{-0.024}$
35	0.000723	$1.496 \pm 0.022^{+0.052}_{-0.061}$	120	0.002473	$1.312 \pm 0.018^{+0.035}_{-0.042}$
45	0.021750	$0.584 \pm 0.006^{+0.013}_{-0.013}$	190	0.085810	$0.430 \pm 0.007^{+0.010}_{-0.009}$
45	0.010540	$0.692 \pm 0.007^{+0.014}_{-0.014}$	190	0.043040	$0.533 \pm 0.007^{+0.011}_{-0.012}$
45	0.006191	$0.832 \pm 0.007^{+0.017}_{-0.017}$	190	0.025630	$0.631 \pm 0.008^{+0.013}_{-0.013}$
45	0.003391	$0.975 \pm 0.008^{+0.020}_{-0.020}$	190	0.014160	$0.773 \pm 0.009^{+0.016}_{-0.016}$
45	0.001996	$1.156 \pm 0.011^{+0.024}_{-0.024}$	190	0.008374	$0.947 \pm 0.013^{+0.019}_{-0.020}$
45	0.001387	$1.276 \pm 0.014^{+0.028}_{-0.027}$	190	0.005830	$1.046 \pm 0.014^{+0.023}_{-0.024}$
45	0.000929	$1.484 \pm 0.017^{+0.049}_{-0.050}$	190	0.003910	$1.121 \pm 0.019^{+0.047}_{-0.089}$
55	0.026450	$0.552 \pm 0.006^{+0.012}_{-0.013}$	320	0.136500	$0.378 \pm 0.007^{+0.009}_{-0.010}$
55	0.012850	$0.672 \pm 0.007^{+0.014}_{-0.014}$	320	0.070420	$0.449 \pm 0.009^{+0.011}_{-0.012}$
55	0.007556	$0.802 \pm 0.008^{+0.016}_{-0.016}$	320	0.042420	$0.528 \pm 0.009^{+0.014}_{-0.015}$
55	0.004142	$0.973 \pm 0.009^{+0.020}_{-0.020}$	320	0.023630	$0.639 \pm 0.010^{+0.017}_{-0.019}$
55	0.002439	$1.170 \pm 0.014^{+0.025}_{-0.024}$	320	0.014020	$0.757 \pm 0.014^{+0.026}_{-0.024}$
55	0.001695	$1.323 \pm 0.015^{+0.028}_{-0.029}$	320	0.009780	$0.907 \pm 0.017^{+0.026}_{-0.031}$
55	0.001135	$1.440 \pm 0.020^{+0.044}_{-0.045}$	320	0.006568	$1.058 \pm 0.024^{+0.026}_{-0.028}$
70	0.033430	$0.542 \pm 0.005^{+0.013}_{-0.013}$			
70	0.016300	$0.658 \pm 0.006^{+0.014}_{-0.014}$			
70	0.009597	$0.775 \pm 0.007^{+0.016}_{-0.016}$			
70	0.005265	$0.952 \pm 0.008^{+0.019}_{-0.019}$			
70	0.003102	$1.142 \pm 0.012^{+0.023}_{-0.023}$			
70	0.002156	$1.257 \pm 0.014^{+0.026}_{-0.027}$			
70	0.001444	$1.419 \pm 0.018^{+0.041}_{-0.044}$			

Table 4: Proton structure function F_2 .

Q^2 (GeV ²)	c	$\alpha_{\overline{P}}^{\text{tot}}(0)$
25	0.184 ± 0.015	1.279 ± 0.013
35	0.199 ± 0.016	1.276 ± 0.014
45	0.181 ± 0.019	1.298 ± 0.018
55	0.167 ± 0.017	1.322 ± 0.017
70	0.175 ± 0.016	1.322 ± 0.017
90	0.196 ± 0.031	1.311 ± 0.029
120	0.214 ± 0.032	1.301 ± 0.028

Table 5: *The results of the fits of F_2 data for $x < 0.01$ in bins of Q^2 to $F_2(x, Q^2) = c \cdot x^{-\lambda}$, where $\alpha_{\overline{P}}^{\text{tot}}(0) = 1 + \lambda$. The errors give the statistical and systematic uncertainties added in quadrature.*

Q^2 (GeV ²)	W (GeV)	$\sigma_{\gamma^*p}^{\text{tot}} \pm \text{stat.} \pm \text{syst.}$ (μb)	Q^2 (GeV ²)	W (GeV)	$\sigma_{\gamma^*p}^{\text{tot}} \pm \text{stat.} \pm \text{syst.}$ (μb)
25	45	$2.733 \pm 0.022^{+0.118}_{-0.060}$	90	45	$0.641 \pm 0.008^{+0.014}_{-0.015}$
25	65	$3.448 \pm 0.030^{+0.076}_{-0.072}$	90	65	$0.797 \pm 0.010^{+0.016}_{-0.016}$
25	85	$4.016 \pm 0.033^{+0.081}_{-0.048}$	90	85	$0.942 \pm 0.011^{+0.019}_{-0.020}$
25	115	$4.731 \pm 0.038^{+0.097}_{-0.097}$	90	115	$1.146 \pm 0.013^{+0.023}_{-0.023}$
25	150	$5.651 \pm 0.055^{+0.118}_{-0.122}$	90	150	$1.376 \pm 0.017^{+0.028}_{-0.028}$
25	180	$6.104 \pm 0.061^{+0.145}_{-0.135}$	90	180	$1.532 \pm 0.022^{+0.032}_{-0.032}$
25	220	$6.571 \pm 0.074^{+0.252}_{-0.236}$	90	220	$1.694 \pm 0.027^{+0.053}_{-0.046}$
35	45	$1.843 \pm 0.022^{+0.093}_{-0.041}$	120	45	$0.459 \pm 0.005^{+0.010}_{-0.010}$
35	65	$2.353 \pm 0.030^{+0.051}_{-0.048}$	120	65	$0.552 \pm 0.007^{+0.011}_{-0.012}$
35	85	$2.856 \pm 0.033^{+0.058}_{-0.059}$	120	85	$0.670 \pm 0.007^{+0.041}_{-0.014}$
35	115	$3.277 \pm 0.036^{+0.068}_{-0.067}$	120	115	$0.827 \pm 0.008^{+0.017}_{-0.017}$
35	150	$3.735 \pm 0.050^{+0.078}_{-0.077}$	120	150	$0.978 \pm 0.012^{+0.020}_{-0.020}$
35	180	$4.178 \pm 0.055^{+0.093}_{-0.090}$	120	180	$1.075 \pm 0.013^{+0.022}_{-0.023}$
35	220	$4.796 \pm 0.069^{+0.166}_{-0.195}$	120	220	$1.227 \pm 0.017^{+0.032}_{-0.039}$
45	45	$1.457 \pm 0.014^{+0.033}_{-0.032}$	190	45	$0.254 \pm 0.004^{+0.005}_{-0.006}$
45	65	$1.726 \pm 0.016^{+0.036}_{-0.036}$	190	65	$0.315 \pm 0.004^{+0.007}_{-0.007}$
45	85	$2.074 \pm 0.017^{+0.042}_{-0.042}$	190	85	$0.373 \pm 0.005^{+0.008}_{-0.008}$
45	115	$2.431 \pm 0.019^{+0.049}_{-0.050}$	190	115	$0.457 \pm 0.005^{+0.009}_{-0.009}$
45	150	$2.883 \pm 0.028^{+0.059}_{-0.060}$	190	150	$0.559 \pm 0.008^{+0.011}_{-0.012}$
45	180	$3.182 \pm 0.034^{+0.070}_{-0.068}$	190	180	$0.618 \pm 0.008^{+0.014}_{-0.014}$
45	220	$3.701 \pm 0.042^{+0.123}_{-0.124}$	190	220	$0.662 \pm 0.011^{+0.028}_{-0.052}$
55	45	$1.127 \pm 0.013^{+0.025}_{-0.027}$	320	45	$0.132 \pm 0.003^{+0.003}_{-0.004}$
55	65	$1.371 \pm 0.015^{+0.028}_{-0.029}$	320	65	$0.158 \pm 0.003^{+0.005}_{-0.005}$
55	85	$1.637 \pm 0.017^{+0.033}_{-0.033}$	320	85	$0.185 \pm 0.003^{+0.005}_{-0.005}$
55	115	$1.985 \pm 0.019^{+0.040}_{-0.041}$	320	115	$0.224 \pm 0.004^{+0.006}_{-0.007}$
55	150	$2.387 \pm 0.028^{+0.050}_{-0.050}$	320	150	$0.265 \pm 0.005^{+0.009}_{-0.008}$
55	180	$2.699 \pm 0.031^{+0.056}_{-0.059}$	320	180	$0.318 \pm 0.006^{+0.009}_{-0.011}$
55	220	$2.938 \pm 0.040^{+0.090}_{-0.092}$	320	220	$0.371 \pm 0.009^{+0.009}_{-0.010}$
70	45	$0.869 \pm 0.008^{+0.020}_{-0.020}$			
70	65	$1.055 \pm 0.010^{+0.022}_{-0.022}$			
70	85	$1.243 \pm 0.011^{+0.025}_{-0.025}$			
70	115	$1.526 \pm 0.013^{+0.031}_{-0.031}$			
70	150	$1.831 \pm 0.019^{+0.037}_{-0.037}$			
70	180	$2.015 \pm 0.022^{+0.042}_{-0.043}$			
70	220	$2.275 \pm 0.028^{+0.066}_{-0.070}$			

Table 6: Total γ^*p cross section $\sigma_{\gamma^*p}^{\text{tot}}$.

M_X	Q^2	W	$\frac{d\sigma_{\gamma^*p \rightarrow XN}^{\text{diff}}}{dM_X}$ $\pm \text{stat.} \pm \text{syst.}$	M_X	Q^2	W	$\frac{d\sigma_{\gamma^*p \rightarrow XN}^{\text{diff}}}{dM_X}$ $\pm \text{stat.} \pm \text{syst.}$
(GeV)	(GeV ²)	(GeV)	(nb/GeV)	(GeV)	(GeV ²)	(GeV)	(nb/GeV)
1.2	25	45	$5.57 \pm 0.91^{+1.21}_{-2.39}$	1.2	90	45	$0.23 \pm 0.10^{+0.03}_{-0.08}$
1.2	25	65	$6.39 \pm 0.88^{+0.54}_{-1.13}$	1.2	90	65	$0.14 \pm 0.11^{+0.07}_{-0.11}$
1.2	25	85	$8.44 \pm 0.98^{+1.09}_{-0.97}$	1.2	90	85	$0.11 \pm 0.06^{+0.06}_{-0.04}$
1.2	25	115	$8.29 \pm 1.02^{+1.36}_{-1.27}$	1.2	90	115	$0.64 \pm 0.20^{+0.04}_{-0.13}$
1.2	25	150	$7.02 \pm 1.15^{+1.07}_{-1.12}$	1.2	90	150	$0.82 \pm 0.34^{+0.21}_{-0.18}$
1.2	25	180	$10.98 \pm 1.50^{+1.73}_{-1.31}$	1.2	90	180	$0.97 \pm 0.40^{+0.28}_{-0.34}$
1.2	25	220	$16.73 \pm 2.29^{+2.58}_{-2.50}$	1.2	90	220	$0.23 \pm 0.13^{+0.10}_{-0.03}$
1.2	35	45	$1.95 \pm 0.69^{+1.59}_{-1.47}$				
1.2	35	65	$3.71 \pm 0.96^{+0.56}_{-0.84}$				
1.2	35	85	$2.63 \pm 0.69^{+0.10}_{-0.21}$	1.2	120	85	$0.09 \pm 0.04^{+0.02}_{-0.02}$
1.2	35	115	$4.56 \pm 0.96^{+0.45}_{-1.72}$	1.2	120	115	$0.23 \pm 0.10^{+0.03}_{-0.09}$
1.2	35	150	$2.33 \pm 0.80^{+0.22}_{-0.51}$	1.2	120	150	$0.36 \pm 0.14^{+0.14}_{-0.06}$
1.2	35	180	$3.09 \pm 0.93^{+0.24}_{-0.21}$	1.2	120	180	$0.27 \pm 0.11^{+0.03}_{-0.10}$
1.2	35	220	$5.75 \pm 1.19^{+1.12}_{-0.37}$	1.2	120	220	$0.65 \pm 0.23^{+0.03}_{-0.01}$
1.2	45	45	$0.77 \pm 0.29^{+0.37}_{-0.65}$	1.2	190	45	$0.05 \pm 0.03^{+0.00}_{-0.00}$
1.2	45	65	$0.83 \pm 0.26^{+0.29}_{-0.32}$	1.2	190	65	$0.03 \pm 0.06^{+0.03}_{-0.01}$
1.2	45	85	$1.39 \pm 0.25^{+0.26}_{-0.22}$	1.2	190	85	$0.03 \pm 0.06^{+0.08}_{-1.65}$
1.2	45	115	$2.21 \pm 0.38^{+0.45}_{-0.09}$				
1.2	45	150	$2.84 \pm 0.52^{+0.36}_{-0.36}$				
1.2	45	180	$2.05 \pm 0.48^{+0.49}_{-0.35}$	1.2	190	180	$0.60 \pm 0.52^{+0.26}_{-0.31}$
1.2	45	220	$3.06 \pm 0.57^{+0.67}_{-0.32}$	1.2	190	220	$0.21 \pm 0.14^{+0.07}_{-0.00}$
1.2	55	45	$0.62 \pm 0.25^{+0.10}_{-0.19}$	1.2	320	45	$0.91 \pm 1.05^{+0.02}_{-0.42}$
1.2	55	65	$0.79 \pm 0.25^{+0.10}_{-0.32}$				
1.2	55	85	$0.75 \pm 0.23^{+0.09}_{-0.16}$				
1.2	55	115	$1.45 \pm 0.33^{+0.12}_{-0.11}$				
1.2	55	150	$2.15 \pm 0.60^{+0.08}_{-0.12}$				
1.2	55	180	$2.08 \pm 0.53^{+0.40}_{-0.29}$	1.2	320	180	$0.07 \pm 0.08^{+0.00}_{-0.00}$
1.2	55	220	$1.50 \pm 0.40^{+0.28}_{-0.28}$	1.2	320	220	$1.26 \pm 1.68^{+0.09}_{-0.05}$
1.2	70	65	$0.54 \pm 0.18^{+0.10}_{-0.26}$				
1.2	70	85	$0.54 \pm 0.16^{+0.02}_{-0.08}$				
1.2	70	115	$0.74 \pm 0.19^{+0.12}_{-0.03}$				
1.2	70	150	$0.51 \pm 0.18^{+0.08}_{-0.08}$				
1.2	70	180	$0.38 \pm 0.20^{+0.14}_{-0.06}$				
1.2	70	220	$0.72 \pm 0.22^{+0.21}_{-0.09}$				

Table 7: Cross section for diffractive scattering, $\gamma^*p \rightarrow XN$, $M_N < 2.3$ GeV, for $M_X = 1.2$ GeV in bins of W and Q^2 .

M_X (GeV)	Q^2 (GeV ²)	W (GeV)	$\frac{d\sigma_{\gamma^*p \rightarrow XN}^{\text{diff}}}{dM_X}$ $\pm \text{stat.} \pm \text{syst.}$ (nb/GeV)	M_X (GeV)	Q^2 (GeV ²)	W (GeV)	$\frac{d\sigma_{\gamma^*p \rightarrow XN}^{\text{diff}}}{dM_X}$ $\pm \text{stat.} \pm \text{syst.}$ (nb/GeV)
3	25	45	$11.68 \pm 2.24^{+4.77}_{-7.18}$	3	90	65	$0.96 \pm 0.29^{+0.22}_{-0.55}$
3	25	65	$27.26 \pm 2.25^{+2.16}_{-4.40}$	3	90	85	$1.24 \pm 0.27^{+0.09}_{-0.21}$
3	25	85	$27.78 \pm 1.91^{+2.12}_{-3.20}$	3	90	115	$1.26 \pm 0.24^{+0.07}_{-0.13}$
3	25	115	$31.88 \pm 2.20^{+2.66}_{-1.38}$	3	90	150	$1.18 \pm 0.32^{+0.36}_{-0.08}$
3	25	150	$42.69 \pm 3.18^{+3.26}_{-6.22}$	3	90	180	$1.46 \pm 0.32^{+0.11}_{-0.21}$
3	25	180	$36.24 \pm 2.86^{+4.32}_{-3.05}$	3	90	220	$1.74 \pm 0.40^{+0.22}_{-0.19}$
3	25	220	$38.58 \pm 2.96^{+3.01}_{-3.26}$				
3	35	45	$6.91 \pm 1.54^{+3.39}_{-5.27}$	3	120	65	$0.12 \pm 0.07^{+0.06}_{-0.11}$
3	35	65	$9.63 \pm 1.57^{+1.37}_{-1.59}$	3	120	85	$0.21 \pm 0.10^{+0.11}_{-0.15}$
3	35	85	$10.25 \pm 1.40^{+2.25}_{-1.90}$	3	120	115	$0.71 \pm 0.15^{+0.05}_{-0.08}$
3	35	115	$14.69 \pm 1.70^{+1.05}_{-0.88}$	3	120	150	$0.40 \pm 0.12^{+0.05}_{-0.04}$
3	35	150	$16.50 \pm 2.12^{+2.63}_{-0.95}$	3	120	180	$0.60 \pm 0.16^{+0.11}_{-0.05}$
3	35	180	$18.53 \pm 2.23^{+3.32}_{-1.48}$	3	120	220	$0.85 \pm 0.19^{+0.14}_{-0.21}$
3	35	220	$16.35 \pm 2.10^{+1.25}_{-2.39}$				
3	45	65	$5.45 \pm 0.70^{+0.74}_{-1.54}$	3	190	45	$0.07 \pm 0.04^{+0.02}_{-0.02}$
3	45	85	$7.14 \pm 0.71^{+0.63}_{-1.20}$	3	190	65	$0.11 \pm 0.07^{+0.03}_{-0.05}$
3	45	115	$8.87 \pm 0.73^{+0.62}_{-1.31}$	3	190	85	$0.03 \pm 0.02^{+0.01}_{-0.03}$
3	45	150	$8.90 \pm 0.91^{+1.28}_{-1.17}$	3	190	115	$0.15 \pm 0.06^{+0.04}_{-0.02}$
3	45	180	$9.10 \pm 0.83^{+0.73}_{-1.61}$	3	190	150	$0.19 \pm 0.07^{+0.05}_{-0.05}$
3	45	220	$9.12 \pm 0.88^{+1.49}_{-0.96}$	3	190	180	$0.05 \pm 0.03^{+0.01}_{-0.01}$
3	45			3	190	220	$0.35 \pm 0.11^{+0.02}_{-0.21}$
3	55	45	$1.98 \pm 0.81^{+0.53}_{-1.03}$				
3	55	65	$2.49 \pm 0.60^{+0.64}_{-1.34}$	3	320	85	$0.01 \pm 0.01^{+0.00}_{-0.01}$
3	55	85	$3.53 \pm 0.50^{+0.35}_{-0.57}$	3	320	115	$0.07 \pm 0.05^{+0.00}_{-0.04}$
3	55	115	$4.99 \pm 0.58^{+0.57}_{-0.64}$	3	320	150	$0.04 \pm 0.08^{+0.01}_{-0.02}$
3	55	150	$5.26 \pm 0.68^{+0.56}_{-1.14}$	3	320	180	$0.12 \pm 0.07^{+0.03}_{-0.01}$
3	55	180	$5.89 \pm 0.78^{+0.60}_{-0.93}$	3	320	220	$0.08 \pm 0.06^{+0.00}_{-0.00}$
3	55	220	$4.92 \pm 0.71^{+0.88}_{-0.90}$				
3	70	65	$1.36 \pm 0.28^{+0.38}_{-0.71}$				
3	70	85	$1.75 \pm 0.25^{+0.31}_{-0.40}$				
3	70	115	$2.70 \pm 0.31^{+0.27}_{-0.38}$				
3	70	150	$3.03 \pm 0.41^{+0.23}_{-0.40}$				
3	70	180	$3.66 \pm 0.48^{+0.44}_{-0.55}$				
3	70	220	$3.81 \pm 0.51^{+0.63}_{-0.53}$				

Table 8: Cross section for diffractive scattering, $\gamma^*p \rightarrow XN$, $M_N < 2.3$ GeV, for $M_X = 3$ GeV in bins of W and Q^2 .

M_X	Q^2	W	$\frac{d\sigma^{\text{diff}}_{\gamma^*p \rightarrow XN}}{dM_X}$ $\pm \text{stat.} \pm \text{syst.}$	M_X	Q^2	W	$\frac{d\sigma^{\text{diff}}_{\gamma^*p \rightarrow XN}}{dM_X}$ $\pm \text{stat.} \pm \text{syst.}$
(GeV)	(GeV ²)	(GeV)	(nb/GeV)	(GeV)	(GeV ²)	(GeV)	(nb/GeV)
6	25	65	$22.6 \pm 4.3^{+5.9}_{-9.7}$	6	90	85	$2.9 \pm 0.4^{+0.4}_{-0.5}$
6	25	85	$28.4 \pm 1.7^{+1.8}_{-2.3}$	6	90	115	$3.2 \pm 0.4^{+0.6}_{-0.5}$
6	25	115	$35.8 \pm 1.9^{+2.7}_{-2.6}$	6	90	150	$4.0 \pm 0.5^{+0.2}_{-0.3}$
6	25	150	$36.1 \pm 2.4^{+1.5}_{-2.7}$	6	90	180	$4.2 \pm 0.5^{+0.6}_{-0.4}$
6	25	180	$44.3 \pm 2.6^{+1.3}_{-1.9}$	6	90	220	$4.5 \pm 0.5^{+0.4}_{-0.6}$
6	25	220	$48.1 \pm 2.7^{+2.9}_{-2.3}$				
6	35	65	$12.5 \pm 3.5^{+3.4}_{-4.1}$	6	120	85	$0.95 \pm 0.18^{+0.39}_{-0.54}$
6	35	85	$18.2 \pm 2.0^{+1.5}_{-2.9}$	6	120	115	$2.1 \pm 0.2^{+0.4}_{-0.3}$
6	35	115	$19.5 \pm 1.6^{+1.1}_{-1.5}$	6	120	150	$1.8 \pm 0.2^{+0.3}_{-0.2}$
6	35	150	$22.7 \pm 2.1^{+1.1}_{-0.9}$	6	120	180	$2.4 \pm 0.3^{+0.2}_{-0.2}$
6	35	180	$27.0 \pm 2.3^{+1.0}_{-2.3}$	6	120	220	$2.2 \pm 0.3^{+0.4}_{-0.1}$
6	35	220	$31.5 \pm 2.6^{+2.8}_{-3.4}$				
6	45	65	$7.3 \pm 1.5^{+2.2}_{-3.4}$				
6	45	85	$10.3 \pm 0.8^{+0.9}_{-1.7}$	6	190	115	$0.46 \pm 0.09^{+0.08}_{-0.08}$
6	45	115	$11.6 \pm 0.7^{+0.7}_{-0.9}$	6	190	150	$0.61 \pm 0.12^{+0.09}_{-0.07}$
6	45	150	$15.6 \pm 1.0^{+0.7}_{-0.8}$	6	190	180	$0.63 \pm 0.11^{+0.14}_{-0.12}$
6	45	180	$15.0 \pm 0.9^{+1.2}_{-0.5}$	6	190	220	$0.42 \pm 0.09^{+0.12}_{-0.08}$
6	45	220	$20.3 \pm 1.1^{+0.7}_{-1.6}$				
6	55	85	$8.2 \pm 0.6^{+0.7}_{-1.2}$	6	320	115	$0.17 \pm 0.06^{+0.03}_{-0.05}$
6	55	115	$8.6 \pm 0.6^{+0.6}_{-0.6}$	6	320	150	$0.10 \pm 0.05^{+0.01}_{-0.03}$
6	55	150	$11.5 \pm 0.9^{+1.0}_{-0.5}$	6	320	180	$0.16 \pm 0.07^{+0.03}_{-0.02}$
6	55	180	$10.1 \pm 0.9^{+1.0}_{-0.5}$	6	320	220	$0.09 \pm 0.07^{+0.06}_{-0.03}$
6	55	220	$15.1 \pm 1.1^{+1.0}_{-0.7}$				
6	70	85	$4.0 \pm 0.3^{+0.5}_{-0.7}$				
6	70	115	$5.8 \pm 0.4^{+0.6}_{-0.6}$				
6	70	150	$6.5 \pm 0.5^{+0.9}_{-0.7}$				
6	70	180	$6.7 \pm 0.5^{+0.9}_{-0.3}$				
6	70	220	$7.6 \pm 0.6^{+0.3}_{-0.8}$				

Table 9: Cross section for diffractive scattering, $\gamma^*p \rightarrow XN$, $M_N < 2.3$ GeV, for $M_X = 6$ GeV in bins of W and Q^2 .

M_X	Q^2	W	$\frac{d\sigma^{\text{diff}}_{\gamma^*p \rightarrow XN}}{dM_X}$	M_X	Q^2	W	$\frac{d\sigma^{\text{diff}}_{\gamma^*p \rightarrow XN}}{dM_X}$
(GeV)	(GeV ²)	(GeV)	$\pm \text{stat.} \pm \text{syst.}$ (nb/GeV)	(GeV)	(GeV ²)	(GeV)	$\pm \text{stat.} \pm \text{syst.}$ (nb/GeV)
11	25	85	$16.6 \pm 4.4^{+4.2}_{-4.8}$	11	90	115	$3.5 \pm 0.6^{+0.6}_{-0.7}$
11	25	115	$16.5 \pm 1.2^{+2.6}_{-4.0}$	11	90	150	$4.1 \pm 0.4^{+0.4}_{-0.4}$
11	25	150	$16.8 \pm 1.5^{+2.7}_{-4.6}$	11	90	180	$4.7 \pm 0.4^{+0.3}_{-0.2}$
11	25	180	$22.9 \pm 1.5^{+1.4}_{-1.8}$	11	90	220	$5.5 \pm 0.5^{+0.4}_{-0.3}$
11	25	220	$24.6 \pm 1.6^{+1.5}_{-1.6}$	11	120	115	$2.3 \pm 0.2^{+0.3}_{-0.6}$
11	35	115	$13.0 \pm 1.1^{+1.8}_{-2.8}$	11	120	150	$2.6 \pm 0.3^{+0.3}_{-0.4}$
11	35	150	$15.0 \pm 1.3^{+0.7}_{-1.1}$	11	120	180	$2.8 \pm 0.2^{+0.2}_{-0.3}$
11	35	180	$13.49 \pm 1.5^{+1.9}_{-1.3}$	11	120	220	$3.3 \pm 0.3^{+0.2}_{-0.2}$
11	35	220	$14.4 \pm 1.3^{+1.0}_{-1.0}$	11	190	115	$0.81 \pm 0.19^{+0.21}_{-0.27}$
11	45	115	$7.7 \pm 0.5^{+1.1}_{-1.8}$	11	190	150	$1.15 \pm 0.14^{+0.11}_{-0.15}$
11	45	150	$10.6 \pm 0.6^{+0.8}_{-1.2}$	11	190	180	$1.01 \pm 0.13^{+0.10}_{-0.09}$
11	45	180	$11.7 \pm 0.7^{+0.7}_{-0.7}$	11	190	220	$1.35 \pm 0.17^{+0.13}_{-0.15}$
11	45	220	$13.6 \pm 0.7^{+0.8}_{-0.6}$	11	320	115	$0.20 \pm 0.05^{+0.05}_{-0.10}$
11	55	115	$6.6 \pm 0.8^{+1.0}_{-1.3}$	11	320	150	$0.33 \pm 0.07^{+0.05}_{-0.05}$
11	55	150	$9.4 \pm 0.7^{+0.5}_{-0.7}$	11	320	180	$0.44 \pm 0.09^{+0.04}_{-0.10}$
11	55	180	$9.3 \pm 0.7^{+0.7}_{-1.0}$	11	320	220	$0.49 \pm 0.12^{+0.04}_{-0.12}$
11	55	220	$10.8 \pm 0.7^{+0.5}_{-1.0}$				
11	70	115	$4.2 \pm 0.4^{+0.7}_{-1.0}$				
11	70	150	$6.1 \pm 0.5^{+0.4}_{-0.6}$				
11	70	180	$6.6 \pm 0.4^{+0.3}_{-0.5}$				
11	70	220	$6.6 \pm 0.4^{+0.5}_{-0.3}$				

Table 10: Cross section for diffractive scattering, $\gamma^*p \rightarrow XN$, $M_N < 2.3$ GeV, for $M_X = 11$ GeV in bins of W and Q^2 .

M_X	Q^2	W	$\frac{d\sigma_{\gamma^*p \rightarrow XN}^{\text{diff}}}{dM_X}$ $\pm \text{stat.} \pm \text{syst.}$	M_X	Q^2	W	$\frac{d\sigma_{\gamma^*p \rightarrow XN}^{\text{diff}}}{dM_X}$ $\pm \text{stat.} \pm \text{syst.}$
(GeV)	(GeV ²)	(GeV)	(nb/GeV)	(GeV)	(GeV ²)	(GeV)	(nb/GeV)
20	25	180	$13.8 \pm 1.2^{+2.4}_{-3.2}$	20	90	150	$2.8 \pm 0.3^{+0.7}_{-0.8}$
20	25	220	$14.5 \pm 1.6^{+2.1}_{-2.0}$	20	90	180	$3.0 \pm 0.5^{+0.5}_{-0.4}$
20	35	150	$9.2 \pm 2.4^{+1.3}_{-1.4}$	20	90	220	$3.3 \pm 0.4^{+0.3}_{-0.3}$
20	35	180	$8.1 \pm 2.5^{+2.2}_{-2.1}$	20	120	180	$2.1 \pm 0.3^{+0.3}_{-0.3}$
20	35	220	$9.9 \pm 1.1^{+1.3}_{-1.8}$	20	120	220	$2.0 \pm 0.2^{+0.2}_{-0.4}$
20	45	150	$5.3 \pm 0.5^{+1.5}_{-1.9}$	20	190	150	$0.9 \pm 0.1^{+0.4}_{-0.3}$
20	45	180	$7.2 \pm 0.7^{+0.8}_{-1.0}$	20	190	180	$1.1 \pm 0.2^{+0.1}_{-0.2}$
20	45	220	$9.1 \pm 0.6^{+0.5}_{-0.7}$	20	190	220	$1.1 \pm 0.1^{+0.1}_{-0.1}$
20	55	150	$5.2 \pm 1.2^{+1.0}_{-1.1}$	20	320	150	$0.37 \pm 0.08^{+0.11}_{-0.11}$
20	55	180	$4.5 \pm 0.5^{+1.0}_{-1.4}$	20	320	180	$0.23 \pm 0.08^{+0.08}_{-0.12}$
20	55	220	$5.1 \pm 0.4^{+0.7}_{-0.8}$	20	320	220	$0.49 \pm 0.11^{+0.08}_{-0.11}$
20	70	180	$3.8 \pm 0.3^{+0.5}_{-0.6}$				
20	70	220	$4.6 \pm 0.4^{+0.3}_{-0.8}$				

Table 11: Cross section for diffractive scattering, $\gamma^*p \rightarrow XN$, $M_N < 2.3$ GeV, for $M_X = 20$ GeV in bins of W and Q^2 .

M_X	Q^2	W	$\frac{d\sigma_{\gamma^*p \rightarrow XN}^{\text{diff}}}{dM_X}$ $\pm \text{stat.} \pm \text{syst.}$	M_X	Q^2	W	$\frac{d\sigma_{\gamma^*p \rightarrow XN}^{\text{diff}}}{dM_X}$ $\pm \text{stat.} \pm \text{syst.}$
(GeV)	(GeV ²)	(GeV)	(nb/GeV)	(GeV)	(GeV ²)	(GeV)	(nb/GeV)
30	25	220	$8.2 \pm 3.3^{+2.7}_{-2.7}$	30	90	180	$2.4 \pm 1.3^{+0.6}_{-0.9}$
30	35	220	$6.6 \pm 1.1^{+1.8}_{-2.2}$	30	90	220	$3.4 \pm 0.6^{+0.6}_{-0.5}$
30	45	180	$5.5 \pm 1.7^{+1.2}_{-1.6}$	30	190	180	$0.91 \pm 0.47^{+0.19}_{-0.43}$
30	45	220	$6.3 \pm 1.1^{+0.9}_{-1.2}$	30	190	220	$1.01 \pm 0.15^{+0.25}_{-0.25}$
30	55	220	$4.6 \pm 0.6^{+0.8}_{-2.1}$				
30	70	220	$2.9 \pm 0.7^{+0.6}_{-0.7}$				

Table 12: Cross section for diffractive scattering, $\gamma^*p \rightarrow XN$, $M_N < 2.3$ GeV, for $M_X = 30$ GeV in bins of W and Q^2 .

M_X (GeV)	Q^2 (GeV ²)	$\alpha_P(0)$
1.2	25	1.150 ± 0.047
1.2	35	1.128 ± 0.091
1.2	45	1.248 ± 0.062
1.2	55	1.214 ± 0.068
3	25	1.142 ± 0.029
3	35	1.156 ± 0.038
3	45	1.132 ± 0.039
3	55	1.174 ± 0.046
3	70	1.241 ± 0.059
3	90	1.126 ± 0.079
6	25	1.167 ± 0.029
6	35	1.198 ± 0.047
6	45	1.216 ± 0.037
6	55	1.198 ± 0.042
6	70	1.178 ± 0.038
6	90	1.149 ± 0.062
6	120	1.189 ± 0.080
11	25	1.190 ± 0.072
11	45	1.234 ± 0.056
11	55	1.183 ± 0.065
11	70	1.172 ± 0.071
11	90	1.219 ± 0.086

Table 13: *The value of $\alpha_P(0)$ deduced from the W dependence of the diffractive cross section, assuming $\alpha'_P = 0.25 \text{ GeV}^{-2}$, for fixed M_X and Q^2 , see text.*

Q^2 (GeV ²)	$\alpha_P(0)$
2.7	1.112 ± 0.023
4	1.127 ± 0.014
6	1.137 ± 0.015
8	1.109 ± 0.012
14	1.130 ± 0.014
25	1.166 ± 0.028
27	1.195 ± 0.021
45	1.194 ± 0.026
55	1.201 ± 0.035
55	1.185 ± 0.030
70	1.197 ± 0.033
90	1.165 ± 0.044

Table 14: *The value of $\alpha_P(0)$ deduced from the W dependence of the diffractive cross section, assuming $\alpha'_P = 0.25$ GeV⁻², for fixed $2 < M_X < 15$ GeV and Q^2 , from FPC I and FPC II, see text.*

M_X (GeV)	Q^2 (GeV ²)	$Q^2 \cdot (Q^2 + M_X^2) \frac{d\sigma_{\gamma^* p \rightarrow XN}^{\text{diff}}}{dM_X^2}$ ($\mu\text{b GeV}^2$)	M_X (GeV)	Q^2 (GeV ²)	$Q^2 \cdot (Q^2 + M_X^2) \frac{d\sigma_{\gamma^* p \rightarrow XN}^{\text{diff}}}{dM_X^2}$ ($\mu\text{b GeV}^2$)
1.2	4	$4.27 \pm 0.44^{+1.36}_{-0.79}$	3	4	$4.98 \pm 0.33^{+0.52}_{-0.53}$
1.2	6	$4.73 \pm 0.52^{+1.10}_{-1.03}$	3	6	$5.84 \pm 0.46^{+0.53}_{-0.61}$
1.2	8	$4.44 \pm 0.45^{+0.96}_{-0.66}$	3	8	$6.01 \pm 0.40^{+0.59}_{-0.54}$
1.2	14	$4.77 \pm 0.45^{+0.70}_{-0.67}$	3	14	$6.12 \pm 0.40^{+0.66}_{-0.58}$
1.2	25	$4.61 \pm 0.63^{+0.95}_{-0.94}$	3	25	$5.47 \pm 0.42^{+0.60}_{-0.62}$
1.2	27	$3.07 \pm 0.63^{+0.90}_{-0.71}$	3	27	$5.58 \pm 0.56^{+0.82}_{-0.85}$
1.2	35	$3.05 \pm 0.63^{+0.87}_{-0.66}$	3	35	$4.20 \pm 0.54^{+0.63}_{-0.82}$
1.2	45	$2.66 \pm 0.50^{+0.77}_{-0.57}$	3	45	$3.69 \pm 0.36^{+0.70}_{-0.53}$
1.2	55	$1.83 \pm 0.96^{+1.00}_{-1.47}$	3	55	$3.88 \pm 0.84^{+1.20}_{-1.03}$
1.2	55	$1.94 \pm 0.51^{+0.63}_{-0.63}$	3	55	$2.89 \pm 0.42^{+0.66}_{-0.67}$
1.2	70	$1.50 \pm 0.45^{+0.63}_{-0.48}$	3	70	$3.51 \pm 0.47^{+0.75}_{-0.68}$
1.2	90	$0.78 \pm 0.44^{+0.57}_{-0.46}$	3	90	$2.59 \pm 0.59^{+0.67}_{-0.65}$
1.2	120	$3.93 \pm 1.37^{+1.38}_{-1.37}$	3	120	$2.18 \pm 0.49^{+0.62}_{-0.73}$
1.2	190	$3.11 \pm 2.07^{+2.32}_{-2.07}$	3	190	$2.19 \pm 0.70^{+0.72}_{-1.49}$
			3	320	$1.46 \pm 1.01^{+1.01}_{-1.02}$

Table 15: *The diffractive cross section multiplied by $Q^2(Q^2 + M_X^2)$, $Q^2(Q^2 + M_X^2)d\sigma_{\gamma^* p \rightarrow XN}^{\text{diff}}/dM_X^2$, $M_N < 2.3$ GeV, for $W = 220$ GeV as a function of Q^2 for $M_X = 1.2$ and 3.0 GeV. The first uncertainties are statistical and the second are the systematic uncertainties.*

M_X (GeV)	Q^2 (GeV ²)	$Q^2 \cdot (Q^2 + M_X^2) \frac{d\sigma_{\gamma^* p \rightarrow XN}^{\text{diff}}}{dM_X^2}$ ($\mu\text{b GeV}^2$)	M_X (GeV)	Q^2 (GeV ²)	$Q^2 \cdot (Q^2 + M_X^2) \frac{d\sigma_{\gamma^* p \rightarrow XN}^{\text{diff}}}{dM_X^2}$ ($\mu\text{b GeV}^2$)
6	4	$3.53 \pm 0.23^{+0.28}_{-0.39}$	11	2.7	$2.30 \pm 0.25^{+0.39}_{-0.25}$
6	6	$3.99 \pm 0.28^{+0.36}_{-0.30}$	11	4	$2.43 \pm 0.18^{+0.21}_{-0.25}$
6	8	$4.14 \pm 0.26^{+0.29}_{-0.34}$	11	6	$3.39 \pm 0.27^{+0.29}_{-0.30}$
6	14	$4.31 \pm 0.25^{+0.36}_{-0.30}$	11	8	$3.26 \pm 0.23^{+0.34}_{-0.24}$
6	25	$6.11 \pm 0.35^{+0.50}_{-0.45}$	11	14	$3.70 \pm 0.23^{+0.27}_{-0.25}$
6	27	$5.78 \pm 0.43^{+0.46}_{-0.58}$	11	25	$4.07 \pm 0.26^{+0.37}_{-0.38}$
6	35	$6.52 \pm 0.53^{+0.79}_{-0.88}$	11	27	$4.07 \pm 0.32^{+0.33}_{-0.46}$
6	45	$6.16 \pm 0.35^{+0.41}_{-0.60}$	11	35	$3.57 \pm 0.33^{+0.42}_{-0.42}$
6	55	$4.35 \pm 0.57^{+0.64}_{-0.69}$	11	45	$4.40 \pm 0.25^{+0.36}_{-0.32}$
6	55	$6.30 \pm 0.30^{+0.64}_{-0.57}$	11	55	$4.46 \pm 0.51^{+0.54}_{-0.58}$
6	70	$4.71 \pm 0.38^{+0.43}_{-0.60}$	11	55	$4.76 \pm 0.31^{+0.37}_{-0.52}$
6	90	$4.22 \pm 0.49^{+0.64}_{-0.77}$	11	70	$3.98 \pm 0.26^{+0.42}_{-0.32}$
6	120	$3.50 \pm 0.45^{+0.81}_{-0.50}$	11	90	$4.78 \pm 0.40^{+0.50}_{-0.50}$
6	190	$1.50 \pm 0.32^{+0.53}_{-0.42}$	11	120	$4.30 \pm 0.38^{+0.44}_{-0.49}$
			11	190	$3.62 \pm 0.45^{+0.57}_{-0.60}$
			11	320	$3.12 \pm 0.78^{+0.82}_{-1.09}$

Table 16: The diffractive cross section multiplied by $Q^2(Q^2 + M_X^2)$, $Q^2(Q^2 + M_X^2)d\sigma_{\gamma^* p \rightarrow XN}^{\text{diff}}/dM_X^2$, $M_N < 2.3$ GeV, for $W = 220$ GeV as a function of Q^2 for $M_X = 6$ and 11 GeV. The first uncertainties are statistical and the second are the systematic uncertainties.

M_X (GeV)	Q^2 (GeV ²)	$Q^2 \cdot (Q^2 + M_X^2) \frac{d\sigma_{\gamma^* p \rightarrow XN}^{\text{diff}}}{dM_X^2}$ ($\mu\text{b GeV}^2$)	M_X (GeV)	Q^2 (GeV ²)	$Q^2 \cdot (Q^2 + M_X^2) \frac{d\sigma_{\gamma^* p \rightarrow XN}^{\text{diff}}}{dM_X^2}$ ($\mu\text{b GeV}^2$)
20	2.7	$2.91 \pm 0.36^{+0.44}_{-0.41}$	30	2.7	$2.57 \pm 0.75^{+0.84}_{-0.79}$
20	4	$2.70 \pm 0.28^{+0.32}_{-0.30}$	30	4	$2.49 \pm 0.71^{+0.72}_{-0.77}$
20	6	$2.92 \pm 0.32^{+0.37}_{-0.41}$	30	6	$2.65 \pm 0.79^{+0.89}_{-0.85}$
20	8	$3.23 \pm 0.34^{+0.36}_{-0.51}$	30	8	$2.80 \pm 0.89^{+1.05}_{-0.90}$
20	14	$3.46 \pm 0.33^{+0.36}_{-0.36}$	30	14	$3.60 \pm 0.96^{+1.02}_{-1.04}$
20	25	$3.85 \pm 0.42^{+0.71}_{-0.69}$	30	25	$3.17 \pm 1.26^{+1.62}_{-1.64}$
20	27	$3.08 \pm 0.41^{+0.49}_{-0.43}$	30	27	$2.82 \pm 0.98^{+1.03}_{-1.04}$
20	35	$3.75 \pm 0.41^{+0.65}_{-0.80}$	30	35	$3.57 \pm 0.61^{+1.17}_{-1.34}$
20	45	$4.53 \pm 0.28^{+0.39}_{-0.44}$	30	45	$4.45 \pm 0.75^{+0.98}_{-1.12}$
20	55	$2.93 \pm 0.54^{+0.87}_{-0.58}$			
20	55	$3.20 \pm 0.27^{+0.53}_{-0.57}$	30	55	$4.04 \pm 0.51^{+0.88}_{-1.93}$
20	70	$3.80 \pm 0.33^{+0.42}_{-0.70}$	30	70	$3.32 \pm 0.84^{+1.07}_{-1.19}$
20	90	$3.66 \pm 0.38^{+0.54}_{-0.53}$	30	90	$5.05 \pm 0.96^{+1.30}_{-1.19}$
20	120	$3.11 \pm 0.32^{+0.48}_{-0.68}$			
20	190	$3.14 \pm 0.38^{+0.48}_{-0.51}$	30	190	$3.50 \pm 0.51^{+1.00}_{-1.00}$
20	320	$2.82 \pm 0.61^{+0.77}_{-0.90}$			

Table 17: The diffractive cross section multiplied by $Q^2(Q^2 + M_X^2)$, $Q^2(Q^2 + M_X^2)d\sigma_{\gamma^* p \rightarrow XN}^{\text{diff}}/dM_X^2$, $M_N < 2.3$ GeV, for $W = 220$ GeV as a function of Q^2 for $M_X = 20$ and 30 GeV. The first uncertainties are statistical and the second are the systematic uncertainties.

Q^2 (GeV ²)	W (GeV)	$\frac{\int_{M_a}^{M_b} dM_X d\sigma_{\gamma^* p \rightarrow XN}^{\text{diff}} / dM_X}{\sigma_{\text{tot}}}$ $\pm \text{stat.} \pm \text{syst.}$	Q^2 (GeV ²)	W (GeV)	$\frac{\int_{M_a}^{M_b} dM_X d\sigma_{\gamma^* p \rightarrow XN}^{\text{diff}} / dM_X}{\sigma_{\text{tot}}}$ $\pm \text{stat.} \pm \text{syst.}$
25	45	$0.00346 \pm 0.00057^{+0.00075}_{-0.00148}$	90	45	$0.00059 \pm 0.00026^{+0.00008}_{-0.00022}$
25	65	$0.00317 \pm 0.00044^{+0.00027}_{-0.00056}$	90	65	$0.00029 \pm 0.00024^{+0.00014}_{-0.00023}$
25	85	$0.00360 \pm 0.00042^{+0.00047}_{-0.00041}$	90	85	$0.00019 \pm 0.00011^{+0.00011}_{-0.00007}$
25	115	$0.00301 \pm 0.00037^{+0.00049}_{-0.00046}$	90	115	$0.00096 \pm 0.00030^{+0.00007}_{-0.00019}$
25	150	$0.00213 \pm 0.00035^{+0.00032}_{-0.00034}$	90	150	$0.00102 \pm 0.00042^{+0.00026}_{-0.00022}$
25	180	$0.00309 \pm 0.00042^{+0.00049}_{-0.00037}$	90	180	$0.00108 \pm 0.00045^{+0.00031}_{-0.00038}$
25	220	$0.00438 \pm 0.00060^{+0.00067}_{-0.00066}$	90	220	$0.00023 \pm 0.00013^{+0.00010}_{-0.00003}$
35	45	$0.00179 \pm 0.00064^{+0.00146}_{-0.00135}$	120	85	$0.00024 \pm 0.00010^{+0.00004}_{-0.00006}$
35	65	$0.00269 \pm 0.00070^{+0.00040}_{-0.00061}$			
35	85	$0.00158 \pm 0.00042^{+0.00006}_{-0.00013}$			
35	115	$0.00239 \pm 0.00050^{+0.00023}_{-0.00090}$			
35	150	$0.00107 \pm 0.00037^{+0.00010}_{-0.00023}$			
35	180	$0.00127 \pm 0.00038^{+0.00010}_{-0.00009}$			
35	220	$0.00206 \pm 0.00043^{+0.00040}_{-0.00013}$			
45	45	$0.00089 \pm 0.00033^{+0.00043}_{-0.00075}$	190	45	$0.00029 \pm 0.00018^{+0.00001}_{-0.00003}$
45	65	$0.00082 \pm 0.00025^{+0.00028}_{-0.00031}$	190	65	$0.00014 \pm 0.00034^{+0.00015}_{-0.00005}$
45	85	$0.00115 \pm 0.00021^{+0.00022}_{-0.00018}$	190	85	$0.00014 \pm 0.00026^{+0.00035}_{-0.000743}$
45	115	$0.00156 \pm 0.00027^{+0.00032}_{-0.00006}$	190	180	$0.00167 \pm 0.00143^{+0.00071}_{-0.00086}$
45	150	$0.00169 \pm 0.00031^{+0.00021}_{-0.00021}$			
45	180	$0.00111 \pm 0.00026^{+0.00026}_{-0.00019}$			
45	220	$0.00142 \pm 0.00026^{+0.00031}_{-0.00015}$	190	220	$0.00053 \pm 0.00035^{+0.00018}_{-0.00001}$
55	45	$0.00092 \pm 0.00037^{+0.00015}_{-0.00028}$	320	45	$0.01020 \pm 0.01184^{+0.00021}_{-0.00476}$
55	65	$0.00098 \pm 0.00031^{+0.00012}_{-0.00039}$	320	180	$0.00039 \pm 0.00041^{+0.00001}_{-0.00001}$
55	85	$0.00078 \pm 0.00024^{+0.00009}_{-0.00017}$			
55	115	$0.00125 \pm 0.00029^{+0.00011}_{-0.00010}$			
55	150	$0.00154 \pm 0.00043^{+0.00006}_{-0.00009}$			
55	180	$0.00132 \pm 0.00034^{+0.00025}_{-0.00018}$			
55	220	$0.00088 \pm 0.00023^{+0.00017}_{-0.00017}$			
70	65	$0.00086 \pm 0.00029^{+0.00016}_{-0.00042}$			
70	85	$0.00074 \pm 0.00022^{+0.00003}_{-0.00011}$			
70	115	$0.00083 \pm 0.00021^{+0.00014}_{-0.00004}$			
70	150	$0.00047 \pm 0.00017^{+0.00008}_{-0.00007}$			
70	180	$0.00033 \pm 0.00017^{+0.00012}_{-0.00005}$			
70	220	$0.00055 \pm 0.00016^{+0.00016}_{-0.00006}$			

Table 18: Ratio of the cross section for diffractive scattering, $\gamma^* p \rightarrow XN$, $M_N < 2.3$ GeV, integrated over $M_X = 0.28 - 2$ GeV, to the total cross section.

Q^2 (GeV ²)	W (GeV)	$\frac{\int_{M_a}^{M_b} dM_X d\sigma_{\gamma^*p \rightarrow XN}^{\text{diff}} / dM_X}{\sigma_{\text{tot}}}$ $\pm \text{stat.} \pm \text{syst.}$	Q^2 (GeV ²)	W (GeV)	$\frac{\int_{M_a}^{M_b} dM_X d\sigma_{\gamma^*p \rightarrow XN}^{\text{diff}} / dM_X}{\sigma_{\text{tot}}}$ $\pm \text{stat.} \pm \text{syst.}$
25	45	$0.00844 \pm 0.00162^{+0.00345}_{-0.00519}$	90	65	$0.00235 \pm 0.00071^{+0.00054}_{-0.00135}$
25	65	$0.01572 \pm 0.00131^{+0.00125}_{-0.00254}$	90	85	$0.00260 \pm 0.00057^{+0.00019}_{-0.00043}$
25	85	$0.01379 \pm 0.00096^{+0.00105}_{-0.00159}$	90	115	$0.00219 \pm 0.00041^{+0.00013}_{-0.00022}$
25	115	$0.01346 \pm 0.00094^{+0.00112}_{-0.00058}$	90	150	$0.00171 \pm 0.00046^{+0.00052}_{-0.00011}$
25	150	$0.01509 \pm 0.00113^{+0.00115}_{-0.00220}$	90	180	$0.00190 \pm 0.00042^{+0.00014}_{-0.00027}$
25	180	$0.01186 \pm 0.00094^{+0.00141}_{-0.00100}$	90	220	$0.00205 \pm 0.00047^{+0.00025}_{-0.00022}$
25	220	$0.01174 \pm 0.00091^{+0.00091}_{-0.00099}$			
35	45	$0.00737 \pm 0.00164^{+0.00361}_{-0.00562}$	120	65	$0.00042 \pm 0.00026^{+0.00020}_{-0.00038}$
35	65	$0.00812 \pm 0.00132^{+0.00115}_{-0.00134}$	120	85	$0.00061 \pm 0.00029^{+0.00033}_{-0.00045}$
35	85	$0.00714 \pm 0.00098^{+0.00157}_{-0.00133}$	120	115	$0.00171 \pm 0.00036^{+0.00011}_{-0.00020}$
35	115	$0.00894 \pm 0.00104^{+0.00064}_{-0.00054}$	120	150	$0.00081 \pm 0.00023^{+0.00010}_{-0.00008}$
35	150	$0.00883 \pm 0.00114^{+0.00140}_{-0.00051}$	120	180	$0.00111 \pm 0.00030^{+0.00020}_{-0.00010}$
35	180	$0.00886 \pm 0.00108^{+0.00159}_{-0.00071}$	120	220	$0.00137 \pm 0.00031^{+0.00023}_{-0.00034}$
35	220	$0.00682 \pm 0.00088^{+0.00052}_{-0.00100}$			
45	65	$0.00625 \pm 0.00081^{+0.00085}_{-0.00176}$	190	65	$0.00065 \pm 0.00040^{+0.00016}_{-0.00030}$
45	85	$0.00684 \pm 0.00069^{+0.00060}_{-0.00115}$	190	85	$0.00017 \pm 0.00013^{+0.00007}_{-0.00016}$
45	115	$0.00728 \pm 0.00061^{+0.00051}_{-0.00108}$	190	115	$0.00064 \pm 0.00026^{+0.00019}_{-0.00007}$
45	150	$0.00617 \pm 0.00063^{+0.00089}_{-0.00081}$	190	150	$0.00067 \pm 0.00025^{+0.00017}_{-0.00017}$
45	180	$0.00571 \pm 0.00052^{+0.00046}_{-0.00101}$	190	180	$0.00015 \pm 0.00010^{+0.00002}_{-0.00004}$
45	220	$0.00493 \pm 0.00048^{+0.00081}_{-0.00052}$	190	220	$0.00105 \pm 0.00034^{+0.00007}_{-0.00063}$
55	45	$0.00342 \pm 0.00139^{+0.00091}_{-0.00178}$	320	65	$0.00005 \pm 0.00007^{+0.00004}_{-0.00005}$
55	65	$0.00358 \pm 0.00086^{+0.00093}_{-0.00193}$	320	85	$0.00008 \pm 0.00009^{+0.00002}_{-0.00010}$
55	85	$0.00428 \pm 0.00061^{+0.00042}_{-0.00069}$	320	115	$0.00058 \pm 0.00041^{+0.00003}_{-0.00039}$
55	115	$0.00501 \pm 0.00058^{+0.00058}_{-0.00064}$	320	150	$0.00027 \pm 0.00060^{+0.00011}_{-0.00012}$
55	150	$0.00440 \pm 0.00057^{+0.00047}_{-0.00095}$	320	180	$0.00072 \pm 0.00047^{+0.00016}_{-0.00003}$
55	180	$0.00436 \pm 0.00058^{+0.00045}_{-0.00069}$	320	220	$0.00044 \pm 0.00031^{+0.00001}_{-0.00003}$
55	220	$0.00335 \pm 0.00049^{+0.00060}_{-0.00061}$			
70	65	$0.00254 \pm 0.00052^{+0.00071}_{-0.00132}$			
70	85	$0.00279 \pm 0.00040^{+0.00049}_{-0.00065}$			
70	115	$0.00352 \pm 0.00041^{+0.00035}_{-0.00050}$			
70	150	$0.00330 \pm 0.00045^{+0.00025}_{-0.00044}$			
70	180	$0.00362 \pm 0.00048^{+0.00044}_{-0.00054}$			
70	220	$0.00335 \pm 0.00045^{+0.00055}_{-0.00047}$			

Table 19: Ratio of the cross section for diffractive scattering, $\gamma^*p \rightarrow XN$, $M_N < 2.3$ GeV, integrated over $M_X = 2 - 4$ GeV, to the total cross section.

Q^2 (GeV ²)	W (GeV)	$\frac{\int_{M_a}^{M_b} dM_X d\sigma_{\gamma^*p \rightarrow XN}^{\text{diff}} / dM_X}{\sigma_{\text{tot}}} \pm \text{stat.} \pm \text{syst.}$	Q^2 (GeV ²)	W (GeV)	$\frac{\int_{M_a}^{M_b} dM_X d\sigma_{\gamma^*p \rightarrow XN}^{\text{diff}} / dM_X}{\sigma_{\text{tot}}} \pm \text{stat.} \pm \text{syst.}$
25	65	$0.02602 \pm 0.00497^{+0.00681}_{-0.01117}$	90	85	$0.01227 \pm 0.00168^{+0.00175}_{-0.00222}$
25	85	$0.02823 \pm 0.00173^{+0.00179}_{-0.00230}$	90	115	$0.01094 \pm 0.00125^{+0.00190}_{-0.00160}$
25	115	$0.03019 \pm 0.00159^{+0.00226}_{-0.00221}$	90	150	$0.01171 \pm 0.00134^{+0.00064}_{-0.00082}$
25	150	$0.02549 \pm 0.00173^{+0.00109}_{-0.00193}$	90	180	$0.01090 \pm 0.00131^{+0.00149}_{-0.00113}$
25	180	$0.02898 \pm 0.00170^{+0.00083}_{-0.00123}$	90	220	$0.01053 \pm 0.00123^{+0.00103}_{-0.00149}$
25	220	$0.02925 \pm 0.00168^{+0.00174}_{-0.00138}$			
35	65	$0.02107 \pm 0.00594^{+0.00568}_{-0.00698}$	120	85	$0.00555 \pm 0.00103^{+0.00227}_{-0.00316}$
35	85	$0.02535 \pm 0.00280^{+0.00203}_{-0.00398}$	120	115	$0.00984 \pm 0.00096^{+0.00173}_{-0.00130}$
35	115	$0.02372 \pm 0.00193^{+0.00128}_{-0.00176}$	120	150	$0.00739 \pm 0.00096^{+0.00118}_{-0.00099}$
35	150	$0.02427 \pm 0.00222^{+0.00118}_{-0.00093}$	120	180	$0.00878 \pm 0.00095^{+0.00081}_{-0.00055}$
35	180	$0.02578 \pm 0.00219^{+0.00091}_{-0.00222}$	120	220	$0.00730 \pm 0.00095^{+0.00140}_{-0.00045}$
35	220	$0.02625 \pm 0.00216^{+0.00235}_{-0.00286}$			
45	65	$0.01668 \pm 0.00343^{+0.00504}_{-0.00790}$	190	115	$0.00396 \pm 0.00077^{+0.00068}_{-0.00073}$
45	85	$0.01975 \pm 0.00151^{+0.00173}_{-0.00332}$	190	150	$0.00434 \pm 0.00086^{+0.00067}_{-0.00052}$
45	115	$0.01900 \pm 0.00111^{+0.00117}_{-0.00141}$	190	180	$0.00404 \pm 0.00072^{+0.00087}_{-0.00077}$
45	150	$0.02164 \pm 0.00135^{+0.00092}_{-0.00110}$	190	220	$0.00253 \pm 0.00054^{+0.00071}_{-0.00047}$
45	180	$0.01881 \pm 0.00119^{+0.00144}_{-0.00062}$			
45	220	$0.02191 \pm 0.00126^{+0.00078}_{-0.00172}$			
55	85	$0.01988 \pm 0.00156^{+0.00180}_{-0.00280}$	320	115	$0.00290 \pm 0.00105^{+0.00057}_{-0.00079}$
55	115	$0.01726 \pm 0.00125^{+0.00117}_{-0.00115}$	320	150	$0.00148 \pm 0.00077^{+0.00015}_{-0.00039}$
55	150	$0.01926 \pm 0.00151^{+0.00159}_{-0.00077}$	320	180	$0.00197 \pm 0.00083^{+0.00031}_{-0.00027}$
55	180	$0.01491 \pm 0.00127^{+0.00147}_{-0.00071}$	320	220	$0.00094 \pm 0.00072^{+0.00064}_{-0.00030}$
55	220	$0.02055 \pm 0.00158^{+0.00138}_{-0.00099}$			
70	85	$0.01288 \pm 0.00108^{+0.00167}_{-0.00212}$			
70	115	$0.01504 \pm 0.00105^{+0.00162}_{-0.00156}$			
70	150	$0.01422 \pm 0.00113^{+0.00193}_{-0.00149}$			
70	180	$0.01323 \pm 0.00106^{+0.00169}_{-0.00064}$			
70	220	$0.01337 \pm 0.00110^{+0.00058}_{-0.00137}$			

Table 20: Ratio of the cross section for diffractive scattering, $\gamma^*p \rightarrow XN$, $M_N < 2.3$ GeV, integrated over $M_X = 4 - 8$ GeV, to the total cross section.

Q^2 (GeV ²)	W (GeV)	$\frac{\int_{M_a}^{M_b} dM_X d\sigma_{\gamma^* p \rightarrow XN}^{\text{diff}} / dM_X}{\sigma_{\text{tot}}} \pm \text{stat.} \pm \text{syst.}$	Q^2 (GeV ²)	W (GeV)	$\frac{\int_{M_a}^{M_b} dM_X d\sigma_{\gamma^* p \rightarrow XN}^{\text{diff}} / dM_X}{\sigma_{\text{tot}}} \pm \text{stat.} \pm \text{syst.}$
25	85	$0.02888 \pm 0.00764^{+0.00727}_{-0.00826}$	90	115	$0.02133 \pm 0.00348^{+0.00350}_{-0.00452}$
25	115	$0.02434 \pm 0.00177^{+0.00377}_{-0.00594}$	90	150	$0.02066 \pm 0.00183^{+0.00193}_{-0.00177}$
25	150	$0.02078 \pm 0.00184^{+0.00337}_{-0.00564}$	90	180	$0.02131 \pm 0.00196^{+0.00128}_{-0.00106}$
25	180	$0.02618 \pm 0.00170^{+0.00163}_{-0.00207}$	90	220	$0.02285 \pm 0.00196^{+0.00144}_{-0.00139}$
25	220	$0.02614 \pm 0.00171^{+0.00164}_{-0.00173}$	120	115	$0.01899 \pm 0.00155^{+0.00248}_{-0.00471}$
35	115	$0.02769 \pm 0.00246^{+0.00380}_{-0.00604}$	120	150	$0.01822 \pm 0.00223^{+0.00233}_{-0.00302}$
35	150	$0.02813 \pm 0.00250^{+0.00129}_{-0.00197}$	120	180	$0.01801 \pm 0.00157^{+0.00109}_{-0.00180}$
35	180	$0.02258 \pm 0.00248^{+0.00324}_{-0.00211}$	120	220	$0.01862 \pm 0.00165^{+0.00097}_{-0.00135}$
35	220	$0.02097 \pm 0.00198^{+0.00147}_{-0.00151}$	190	115	$0.01221 \pm 0.00286^{+0.00311}_{-0.00411}$
45	115	$0.02204 \pm 0.00141^{+0.00326}_{-0.00504}$	190	150	$0.01434 \pm 0.00174^{+0.00134}_{-0.00183}$
45	150	$0.02572 \pm 0.00158^{+0.00188}_{-0.00289}$	190	180	$0.01134 \pm 0.00146^{+0.00118}_{-0.00097}$
45	180	$0.02571 \pm 0.00149^{+0.00159}_{-0.00154}$	190	220	$0.01419 \pm 0.00177^{+0.00137}_{-0.00156}$
45	220	$0.02564 \pm 0.00143^{+0.00142}_{-0.00113}$	320	115	$0.00617 \pm 0.00141^{+0.00144}_{-0.00316}$
55	115	$0.02304 \pm 0.00285^{+0.00350}_{-0.00452}$	320	150	$0.00866 \pm 0.00193^{+0.00119}_{-0.00138}$
55	150	$0.02740 \pm 0.00196^{+0.00137}_{-0.00205}$	320	180	$0.00961 \pm 0.00196^{+0.00091}_{-0.00229}$
55	180	$0.02399 \pm 0.00173^{+0.00175}_{-0.00248}$	320	220	$0.00911 \pm 0.00228^{+0.00073}_{-0.00224}$
55	220	$0.02577 \pm 0.00172^{+0.00108}_{-0.00228}$			
70	115	$0.01924 \pm 0.00165^{+0.00313}_{-0.00456}$			
70	150	$0.02323 \pm 0.00178^{+0.00152}_{-0.00226}$			
70	180	$0.02276 \pm 0.00146^{+0.00107}_{-0.00182}$			
70	220	$0.02015 \pm 0.00134^{+0.00166}_{-0.00092}$			

Table 21: Ratio of the cross section for diffractive scattering, $\gamma^* p \rightarrow XN$, $M_N < 2.3$ GeV, integrated over $M_X = 8 - 15$ GeV, to the total cross section.

Q^2 (GeV ²)	W (GeV)	$\frac{\int_{M_a}^{M_b} dM_X d\sigma_{\gamma^*p \rightarrow XN}^{\text{diff}} / dM_X}{\sigma_{\text{tot}}}$ $\pm \text{stat.} \pm \text{syst.}$	Q^2 (GeV ²)	W (GeV)	$\frac{\int_{M_a}^{M_b} dM_X d\sigma_{\gamma^*p \rightarrow XN}^{\text{diff}} / dM_X}{\sigma_{\text{tot}}}$ $\pm \text{stat.} \pm \text{syst.}$
25	180	$0.02250 \pm 0.00197^{+0.00390}_{-0.00516}$	90	180	$0.01969 \pm 0.00293^{+0.00292}_{-0.00284}$
25	220	$0.02207 \pm 0.00243^{+0.00324}_{-0.00310}$	90	220	$0.01957 \pm 0.00207^{+0.00201}_{-0.00196}$
35	150	$0.02464 \pm 0.00632^{+0.00357}_{-0.00371}$	120	180	$0.01939 \pm 0.00300^{+0.00270}_{-0.00308}$
35	180	$0.01927 \pm 0.00601^{+0.00526}_{-0.00501}$	120	220	$0.01623 \pm 0.00166^{+0.00189}_{-0.00312}$
35	220	$0.02054 \pm 0.00229^{+0.00277}_{-0.00372}$	190	150	$0.01617 \pm 0.00239^{+0.00719}_{-0.00517}$
45	150	$0.01819 \pm 0.00180^{+0.00510}_{-0.00661}$	190	180	$0.01800 \pm 0.00299^{+0.00175}_{-0.00366}$
45	180	$0.02273 \pm 0.00220^{+0.00246}_{-0.00313}$	190	220	$0.01687 \pm 0.00207^{+0.00158}_{-0.00181}$
45	220	$0.02445 \pm 0.00153^{+0.00144}_{-0.00185}$	320	150	$0.01389 \pm 0.00296^{+0.00409}_{-0.00425}$
55	150	$0.02160 \pm 0.00501^{+0.00429}_{-0.00461}$	320	180	$0.00704 \pm 0.00254^{+0.00260}_{-0.00377}$
55	180	$0.01668 \pm 0.00179^{+0.00378}_{-0.00525}$	320	220	$0.01311 \pm 0.00287^{+0.00217}_{-0.00308}$
55	220	$0.01742 \pm 0.00149^{+0.00245}_{-0.00271}$			
70	180	$0.01904 \pm 0.00149^{+0.00243}_{-0.00290}$			
70	220	$0.02028 \pm 0.00176^{+0.00140}_{-0.00334}$			

Table 22: Ratio of the cross section for diffractive scattering, $\gamma^*p \rightarrow XN$, $M_N < 2.3$ GeV, integrated over $M_X = 15 - 25$ GeV, to the total cross section.

Q^2 (GeV ²)	W (GeV)	$\frac{\int_{M_a}^{M_b} dM_X d\sigma_{\gamma^*p \rightarrow XN}^{\text{diff}} / dM_X}{\sigma_{\text{tot}}}$ $\pm \text{stat.} \pm \text{syst.}$	Q^2 (GeV ²)	W (GeV)	$\frac{\int_{M_a}^{M_b} dM_X d\sigma_{\gamma^*p \rightarrow XN}^{\text{diff}} / dM_X}{\sigma_{\text{tot}}}$ $\pm \text{stat.} \pm \text{syst.}$
25	220	$0.01252 \pm 0.00496^{+0.00403}_{-0.00417}$	90	180	$0.01581 \pm 0.00827^{+0.00364}_{-0.00571}$
35	220	$0.01366 \pm 0.00234^{+0.00381}_{-0.00458}$	90	220	$0.02010 \pm 0.00381^{+0.00348}_{-0.00283}$
45	180	$0.01725 \pm 0.00539^{+0.00369}_{-0.00507}$	190	180	$0.01465 \pm 0.00761^{+0.00310}_{-0.00689}$
45	220	$0.01694 \pm 0.00286^{+0.00239}_{-0.00317}$	190	220	$0.01525 \pm 0.00222^{+0.00378}_{-0.00376}$
55	220	$0.01569 \pm 0.00198^{+0.00277}_{-0.00723}$			
70	220	$0.01289 \pm 0.00327^{+0.00254}_{-0.00327}$			

Table 23: Ratio of the cross section for diffractive scattering, $\gamma^*p \rightarrow XN$, $M_N < 2.3$ GeV, integrated over $M_X = 25 - 35$ GeV, to the total cross section.

Q^2	$\sigma_{0.28 < M_X < 35 \text{ GeV}}^{\text{diff}} / \sigma^{\text{tot}} \pm \text{stat.} \pm \text{syst.}$
4	$0.158 \pm 0.007^{+0.009}_{-0.007}$
6	$0.149 \pm 0.007^{+0.005}_{-0.005}$
8	$0.134 \pm 0.006^{+0.005}_{-0.004}$
14	$0.118 \pm 0.005^{+0.003}_{-0.002}$
25	$0.106 \pm 0.006^{+0.012}_{-0.012}$
27	$0.096 \pm 0.006^{+0.003}_{-0.004}$
35	$0.090 \pm 0.005^{+0.011}_{-0.014}$
45	$0.095 \pm 0.004^{+0.007}_{-0.009}$
55	$0.084 \pm 0.003^{+0.008}_{-0.014}$
70	$0.071 \pm 0.004^{+0.007}_{-0.009}$
90	$0.075 \pm 0.005^{+0.008}_{-0.008}$
120	$0.044 \pm 0.003^{+0.005}_{-0.005}$
190	$0.050 \pm 0.004^{+0.008}_{-0.008}$

Table 24: *Ratio of the cross section for diffractive scattering, $\gamma^*p \rightarrow XN$, $M_N < 2.3$ GeV, integrated over $M_X = 0.28 - 35$ GeV, to the total cross section, for $W = 220$ GeV.*

β	x_P	Q^2	$x_P F_2^{D(3)}$ $\pm \text{stat.} \pm \text{syst.}$	β	x_P	Q^2	$x_P F_2^{D(3)}$ $\pm \text{stat.} \pm \text{syst.}$
(GeV ²)				(GeV ²)			
0.9455	0.01290	25	$0.0137 \pm 0.0022^{+0.0030}_{-0.0059}$	0.9605	0.01769	35	$0.0092 \pm 0.0033^{+0.0075}_{-0.0070}$
0.9455	0.00622	25	$0.0157 \pm 0.0022^{+0.0013}_{-0.0028}$	0.9605	0.00855	35	$0.0176 \pm 0.0046^{+0.0026}_{-0.0040}$
0.9455	0.00365	25	$0.0207 \pm 0.0024^{+0.0027}_{-0.0024}$	0.9605	0.00502	35	$0.0125 \pm 0.0033^{+0.0005}_{-0.0010}$
0.9455	0.00200	25	$0.0203 \pm 0.0025^{+0.0033}_{-0.0031}$	0.9605	0.00275	35	$0.0216 \pm 0.0046^{+0.0021}_{-0.0081}$
0.9455	0.00117	25	$0.0172 \pm 0.0028^{+0.0026}_{-0.0027}$	0.9605	0.00162	35	$0.0110 \pm 0.0038^{+0.0010}_{-0.0024}$
0.9455	0.00082	25	$0.0270 \pm 0.0037^{+0.0042}_{-0.0032}$	0.9605	0.00112	35	$0.0146 \pm 0.0044^{+0.0011}_{-0.0010}$
0.9455	0.00055	25	$0.0411 \pm 0.0056^{+0.0063}_{-0.0061}$	0.9605	0.00075	35	$0.0272 \pm 0.0056^{+0.0053}_{-0.0017}$
0.7353	0.01659	25	$0.0148 \pm 0.0028^{+0.0060}_{-0.0091}$	0.7955	0.02136	35	$0.0158 \pm 0.0035^{+0.0077}_{-0.0121}$
0.7353	0.00800	25	$0.0344 \pm 0.0028^{+0.0027}_{-0.0056}$	0.7955	0.01033	35	$0.0220 \pm 0.0036^{+0.0031}_{-0.0036}$
0.7353	0.00469	25	$0.0351 \pm 0.0024^{+0.0027}_{-0.0040}$	0.7955	0.00606	35	$0.0234 \pm 0.0032^{+0.0052}_{-0.0044}$
0.7353	0.00257	25	$0.0403 \pm 0.0028^{+0.0034}_{-0.0018}$	0.7955	0.00332	35	$0.0336 \pm 0.0039^{+0.0024}_{-0.0020}$
0.7353	0.00151	25	$0.0539 \pm 0.0040^{+0.0041}_{-0.0078}$	0.7955	0.00195	35	$0.0378 \pm 0.0049^{+0.0060}_{-0.0022}$
0.7353	0.00105	25	$0.0458 \pm 0.0036^{+0.0055}_{-0.0038}$	0.7955	0.00136	35	$0.0424 \pm 0.0051^{+0.0076}_{-0.0034}$
0.7353	0.00070	25	$0.0487 \pm 0.0037^{+0.0038}_{-0.0041}$	0.7955	0.00091	35	$0.0374 \pm 0.0048^{+0.0029}_{-0.0055}$
0.4098	0.01435	25	$0.0256 \pm 0.0049^{+0.0067}_{-0.0110}$	0.4930	0.01667	35	$0.0231 \pm 0.0065^{+0.0062}_{-0.0076}$
0.4098	0.00841	25	$0.0322 \pm 0.0020^{+0.0020}_{-0.0026}$	0.4930	0.00978	35	$0.0336 \pm 0.0037^{+0.0027}_{-0.0053}$
0.4098	0.00460	25	$0.0405 \pm 0.0021^{+0.0030}_{-0.0030}$	0.4930	0.00535	35	$0.0360 \pm 0.0029^{+0.0019}_{-0.0027}$
0.4098	0.00271	25	$0.0408 \pm 0.0027^{+0.0017}_{-0.0031}$	0.4930	0.00315	35	$0.0419 \pm 0.0038^{+0.0020}_{-0.0016}$
0.4098	0.00188	25	$0.0501 \pm 0.0029^{+0.0014}_{-0.0021}$	0.4930	0.00219	35	$0.0498 \pm 0.0042^{+0.0018}_{-0.0043}$
0.4098	0.00126	25	$0.0545 \pm 0.0031^{+0.0032}_{-0.0026}$	0.4930	0.00147	35	$0.0581 \pm 0.0047^{+0.0052}_{-0.0063}$
0.1712	0.02014	25	$0.0246 \pm 0.0065^{+0.0062}_{-0.0070}$	0.2244	0.01176	35	$0.0288 \pm 0.0025^{+0.0039}_{-0.0063}$
0.1712	0.01102	25	$0.0244 \pm 0.0018^{+0.0038}_{-0.0060}$	0.2244	0.00692	35	$0.0332 \pm 0.0029^{+0.0015}_{-0.0023}$
0.1712	0.00648	25	$0.0248 \pm 0.0022^{+0.0040}_{-0.0067}$	0.2244	0.00481	35	$0.0298 \pm 0.0033^{+0.0043}_{-0.0028}$
0.1712	0.00450	25	$0.0338 \pm 0.0022^{+0.0021}_{-0.0027}$	0.2244	0.00322	35	$0.0318 \pm 0.0030^{+0.0022}_{-0.0023}$
0.1712	0.00301	25	$0.0363 \pm 0.0023^{+0.0023}_{-0.0024}$	0.0805	0.01930	35	$0.0313 \pm 0.0080^{+0.0045}_{-0.0047}$
0.0588	0.01311	25	$0.0325 \pm 0.0028^{+0.0056}_{-0.0075}$	0.0805	0.01341	35	$0.0273 \pm 0.0085^{+0.0075}_{-0.0071}$
0.0588	0.00878	25	$0.0343 \pm 0.0038^{+0.0050}_{-0.0048}$	0.0805	0.00898	35	$0.0334 \pm 0.0037^{+0.0045}_{-0.0061}$
0.0270	0.01910	25	$0.0283 \pm 0.0112^{+0.0091}_{-0.0094}$	0.0374	0.01930	35	$0.0319 \pm 0.0054^{+0.0089}_{-0.0107}$

Table 25: The diffractive structure function multiplied by x_P , $x_P F_2^{D(3)}(\beta, x_P, Q^2)$, for diffractive scattering, $\gamma^* p \rightarrow XN$, $M_N < 2.3$ GeV, for $Q^2 = 25$ and 35 GeV², in bins of β and x_P .

β	x_P	Q^2	$x_P F_2^{D(3)}$ $\pm \text{stat.} \pm \text{syst.}$	β	x_P	Q^2	$x_P F_2^{D(3)}$ $\pm \text{stat.} \pm \text{syst.}$
(GeV ²)				(GeV ²)			
0.9690	0.02243	45	$0.0060 \pm 0.0022^{+0.0029}_{-0.0050}$	0.9745	0.02713	55	$0.0071 \pm 0.0028^{+0.0011}_{-0.0022}$
0.9690	0.01088	45	$0.0065 \pm 0.0020^{+0.0022}_{-0.0025}$	0.9745	0.01319	55	$0.0091 \pm 0.0029^{+0.0012}_{-0.0037}$
0.9690	0.00639	45	$0.0108 \pm 0.0020^{+0.0021}_{-0.0017}$	0.9745	0.00775	55	$0.0086 \pm 0.0027^{+0.0010}_{-0.0018}$
0.9690	0.00350	45	$0.0172 \pm 0.0030^{+0.0035}_{-0.0007}$	0.9745	0.00425	55	$0.0167 \pm 0.0038^{+0.0014}_{-0.0013}$
0.9690	0.00206	45	$0.0221 \pm 0.0041^{+0.0028}_{-0.0028}$	0.9745	0.00250	55	$0.0247 \pm 0.0069^{+0.0009}_{-0.0014}$
0.9690	0.00143	45	$0.0159 \pm 0.0037^{+0.0038}_{-0.0027}$	0.9745	0.00174	55	$0.0239 \pm 0.0062^{+0.0046}_{-0.0033}$
0.9690	0.00096	45	$0.0237 \pm 0.0044^{+0.0052}_{-0.0025}$	0.9745	0.00117	55	$0.0173 \pm 0.0046^{+0.0033}_{-0.0033}$
0.8333	0.01265	45	$0.0197 \pm 0.0025^{+0.0027}_{-0.0055}$	0.8594	0.03077	55	$0.0103 \pm 0.0042^{+0.0028}_{-0.0054}$
0.8333	0.00743	45	$0.0258 \pm 0.0026^{+0.0023}_{-0.0043}$	0.8594	0.01495	55	$0.0130 \pm 0.0031^{+0.0034}_{-0.0070}$
0.8333	0.00407	45	$0.0320 \pm 0.0027^{+0.0022}_{-0.0047}$	0.8594	0.00879	55	$0.0184 \pm 0.0026^{+0.0018}_{-0.0030}$
0.8333	0.00240	45	$0.0322 \pm 0.0033^{+0.0046}_{-0.0042}$	0.8594	0.00482	55	$0.0261 \pm 0.0030^{+0.0030}_{-0.0033}$
0.8333	0.00166	45	$0.0329 \pm 0.0030^{+0.0026}_{-0.0058}$	0.8594	0.00284	55	$0.0275 \pm 0.0036^{+0.0029}_{-0.0060}$
0.8333	0.00111	45	$0.0329 \pm 0.0032^{+0.0054}_{-0.0035}$	0.8594	0.00197	55	$0.0308 \pm 0.0041^{+0.0032}_{-0.0049}$
0.5556	0.01897	45	$0.0197 \pm 0.0040^{+0.0059}_{-0.0093}$	0.6044	0.01250	55	$0.0305 \pm 0.0024^{+0.0028}_{-0.0043}$
0.5556	0.01114	45	$0.0279 \pm 0.0021^{+0.0024}_{-0.0047}$	0.6044	0.00685	55	$0.0320 \pm 0.0023^{+0.0022}_{-0.0021}$
0.5556	0.00610	45	$0.0314 \pm 0.0018^{+0.0019}_{-0.0023}$	0.6044	0.00404	55	$0.0428 \pm 0.0033^{+0.0035}_{-0.0017}$
0.5556	0.00359	45	$0.0423 \pm 0.0026^{+0.0018}_{-0.0022}$	0.6044	0.00280	55	$0.0375 \pm 0.0032^{+0.0037}_{-0.0018}$
0.5556	0.00250	45	$0.0406 \pm 0.0025^{+0.0031}_{-0.0013}$	0.6044	0.00188	55	$0.0562 \pm 0.0043^{+0.0038}_{-0.0027}$
0.5556	0.00167	45	$0.0549 \pm 0.0031^{+0.0020}_{-0.0043}$	0.3125	0.01325	55	$0.0257 \pm 0.0032^{+0.0039}_{-0.0050}$
0.2711	0.01251	45	$0.0232 \pm 0.0015^{+0.0034}_{-0.0053}$	0.3125	0.00780	55	$0.0367 \pm 0.0026^{+0.0018}_{-0.0028}$
0.2711	0.00736	45	$0.0321 \pm 0.0019^{+0.0023}_{-0.0036}$	0.3125	0.00542	55	$0.0363 \pm 0.0026^{+0.0026}_{-0.0038}$
0.2711	0.00512	45	$0.0354 \pm 0.0020^{+0.0022}_{-0.0021}$	0.3125	0.00363	55	$0.0424 \pm 0.0028^{+0.0018}_{-0.0038}$
0.2711	0.00343	45	$0.0410 \pm 0.0022^{+0.0023}_{-0.0018}$	0.1209	0.02017	55	$0.0288 \pm 0.0067^{+0.0057}_{-0.0061}$
0.1011	0.01974	45	$0.0234 \pm 0.0023^{+0.0066}_{-0.0085}$	0.1209	0.01402	55	$0.0251 \pm 0.0027^{+0.0057}_{-0.0079}$
0.1011	0.01372	45	$0.0323 \pm 0.0031^{+0.0035}_{-0.0045}$	0.1209	0.00939	55	$0.0286 \pm 0.0024^{+0.0040}_{-0.0044}$
0.1011	0.00919	45	$0.0404 \pm 0.0025^{+0.0024}_{-0.0031}$				
0.0476	0.02913	45	$0.0347 \pm 0.0108^{+0.0074}_{-0.0102}$	0.0576	0.01971	55	$0.0360 \pm 0.0045^{+0.0064}_{-0.0166}$
0.0476	0.01951	45	$0.0396 \pm 0.0067^{+0.0056}_{-0.0074}$				

Table 26: The diffractive structure function multiplied by x_P , $x_P F_2^{D(3)}(\beta, x_P, Q^2)$, for diffractive scattering, $\gamma^* p \rightarrow XN$, $M_N < 2.3$ GeV, for $Q^2 = 45$ and 55 GeV², in bins of β and x_P .

β	x_P	Q^2	$x_P F_2^{D(3)}$ $\pm \text{stat.} \pm \text{syst.}$	β	x_P	Q^2	$x_P F_2^{D(3)}$ $\pm \text{stat.} \pm \text{syst.}$
(GeV ²)				(GeV ²)			
0.9798	0.01663	70	$0.0100 \pm 0.0034^{+0.0018}_{-0.0048}$	0.9843	0.04323	90	$0.0070 \pm 0.0031^{+0.0010}_{-0.0026}$
0.9798	0.00979	70	$0.0100 \pm 0.0030^{+0.0004}_{-0.0016}$	0.9843	0.02119	90	$0.0042 \pm 0.0034^{+0.0020}_{-0.0034}$
0.9798	0.00537	70	$0.0138 \pm 0.0035^{+0.0022}_{-0.0006}$	0.9843	0.01250	90	$0.0032 \pm 0.0018^{+0.0018}_{-0.0012}$
0.9798	0.00316	70	$0.0094 \pm 0.0033^{+0.0015}_{-0.0014}$	0.9843	0.00687	90	$0.0196 \pm 0.0061^{+0.0013}_{-0.0039}$
0.9798	0.00220	70	$0.0071 \pm 0.0038^{+0.0026}_{-0.0011}$	0.9843	0.00405	90	$0.0249 \pm 0.0103^{+0.0065}_{-0.0055}$
0.9798	0.00147	70	$0.0134 \pm 0.0040^{+0.0040}_{-0.0016}$	0.9843	0.00281	90	$0.0296 \pm 0.0122^{+0.0085}_{-0.0103}$
0.9843	0.00189	90	$0.0070 \pm 0.0039^{+0.0032}_{-0.0010}$	0.9843	0.00189	90	$0.0070 \pm 0.0039^{+0.0032}_{-0.0010}$
0.8861	0.01839	70	$0.0112 \pm 0.0023^{+0.0031}_{-0.0058}$	0.9091	0.02294	90	$0.0126 \pm 0.0038^{+0.0029}_{-0.0073}$
0.8861	0.01083	70	$0.0144 \pm 0.0020^{+0.0025}_{-0.0033}$	0.9091	0.01353	90	$0.0164 \pm 0.0036^{+0.0012}_{-0.0027}$
0.8861	0.00594	70	$0.0222 \pm 0.0026^{+0.0022}_{-0.0031}$	0.9091	0.00744	90	$0.0167 \pm 0.0031^{+0.0010}_{-0.0017}$
0.8861	0.00350	70	$0.0249 \pm 0.0034^{+0.0019}_{-0.0033}$	0.9091	0.00438	90	$0.0156 \pm 0.0042^{+0.0048}_{-0.0010}$
0.8861	0.00243	70	$0.0300 \pm 0.0039^{+0.0036}_{-0.0045}$	0.9091	0.00305	90	$0.0193 \pm 0.0043^{+0.0014}_{-0.0028}$
0.8861	0.00163	70	$0.0313 \pm 0.0042^{+0.0052}_{-0.0044}$	0.9091	0.00204	90	$0.0231 \pm 0.0053^{+0.0029}_{-0.0025}$
0.6604	0.01453	70	$0.0223 \pm 0.0019^{+0.0029}_{-0.0037}$	0.7143	0.01722	90	$0.0247 \pm 0.0034^{+0.0035}_{-0.0045}$
0.6604	0.00797	70	$0.0318 \pm 0.0022^{+0.0034}_{-0.0033}$	0.7143	0.00946	90	$0.0266 \pm 0.0030^{+0.0046}_{-0.0039}$
0.6604	0.00470	70	$0.0360 \pm 0.0028^{+0.0049}_{-0.0038}$	0.7143	0.00558	90	$0.0341 \pm 0.0039^{+0.0019}_{-0.0024}$
0.6604	0.00326	70	$0.0368 \pm 0.0029^{+0.0047}_{-0.0018}$	0.7143	0.00388	90	$0.0353 \pm 0.0042^{+0.0048}_{-0.0036}$
0.6604	0.00219	70	$0.0420 \pm 0.0034^{+0.0018}_{-0.0043}$	0.7143	0.00260	90	$0.0376 \pm 0.0044^{+0.0037}_{-0.0053}$
0.3665	0.01437	70	$0.0228 \pm 0.0019^{+0.0037}_{-0.0054}$	0.4265	0.01585	90	$0.0270 \pm 0.0044^{+0.0044}_{-0.0057}$
0.3665	0.00846	70	$0.0330 \pm 0.0025^{+0.0022}_{-0.0032}$	0.4265	0.00934	90	$0.0314 \pm 0.0027^{+0.0029}_{-0.0027}$
0.3665	0.00588	70	$0.0355 \pm 0.0022^{+0.0017}_{-0.0028}$	0.4265	0.00649	90	$0.0360 \pm 0.0033^{+0.0022}_{-0.0018}$
0.3665	0.00394	70	$0.0355 \pm 0.0023^{+0.0029}_{-0.0016}$	0.4265	0.00435	90	$0.0426 \pm 0.0036^{+0.0027}_{-0.0026}$
0.1489	0.01447	70	$0.0282 \pm 0.0022^{+0.0036}_{-0.0043}$	0.1837	0.02169	90	$0.0276 \pm 0.0033^{+0.0064}_{-0.0075}$
0.1489	0.00970	70	$0.0339 \pm 0.0029^{+0.0023}_{-0.0056}$	0.1837	0.01508	90	$0.0297 \pm 0.0044^{+0.0044}_{-0.0043}$
0.1837	0.01011	90	$0.0326 \pm 0.0034^{+0.0034}_{-0.0033}$	0.1837	0.01011	90	$0.0326 \pm 0.0034^{+0.0034}_{-0.0033}$
0.0722	0.02001	70	$0.0296 \pm 0.0075^{+0.0058}_{-0.0075}$	0.0909	0.03047	90	$0.0322 \pm 0.0168^{+0.0074}_{-0.0116}$
0.0909	0.02042	90	$0.0452 \pm 0.0085^{+0.0078}_{-0.0064}$	0.0909	0.02042	90	$0.0452 \pm 0.0085^{+0.0078}_{-0.0064}$

Table 27: The diffractive structure function multiplied by x_P , $x_P F_2^{D(3)}(\beta, x_P, Q^2)$, for diffractive scattering, $\gamma^* p \rightarrow XN$, $M_N < 2.3$ GeV, for $Q^2 = 70$ and 90 GeV², in bins of β and x_P .

β	x_P	Q^2	$x_P F_2^{D(3)}$ $\pm \text{stat.} \pm \text{syst.}$	β	x_P	Q^2	$x_P F_2^{D(3)}$ $\pm \text{stat.} \pm \text{syst.}$
(GeV ²)				(GeV ²)			
0.9881	0.01653	120	$0.0051 \pm 0.0022^{+0.0009}_{-0.0013}$	0.9925	0.08643	190	$0.0064 \pm 0.0040^{+0.0002}_{-0.0006}$
0.9881	0.00910	120	$0.0126 \pm 0.0054^{+0.0018}_{-0.0048}$	0.9925	0.04336	190	$0.0035 \pm 0.0088^{+0.0038}_{-0.0012}$
0.9881	0.00537	120	$0.0197 \pm 0.0077^{+0.0074}_{-0.0033}$	0.9925	0.02582	190	$0.0042 \pm 0.0078^{+0.0104}_{-0.2232}$
0.9881	0.00373	120	$0.0146 \pm 0.0061^{+0.0016}_{-0.0054}$	0.9925	0.00587	190	$0.0815 \pm 0.0698^{+0.0345}_{-0.0420}$
0.9881	0.00250	120	$0.0351 \pm 0.0122^{+0.0016}_{-0.0007}$	0.9925	0.00394	190	$0.0278 \pm 0.0184^{+0.0095}_{-0.0006}$
0.9302	0.02969	120	$0.0027 \pm 0.0017^{+0.0013}_{-0.0025}$	0.9548	0.08984	190	$0.0042 \pm 0.0021^{+0.0010}_{-0.0010}$
0.9302	0.01756	120	$0.0048 \pm 0.0023^{+0.0026}_{-0.0035}$	0.9548	0.04507	190	$0.0060 \pm 0.0037^{+0.0015}_{-0.0028}$
0.9302	0.00967	120	$0.0164 \pm 0.0034^{+0.0011}_{-0.0019}$	0.9548	0.02684	190	$0.0018 \pm 0.0013^{+0.0007}_{-0.0017}$
0.9302	0.00570	120	$0.0091 \pm 0.0026^{+0.0011}_{-0.0009}$	0.9548	0.01483	190	$0.0084 \pm 0.0034^{+0.0024}_{-0.0009}$
0.9302	0.00397	120	$0.0138 \pm 0.0037^{+0.0025}_{-0.0012}$	0.9548	0.00877	190	$0.0106 \pm 0.0039^{+0.0027}_{-0.0026}$
0.9302	0.00266	120	$0.0194 \pm 0.0044^{+0.0033}_{-0.0049}$	0.9548	0.00611	190	$0.0026 \pm 0.0018^{+0.0003}_{-0.0007}$
0.7692	0.02124	120	$0.0132 \pm 0.0024^{+0.0054}_{-0.0075}$	0.9548	0.00410	190	$0.0195 \pm 0.0063^{+0.0014}_{-0.0117}$
0.7692	0.01169	120	$0.0285 \pm 0.0028^{+0.0050}_{-0.0038}$	0.8407	0.01685	190	$0.0146 \pm 0.0028^{+0.0025}_{-0.0027}$
0.7692	0.00690	120	$0.0253 \pm 0.0033^{+0.0040}_{-0.0034}$	0.8407	0.00996	190	$0.0195 \pm 0.0039^{+0.0030}_{-0.0023}$
0.7692	0.00480	120	$0.0329 \pm 0.0036^{+0.0030}_{-0.0021}$	0.8407	0.00693	190	$0.0200 \pm 0.0036^{+0.0043}_{-0.0038}$
0.7692	0.00322	120	$0.0312 \pm 0.0040^{+0.0060}_{-0.0019}$	0.8407	0.00465	190	$0.0134 \pm 0.0028^{+0.0038}_{-0.0025}$
0.4979	0.01806	120	$0.0265 \pm 0.0021^{+0.0035}_{-0.0066}$	0.6109	0.02318	190	$0.0193 \pm 0.0045^{+0.0049}_{-0.0065}$
0.4979	0.01065	120	$0.0300 \pm 0.0036^{+0.0038}_{-0.0050}$	0.6109	0.01371	190	$0.0277 \pm 0.0033^{+0.0026}_{-0.0035}$
0.4979	0.00741	120	$0.0325 \pm 0.0028^{+0.0020}_{-0.0032}$	0.6109	0.00954	190	$0.0241 \pm 0.0031^{+0.0025}_{-0.0021}$
0.4979	0.00497	120	$0.0383 \pm 0.0034^{+0.0020}_{-0.0028}$	0.6109	0.00640	190	$0.0322 \pm 0.0040^{+0.0031}_{-0.0035}$
0.2308	0.01599	120	$0.0291 \pm 0.0045^{+0.0040}_{-0.0046}$	0.3220	0.02600	190	$0.0228 \pm 0.0034^{+0.0101}_{-0.0073}$
0.2308	0.01072	120	$0.0278 \pm 0.0028^{+0.0032}_{-0.0053}$	0.3220	0.01810	190	$0.0279 \pm 0.0046^{+0.0027}_{-0.0057}$
				0.3220	0.01214	190	$0.0280 \pm 0.0034^{+0.0026}_{-0.0030}$
				0.1743	0.03345	190	$0.0280 \pm 0.0145^{+0.0059}_{-0.0132}$
				0.1743	0.02243	190	$0.0312 \pm 0.0045^{+0.0077}_{-0.0077}$

Table 28: The diffractive structure function multiplied by x_P , $x_P F_2^{D(3)}(\beta, x_P, Q^2)$, for diffractive scattering, $\gamma^* p \rightarrow XN$, $M_N < 2.3$ GeV, for $Q^2 = 120$ and 190 GeV², in bins of β and x_P .

β	x_P	Q^2	$x_P F_2^{D(3)}$
			$\pm \text{stat.} \pm \text{syst.}$
		(GeV ²)	
0.9726	0.07239	320	$0.0006 \pm 0.0010^{+0.0005}_{-0.0006}$
0.9726	0.04361	320	$0.0011 \pm 0.0013^{+0.0002}_{-0.0014}$
0.9726	0.02429	320	$0.0104 \pm 0.0074^{+0.0005}_{-0.0070}$
0.9726	0.01442	320	$0.0057 \pm 0.0126^{+0.0023}_{-0.0025}$
0.9726	0.01006	320	$0.0182 \pm 0.0117^{+0.0041}_{-0.0008}$
0.9726	0.00675	320	$0.0130 \pm 0.0090^{+0.0003}_{-0.0008}$
0.8989	0.02628	320	$0.0141 \pm 0.0051^{+0.0028}_{-0.0038}$
0.8989	0.01560	320	$0.0084 \pm 0.0044^{+0.0009}_{-0.0022}$
0.8989	0.01088	320	$0.0134 \pm 0.0056^{+0.0021}_{-0.0018}$
0.8989	0.00731	320	$0.0074 \pm 0.0057^{+0.0050}_{-0.0024}$
0.7256	0.03256	320	$0.0116 \pm 0.0026^{+0.0027}_{-0.0059}$
0.7256	0.01933	320	$0.0190 \pm 0.0042^{+0.0026}_{-0.0030}$
0.7256	0.01348	320	$0.0252 \pm 0.0051^{+0.0024}_{-0.0060}$
0.7256	0.00905	320	$0.0278 \pm 0.0069^{+0.0022}_{-0.0068}$
0.4444	0.03155	320	$0.0192 \pm 0.0041^{+0.0057}_{-0.0059}$
0.4444	0.02200	320	$0.0116 \pm 0.0042^{+0.0043}_{-0.0062}$
0.4444	0.01478	320	$0.0251 \pm 0.0055^{+0.0042}_{-0.0059}$

Table 29: The diffractive structure function multiplied by x_P , $x_P F_2^{D(3)}(\beta, x_P, Q^2)$, for diffractive scattering, $\gamma^* p \rightarrow XN$, $M_N < 2.3$ GeV, for $Q^2 = 320$ GeV², in bins of β and x_P .

x_P	β	Q^2 (GeV ²)	$x_P F_2^{D(3)}$
0.00015	0.700	2.7	$0.0378^{+0.0066}_{-0.0058}$
0.00015	0.700	4	$0.0480^{+0.0093}_{-0.0072}$
0.00015	0.900	6	$0.0343^{+0.0082}_{-0.0083}$
0.00015	0.900	8	$0.0358^{+0.0086}_{-0.0064}$
0.0003	0.400	2.7	$0.0477^{+0.0076}_{-0.0074}$
0.0003	0.400	4	$0.0476^{+0.0059}_{-0.0059}$
0.0003	0.400	6	$0.0523^{+0.0063}_{-0.0068}$
0.0003	0.400	8	$0.0539^{+0.0064}_{-0.0060}$
0.0003	0.700	2.7	$0.0382^{+0.0057}_{-0.0054}$
0.0003	0.700	4	$0.0394^{+0.0066}_{-0.0056}$
0.0003	0.900	6	$0.0331^{+0.0054}_{-0.0047}$
0.0003	0.900	8	$0.0431^{+0.0056}_{-0.0076}$
0.0003	0.900	14	$0.0439^{+0.0076}_{-0.0074}$
0.0006	0.400	2.7	$0.0438^{+0.0063}_{-0.0067}$
0.0006	0.400	4	$0.0460^{+0.0051}_{-0.0046}$
0.0006	0.400	6	$0.0535^{+0.0053}_{-0.0057}$
0.0006	0.400	8	$0.0473^{+0.0052}_{-0.0045}$
0.0006	0.700	2.7	$0.0376^{+0.0060}_{-0.0059}$
0.0006	0.700	4	$0.0437^{+0.0063}_{-0.0060}$
0.0006	0.700	14	$0.0468^{+0.0058}_{-0.0052}$
0.0006	0.700	27	$0.0575^{+0.0102}_{-0.0105}$
0.0006	0.900	6	$0.0300^{+0.0045}_{-0.0054}$
0.0006	0.900	8	$0.0370^{+0.0050}_{-0.0049}$
0.0006	0.900	14	$0.0305^{+0.0043}_{-0.0046}$
0.0006	0.900	27	$0.0340^{+0.0122}_{-0.0104}$

Table 30: The diffractive structure function multiplied by x_P , $x_P F_2^{D(3)}(\beta, x_P, Q^2)$, for diffractive scattering, $\gamma^* p \rightarrow XN$, $M_N < 2.3$ GeV, for fixed $x_P = 0.00015, 0.0003, 0.0006$ and fixed β . The errors are the statistical and systematic uncertainties added in quadrature.

x_P	β	Q^2 (GeV ²)	$x_P F_2^{D(3)}$
0.0012	0.125	2.7	$0.0247^{+0.0037}_{-0.0040}$
0.0012	0.125	4	$0.0292^{+0.0029}_{-0.0032}$
0.0012	0.125	6	$0.0323^{+0.0034}_{-0.0033}$
0.0012	0.125	8	$0.0325^{+0.0029}_{-0.0030}$
0.0012	0.400	2.7	$0.0306^{+0.0052}_{-0.0048}$
0.0012	0.400	4	$0.0335^{+0.0037}_{-0.0040}$
0.0012	0.400	6	$0.0366^{+0.0041}_{-0.0040}$
0.0012	0.400	8	$0.0409^{+0.0036}_{-0.0038}$
0.0012	0.400	14	$0.0434^{+0.0035}_{-0.0032}$
0.0012	0.400	25	$0.0554^{+0.0046}_{-0.0046}$
0.0012	0.400	27	$0.0510^{+0.0050}_{-0.0059}$
0.0012	0.400	35	$0.0600^{+0.0087}_{-0.0095}$
0.0012	0.400	45	$0.0601^{+0.0053}_{-0.0067}$
0.0012	0.700	2.7	$0.0352^{+0.0074}_{-0.0066}$
0.0012	0.700	4	$0.0358^{+0.0058}_{-0.0063}$
0.0012	0.700	14	$0.0401^{+0.0035}_{-0.0035}$
0.0012	0.700	25	$0.0540^{+0.0071}_{-0.0091}$
0.0012	0.700	27	$0.0456^{+0.0085}_{-0.0078}$
0.0012	0.700	35	$0.0524^{+0.0120}_{-0.0088}$
0.0012	0.700	35	$0.0416^{+0.0082}_{-0.0097}$
0.0012	0.700	55	$0.0401^{+0.0079}_{-0.0082}$
0.0012	0.700	55	$0.0575^{+0.0073}_{-0.0068}$
0.0012	0.900	6	$0.0292^{+0.0060}_{-0.0046}$
0.0012	0.900	8	$0.0332^{+0.0062}_{-0.0053}$
0.0012	0.900	14	$0.0316^{+0.0046}_{-0.0042}$
0.0012	0.900	25	$0.0246^{+0.0055}_{-0.0055}$
0.0012	0.900	25	$0.0286^{+0.0071}_{-0.0065}$
0.0012	0.900	27	$0.0352^{+0.0090}_{-0.0122}$
0.0012	0.900	45	$0.0272^{+0.0045}_{-0.0050}$
0.0012	0.900	55	$0.0302^{+0.0092}_{-0.0100}$
0.0012	0.900	55	$0.0270^{+0.0057}_{-0.0063}$
0.0012	0.900	70	$0.0324^{+0.0082}_{-0.0076}$

Table 31: The diffractive structure function multiplied by x_P , $x_P F_2^{D(3)}(\beta, x_P, Q^2)$, for diffractive scattering, $\gamma^* p \rightarrow XN$, $M_N < 2.3$ GeV, for fixed $x_P = 0.0012$ and fixed β . The errors are the statistical and systematic uncertainties added in quadrature.

$x_{\mathcal{P}}$	β	Q^2 (GeV ²)	$x_{\mathcal{P}} F_2^{D(3)}$
0.0012	0.970	35	$0.0127^{+0.0052}_{-0.0054}$
0.0012	0.970	45	$0.0200^{+0.0067}_{-0.0057}$
0.0012	0.970	55	$0.0168^{+0.0128}_{-0.0162}$
0.0012	0.970	55	$0.0228^{+0.0082}_{-0.0079}$
0.0012	0.970	70	$0.0155^{+0.0080}_{-0.0068}$
0.0012	0.970	120	$0.0093^{+0.0085}_{-0.0075}$
0.0025	0.025	2.7	$0.0205^{+0.0041}_{-0.0032}$
0.0025	0.025	4	$0.0221^{+0.0025}_{-0.0028}$
0.0025	0.025	6	$0.0324^{+0.0038}_{-0.0039}$
0.0025	0.125	2.7	$0.0234^{+0.0044}_{-0.0040}$
0.0025	0.125	8.	$0.0277^{+0.0035}_{-0.0028}$
0.0025	0.125	14	$0.0331^{+0.0032}_{-0.0031}$
0.0025	0.400	2.7	$0.0280^{+0.0051}_{-0.0053}$
0.0025	0.400	6	$0.0385^{+0.0053}_{-0.0053}$
0.0025	0.400	8	$0.0400^{+0.0060}_{-0.0043}$
0.0025	0.400	14	$0.0364^{+0.0033}_{-0.0030}$
0.0025	0.400	25	$0.0414^{+0.0043}_{-0.0050}$
0.0025	0.400	27	$0.0369^{+0.0046}_{-0.0046}$
0.0025	0.400	35	$0.0469^{+0.0058}_{-0.0069}$
0.0025	0.400	45	$0.0402^{+0.0047}_{-0.0038}$
0.0025	0.700	2.7	$0.0301^{+0.0060}_{-0.0052}$
0.0025	0.700	4	$0.0327^{+0.0043}_{-0.0053}$
0.0025	0.700	25	$0.0429^{+0.0055}_{-0.0046}$
0.0025	0.700	27	$0.0373^{+0.0062}_{-0.0061}$
0.0025	0.700	55	$0.0427^{+0.0071}_{-0.0086}$
0.0025	0.700	55	$0.0347^{+0.0054}_{-0.0045}$
0.0025	0.700	70	$0.0380^{+0.0047}_{-0.0058}$
0.0025	0.700	90	$0.0390^{+0.0075}_{-0.0085}$

Table 32: The diffractive structure function multiplied by $x_{\mathcal{P}}$, $x_{\mathcal{P}} F_2^{D(3)}(\beta, x_{\mathcal{P}}, Q^2)$, for diffractive scattering, $\gamma^* p \rightarrow XN$, $M_N < 2.3$ GeV, for fixed $x_{\mathcal{P}} = 0.0012, 0.0025$ and fixed β . The errors are the statistical and systematic uncertainties added in quadrature.

x_P	β	Q^2 (GeV ²)	$x_P F_2^{D(3)}$
0.0025	0.900	8	$0.0319^{+0.0055}_{-0.0052}$
0.0025	0.900	14	$0.0320^{+0.0054}_{-0.0063}$
0.0025	0.900	27	$0.0148^{+0.0058}_{-0.0057}$
0.0025	0.900	45	$0.0251^{+0.0051}_{-0.0049}$
0.0025	0.900	55	$0.0190^{+0.0105}_{-0.0084}$
0.0025	0.900	55	$0.0244^{+0.0052}_{-0.0069}$
0.0025	0.900	70	$0.0279^{+0.0062}_{-0.0067}$
0.0025	0.900	90	$0.0226^{+0.0078}_{-0.0077}$
0.0025	0.900	120	$0.0240^{+0.0087}_{-0.0097}$
0.0025	0.970	35	$0.0212^{+0.0067}_{-0.0102}$
0.0025	0.970	45	$0.0207^{+0.0060}_{-0.0060}$
0.0025	0.970	55	$0.0255^{+0.0101}_{-0.0102}$
0.0025	0.970	70	$0.0074^{+0.0062}_{-0.0057}$
0.0025	0.970	90	$0.0353^{+0.0230}_{-0.0240}$
0.0025	0.970	120	$0.0431^{+0.0213}_{-0.0213}$
0.0050	0.025	2.7	$0.0183^{+0.0030}_{-0.0032}$
0.0050	0.025	4	$0.0205^{+0.0024}_{-0.0026}$
0.0050	0.025	6	$0.0239^{+0.0030}_{-0.0030}$
0.0050	0.125	2.7	$0.0218^{+0.0036}_{-0.0035}$
0.0050	0.125	4	$0.0214^{+0.0030}_{-0.0028}$
0.0050	0.125	6	$0.0229^{+0.0025}_{-0.0028}$
0.0050	0.125	8	$0.0257^{+0.0028}_{-0.0025}$
0.0050	0.125	14	$0.0260^{+0.0024}_{-0.0025}$
0.0050	0.125	25	$0.0327^{+0.0036}_{-0.0037}$
0.0050	0.125	27	$0.0290^{+0.0036}_{-0.0037}$

Table 33: The diffractive structure function multiplied by x_P , $x_P F_2^{D(3)}(\beta, x_P, Q^2)$, for diffractive scattering, $\gamma^* p \rightarrow XN$, $M_N < 2.3$ GeV, for fixed $x_P = 0.0025, 0.0050$ and fixed β . The errors are the statistical and systematic uncertainties added in quadrature.

x_P	β	Q^2 (GeV ²)	$x_P F_2^{D(3)}$
0.005	0.400	2.7	$0.0296^{+0.0053}_{-0.0052}$
0.005	0.400	4	$0.0287^{+0.0035}_{-0.0032}$
0.005	0.400	6	$0.0313^{+0.0048}_{-0.0038}$
0.005	0.400	8	$0.0339^{+0.0038}_{-0.0052}$
0.005	0.400	14	$0.0329^{+0.0034}_{-0.0037}$
0.005	0.400	25	$0.0395^{+0.0041}_{-0.0041}$
0.005	0.400	27	$0.0336^{+0.0041}_{-0.0054}$
0.005	0.400	35	$0.0359^{+0.0042}_{-0.0043}$
0.005	0.400	45	$0.0354^{+0.0032}_{-0.0035}$
0.005	0.400	55	$0.0401^{+0.0041}_{-0.0051}$
0.005	0.400	70	$0.0359^{+0.0036}_{-0.0036}$
0.005	0.400	90	$0.0396^{+0.0049}_{-0.0048}$
0.005	0.400	120	$0.0375^{+0.0050}_{-0.0053}$
0.005	0.700	14	$0.0311^{+0.0048}_{-0.0036}$
0.005	0.700	25	$0.0365^{+0.0045}_{-0.0055}$
0.005	0.700	27	$0.0306^{+0.0067}_{-0.0073}$
0.005	0.700	35	$0.0334^{+0.0070}_{-0.0066}$
0.005	0.700	55	$0.0267^{+0.0056}_{-0.0053}$
0.005	0.700	55	$0.0335^{+0.0040}_{-0.0036}$
0.005	0.700	70	$0.0318^{+0.0052}_{-0.0040}$
0.005	0.700	90	$0.0348^{+0.0060}_{-0.0058}$
0.005	0.700	120	$0.0355^{+0.0068}_{-0.0062}$
0.005	0.700	190	$0.0316^{+0.0063}_{-0.0065}$
0.005	0.900	6	$0.0253^{+0.0041}_{-0.0044}$
0.005	0.900	8	$0.0289^{+0.0044}_{-0.0046}$
0.005	0.900	14	$0.0236^{+0.0040}_{-0.0043}$
0.005	0.900	25	$0.0212^{+0.0040}_{-0.0045}$
0.005	0.900	27	$0.0231^{+0.0060}_{-0.0058}$
0.005	0.900	45	$0.0239^{+0.0033}_{-0.0045}$
0.005	0.900	55	$0.0186^{+0.0071}_{-0.0059}$
0.005	0.900	55	$0.0220^{+0.0044}_{-0.0046}$
0.005	0.900	70	$0.0215^{+0.0038}_{-0.0044}$
0.005	0.900	90	$0.0166^{+0.0059}_{-0.0053}$
0.005	0.900	120	$0.0136^{+0.0052}_{-0.0049}$
0.005	0.900	190	$0.0139^{+0.0044}_{-0.0039}$

Table 34: The diffractive structure function multiplied by x_P , $x_P F_2^{D(3)}(\beta, x_P, Q^2)$, for diffractive scattering, $\gamma^* p \rightarrow XN$, $M_N < 2.3$ GeV, for fixed $x_P = 0.005$ and fixed β . The errors are the statistical and systematic uncertainties added in quadrature.

x_P	β	Q^2 (GeV ²)	$x_P F_2^{D(3)}$
0.005	0.970	35	$0.0119^{+0.0045}_{-0.0045}$
0.005	0.970	45	$0.0136^{+0.0040}_{-0.0033}$
0.005	0.970	55	$0.0136^{+0.0068}_{-0.0072}$
0.005	0.970	55	$0.0164^{+0.0055}_{-0.0055}$
0.005	0.970	70	$0.0131^{+0.0047}_{-0.0044}$
0.005	0.970	90	$0.0255^{+0.0123}_{-0.0127}$
0.005	0.970	120	$0.0208^{+0.0115}_{-0.0112}$
0.005	0.970	190	$0.0130^{+0.0055}_{-0.0074}$
0.010	0.005	2.7	$0.0230^{+0.0047}_{-0.0043}$
0.010	0.005	4	$0.0232^{+0.0040}_{-0.0038}$
0.010	0.025	2.7	$0.0189^{+0.0037}_{-0.0036}$
0.010	0.025	4	$0.0189^{+0.0034}_{-0.0032}$
0.010	0.025	6	$0.0235^{+0.0034}_{-0.0043}$
0.010	0.025	8	$0.0286^{+0.0043}_{-0.0053}$
0.010	0.025	14	$0.0306^{+0.0046}_{-0.0047}$
0.010	0.125	2.7	$0.0180^{+0.0031}_{-0.0031}$
0.010	0.125	4	$0.0186^{+0.0030}_{-0.0027}$
0.010	0.125	6	$0.0230^{+0.0035}_{-0.0036}$
0.010	0.125	8	$0.0220^{+0.0030}_{-0.0029}$
0.010	0.125	14	$0.0241^{+0.0031}_{-0.0035}$
0.010	0.125	25	$0.0256^{+0.0047}_{-0.0068}$
0.010	0.125	27	$0.0218^{+0.0055}_{-0.0046}$
0.010	0.125	35	$0.0293^{+0.0087}_{-0.0092}$
0.010	0.125	45	$0.0365^{+0.0045}_{-0.0051}$
0.010	0.125	55	$0.0245^{+0.0080}_{-0.0070}$
0.010	0.125	55	$0.0278^{+0.0060}_{-0.0073}$
0.010	0.125	70	$0.0338^{+0.0048}_{-0.0064}$
0.010	0.125	90	$0.0355^{+0.0064}_{-0.0063}$

Table 35: The diffractive structure function multiplied by x_P , $x_P F_2^{D(3)}(\beta, x_P, Q^2)$, for diffractive scattering, $\gamma^* p \rightarrow XN$, $M_N < 2.3$ GeV, for fixed $x_P = 0.005, 0.010$ and fixed β . The errors are the statistical and systematic uncertainties added in quadrature.

x_P	β	Q^2 (GeV ²)	$x_P F_2^{D(3)}$
0.010	0.400	6	$0.0288^{+0.0039}_{-0.0044}$
0.010	0.400	8	$0.0305^{+0.0027}_{-0.0028}$
0.010	0.400	14	$0.0273^{+0.0041}_{-0.0040}$
0.010	0.400	25	$0.0304^{+0.0061}_{-0.0083}$
0.010	0.400	27	$0.0282^{+0.0042}_{-0.0047}$
0.010	0.400	35	$0.0326^{+0.0057}_{-0.0072}$
0.010	0.400	45	$0.0286^{+0.0040}_{-0.0057}$
0.010	0.400	55	$0.0299^{+0.0056}_{-0.0056}$
0.010	0.400	55	$0.0344^{+0.0050}_{-0.0057}$
0.010	0.400	70	$0.0293^{+0.0044}_{-0.0055}$
0.010	0.400	90	$0.0303^{+0.0047}_{-0.0046}$
0.010	0.400	120	$0.0292^{+0.0046}_{-0.0054}$
0.010	0.400	190	$0.0313^{+0.0061}_{-0.0064}$
0.010	0.400	320	$0.0292^{+0.0102}_{-0.0113}$
0.010	0.700	14	$0.0280^{+0.0026}_{-0.0030}$
0.010	0.700	25	$0.0344^{+0.0049}_{-0.0068}$
0.010	0.700	27	$0.0241^{+0.0073}_{-0.0051}$
0.010	0.700	35	$0.0267^{+0.0072}_{-0.0076}$
0.010	0.700	55	$0.0213^{+0.0078}_{-0.0057}$
0.010	0.700	55	$0.0291^{+0.0041}_{-0.0052}$
0.010	0.700	70	$0.0262^{+0.0039}_{-0.0042}$
0.010	0.700	90	$0.0267^{+0.0063}_{-0.0058}$
0.010	0.700	120	$0.0348^{+0.0078}_{-0.0066}$
0.010	0.700	190	$0.0246^{+0.0044}_{-0.0045}$
0.010	0.700	320	$0.0292^{+0.0084}_{-0.0106}$
0.010	0.900	14	$0.0246^{+0.0042}_{-0.0038}$
0.010	0.900	25	$0.0171^{+0.0054}_{-0.0083}$
0.010	0.900	27	$0.0191^{+0.0046}_{-0.0056}$
0.010	0.900	45	$0.0180^{+0.0032}_{-0.0046}$
0.010	0.900	55	$0.0168^{+0.0052}_{-0.0050}$
0.010	0.900	55	$0.0144^{+0.0040}_{-0.0056}$
0.010	0.900	70	$0.0138^{+0.0037}_{-0.0042}$
0.010	0.900	90	$0.0172^{+0.0044}_{-0.0049}$
0.010	0.900	120	$0.0196^{+0.0059}_{-0.0062}$
0.010	0.900	190	$0.0145^{+0.0046}_{-0.0044}$
0.010	0.900	320	$0.0121^{+0.0076}_{-0.0070}$

Table 36: The diffractive structure function multiplied by x_P , $x_P F_2^{D(3)}(\beta, x_P, Q^2)$, for diffractive scattering, $\gamma^* p \rightarrow XN$, $M_N < 2.3$ GeV, for fixed $x_P = 0.010$ and fixed β . The errors are the statistical and systematic uncertainties added in quadrature.

x_P	β	Q^2 (GeV ²)	$x_P F_2^{D(3)}$
0.010	0.970	35	$0.0161^{+0.0064}_{-0.0069}$
0.010	0.970	45	$0.0066^{+0.0037}_{-0.0038}$
0.010	0.970	55	$0.0118^{+0.0079}_{-0.0066}$
0.010	0.970	55	$0.0092^{+0.0037}_{-0.0046}$
0.010	0.970	70	$0.0108^{+0.0045}_{-0.0048}$
0.010	0.970	90	$0.0040^{+0.0039}_{-0.0035}$
0.010	0.970	120	$0.0150^{+0.0094}_{-0.0108}$
0.010	0.970	190	$0.0083^{+0.0045}_{-0.0042}$
0.020	0.005	2.7	$0.0196^{+0.0084}_{-0.0082}$
0.020	0.005	4	$0.0172^{+0.0078}_{-0.0079}$
0.020	0.005	6	$0.0235^{+0.0106}_{-0.0103}$
0.020	0.005	8	$0.0251^{+0.0124}_{-0.0114}$
0.020	0.025	2.7	$0.0167^{+0.0060}_{-0.0052}$
0.020	0.025	4	$0.0142^{+0.0053}_{-0.0053}$
0.020	0.025	6	$0.0188^{+0.0071}_{-0.0061}$
0.020	0.025	8	$0.0219^{+0.0083}_{-0.0083}$
0.020	0.025	14	$0.0234^{+0.0096}_{-0.0095}$
0.020	0.025	25	$0.0282^{+0.0182}_{-0.0182}$
0.020	0.025	27	$0.0254^{+0.0128}_{-0.0129}$
0.020	0.025	35	$0.0333^{+0.0123}_{-0.0138}$
0.020	0.025	45	$0.0435^{+0.0120}_{-0.0132}$
0.020	0.125	4	$0.0183^{+0.0047}_{-0.0044}$
0.020	0.125	6	$0.0174^{+0.0052}_{-0.0051}$
0.020	0.125	8	$0.0201^{+0.0056}_{-0.0054}$
0.020	0.125	14	$0.0225^{+0.0072}_{-0.0069}$
0.020	0.125	25	$0.0252^{+0.0114}_{-0.0119}$
0.020	0.125	27	$0.0202^{+0.0092}_{-0.0080}$
0.020	0.125	35	$0.0282^{+0.0110}_{-0.0111}$
0.020	0.125	45	$0.0223^{+0.0070}_{-0.0087}$
0.020	0.125	55	$0.0231^{+0.0123}_{-0.0127}$
0.020	0.125	55	$0.0287^{+0.0110}_{-0.0112}$
0.020	0.125	70	$0.0255^{+0.0104}_{-0.0112}$
0.020	0.125	90	$0.0302^{+0.0078}_{-0.0081}$
0.020	0.125	190	$0.0359^{+0.0115}_{-0.0115}$

Table 37: The diffractive structure function multiplied by x_P , $x_P F_2^{D(3)}(\beta, x_P, Q^2)$, for diffractive scattering, $\gamma^* p \rightarrow XN$, $M_N < 2.3$ GeV, for fixed $x_P = 0.010, 0.020$ and fixed β . The errors are the statistical and systematic uncertainties added in quadrature.

x_P	β	Q^2 (GeV ²)	$x_P F_2^{D(3)}$
0.020	0.400	35	$0.0214^{+0.0103}_{-0.0111}$
0.020	0.400	45	$0.0192^{+0.0081}_{-0.0107}$
0.020	0.400	90	$0.0247^{+0.0070}_{-0.0077}$
0.020	0.400	120	$0.0251^{+0.0043}_{-0.0069}$
0.020	0.400	190	$0.0280^{+0.0071}_{-0.0087}$
0.020	0.400	320	$0.0119^{+0.0075}_{-0.0088}$
0.020	0.700	25	$0.0149^{+0.0073}_{-0.0100}$
0.020	0.700	27	$0.0153^{+0.0037}_{-0.0033}$
0.020	0.700	35	$0.0194^{+0.0113}_{-0.0160}$
0.020	0.700	55	$0.0144^{+0.0055}_{-0.0052}$
0.020	0.700	90	$0.0240^{+0.0058}_{-0.0063}$
0.020	0.700	120	$0.0155^{+0.0075}_{-0.0097}$
0.020	0.700	190	$0.0182^{+0.0076}_{-0.0086}$
0.020	0.700	320	$0.0197^{+0.0068}_{-0.0070}$
0.020	0.900	70	$0.0102^{+0.0041}_{-0.0061}$
0.020	0.900	90	$0.0139^{+0.0067}_{-0.0099}$
0.020	0.900	120	$0.0055^{+0.0047}_{-0.0055}$
0.020	0.900	190	$0.0102^{+0.0033}_{-0.0034}$
0.020	0.900	320	$0.0076^{+0.0056}_{-0.0059}$
0.020	0.970	35	$0.0085^{+0.0082}_{-0.0077}$
0.020	0.970	45	$0.0062^{+0.0044}_{-0.0061}$
0.020	0.970	70	$0.0102^{+0.0052}_{-0.0069}$
0.020	0.970	120	$0.0058^{+0.0038}_{-0.0039}$
0.020	0.970	320	$0.0118^{+0.0118}_{-0.0142}$
0.030	0.025	45	$0.0381^{+0.0187}_{-0.0202}$
0.030	0.125	90	$0.0295^{+0.0228}_{-0.0242}$
0.030	0.125	190	$0.0322^{+0.0246}_{-0.0280}$
0.030	0.040	190	$0.0224^{+0.0110}_{-0.0086}$
0.030	0.040	320	$0.0193^{+0.0081}_{-0.0083}$
0.030	0.700	320	$0.0126^{+0.0050}_{-0.0076}$
0.030	0.900	55	$0.0089^{+0.0056}_{-0.0069}$
0.030	0.900	320	$0.0132^{+0.0073}_{-0.0077}$
0.030	0.970	55	$0.0120^{+0.0075}_{-0.0079}$
0.060	0.970	90	$0.0072^{+0.0046}_{-0.0052}$
0.060	0.970	190	$0.0072^{+0.0070}_{-0.0070}$

Table 38: The diffractive structure function multiplied by x_P , $x_P F_2^{D(3)}(\beta, x_P, Q^2)$, for diffractive scattering, $\gamma^* p \rightarrow XN$, $M_N < 2.3$ GeV, for fixed $x_P = 0.020, 0.030$ and fixed β . The errors are the statistical and systematic uncertainties added in quadrature.

x_P	$\beta = 0.125$	0.40	0.70	0.90
0.0012		$c = 0.0144 \pm 0.0051$ $a = 0.0117 \pm 0.0020$	0.0258 ± 0.0072 0.0060 ± 0.0024	0.0347 ± 0.0082 -0.0017 ± 0.0025
0.0025		0.0278 ± 0.0062 0.0037 ± 0.0022	0.0293 ± 0.0056 0.0024 ± 0.0017	0.0368 ± 0.0097 -0.0033 ± 0.0027
0.0050	0.0134 ± 0.0039 0.0051 ± 0.0017	0.0255 ± 0.0036 0.0029 ± 0.0011	0.0317 ± 0.0095 0.0002 ± 0.0024	0.0347 ± 0.0049 -0.0037 ± 0.0013
0.0100	0.0121 ± 0.0031 0.0046 ± 0.0012	0.0288 ± 0.0042 0.0003 ± 0.0012	0.0296 ± 0.0062 -0.0005 ± 0.0016	0.0306 ± 0.0220 -0.0033 ± 0.0053

Table 39: Fits of $x_P F_2^{D(3)} = c + a \cdot \ln(1 + Q^2)$ for the x_P, β - values indicated: shown are the values for c and a .

Exp't	c_T	c_L	c_g	n_1	γ	χ^2/n_D
FPC II	0.120 ± 0.003	0.074 ± 0.006	0.0111 ± 0.0015	0.067 ± 0.003	7.98 ± 0.92	0.75
FPC I	0.115 ± 0.003	0.107 ± 0.009	0.0091 ± 0.0003	0.062 ± 0.003	8.60 ± 0.56	0.62
FPC I + FPC II	0.118 ± 0.002	0.087 ± 0.005	0.0090 ± 0.0003	0.062 ± 0.002	8.22 ± 0.46	0.79

Table 40: Results from fitting the data from FPC II, from FPC I, and from the combined data from FPC I and FPC II to BEKW(mod). The fit procedure includes the statistical and systematic uncertainties of the data.

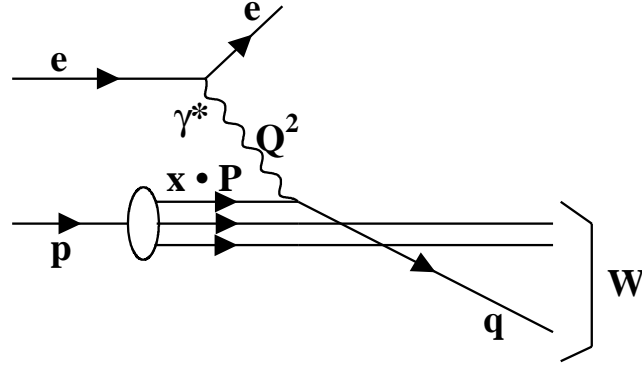


Figure 1: *Diagram for non-peripheral deep inelastic scattering.*

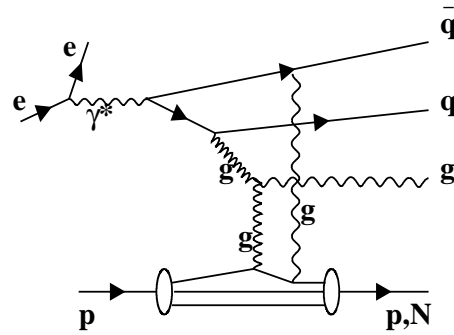
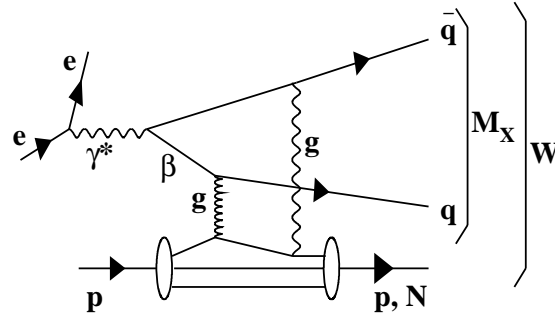


Figure 2: *Diagrams of diffractive deep inelastic scattering, $ep \rightarrow eXN$, proceeding by the exchange of two gluons.*

ZEUS

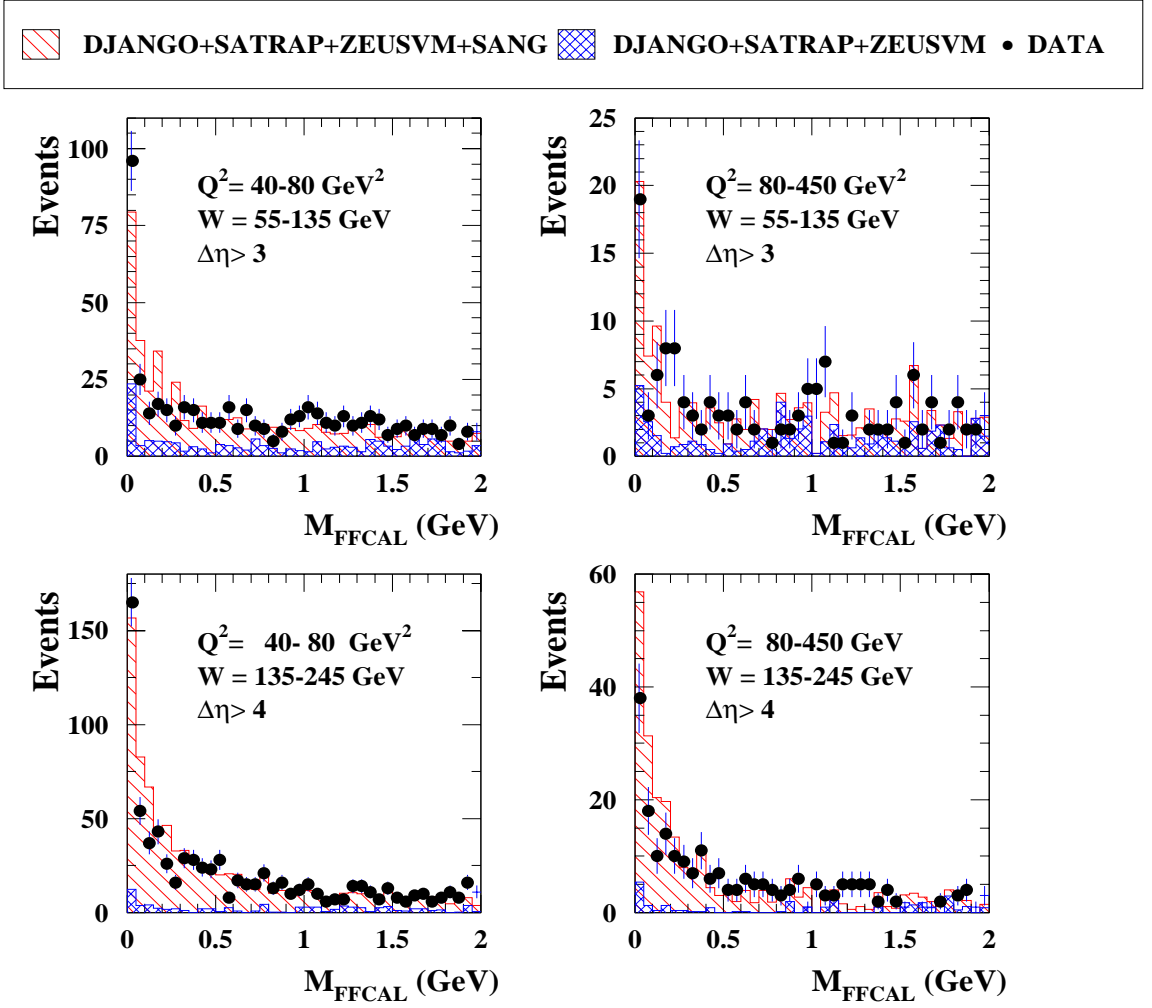


Figure 3: Distributions of M_{FFCAL} for four different $(Q^2, W, \Delta\eta)$ regions. The points with error bars show the data. The cross hatched histograms show the MC predictions for the sum of contributions from Xp , $\rho^0 p$ and non-peripheral processes; the hatched histograms show the sum of contributions from Xp , $\rho^0 p$, diffractive double dissociation (XN) and non-peripheral processes. The MC distributions are normalised according to the luminosity of the data.

ZEUS

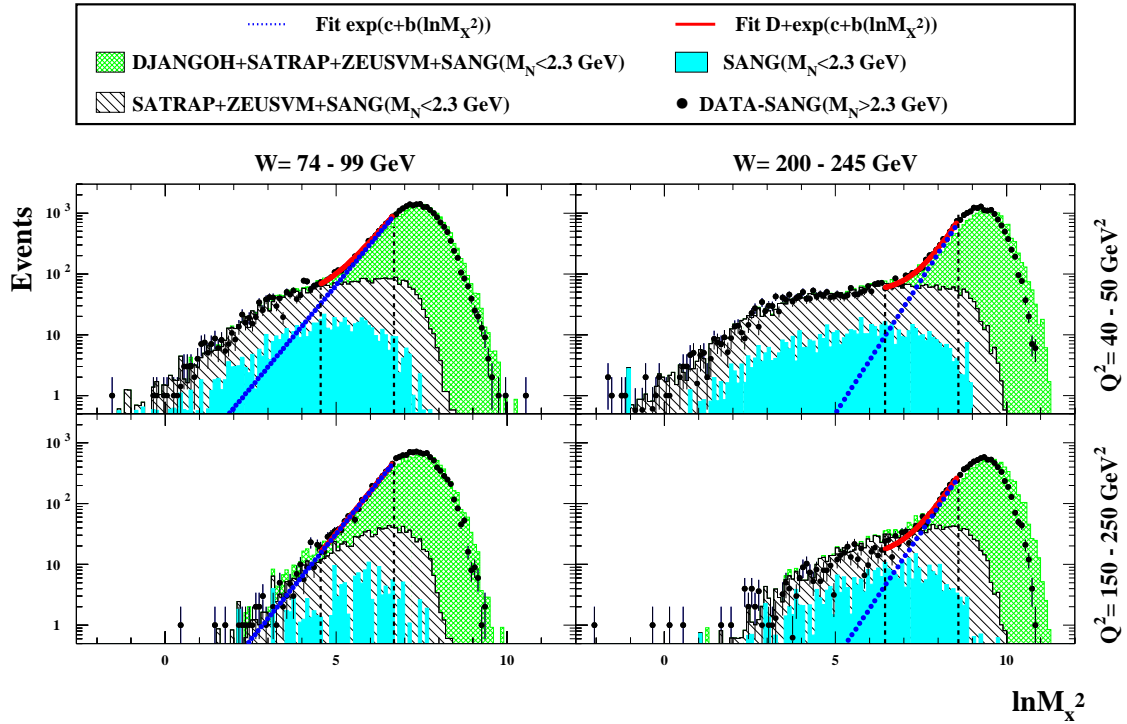


Figure 4: Distributions of $\ln M_X^2$ (M_X in units of GeV) at the detector level for the $W = 74 - 99$ GeV, $W = 200 - 245$ GeV and $Q^2 = 40 - 50$ GeV², $Q^2 = 150 - 250$ GeV² bins. The points with error bars show the data, with the contribution from proton dissociation, as predicted by SANG, for $M_N > 2.3$ GeV subtracted. The light shaded areas show the non-peripheral contributions as predicted by DJANGO plus the diffractive contributions from SATRAP+ZEUSVM+SANG($M_N < 2.3$ GeV). The diffractive contributions from $\gamma^*p \rightarrow XN$, $M_N < 2.3$ GeV, as predicted by SATRAP+ZEUSVM+SANG($M_N < 2.3$ GeV), are shown as hatched areas. The dark grey areas show the contribution of diffractive events in which the proton dissociates into a system N , with $M_N < 2.3$ GeV. The dash-dotted lines show the results for the non-diffractive contribution from fitting the data in the $\ln M_X^2$ range delimited by the two vertical dashed lines.

ZEUS

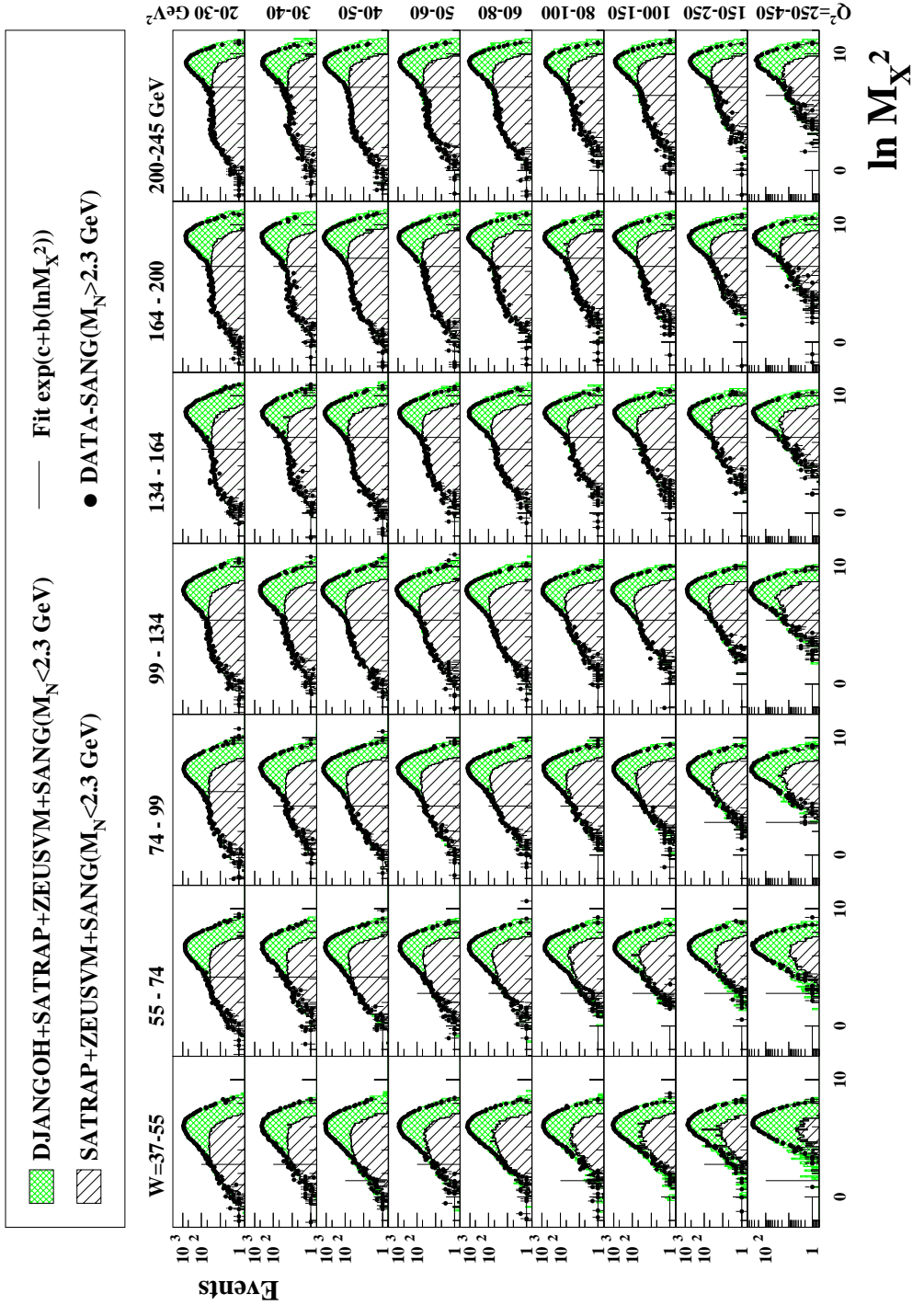


Figure 5: Distributions of $\ln M_X^2$ (M_X in units of GeV) at the detector level for different (W, Q^2) bins. The points with error bars show the data, with the contribution from proton dissociation, as predicted by SANG, for $M_N > 2.3$ GeV subtracted. The diffractive contributions from $\gamma^*p \rightarrow XN$, $M_N < 2.3$ GeV, as predicted by SATRAP+ZEUSVM+SANG($M_N < 2.3$ GeV), are shown by the hatched histograms. The cross-hatched histograms show the non-peripheral contributions as predicted by DJANGO plus the diffractive contributions. The slanted straight lines show the result for the non-diffractive contribution from fitting the data in the range $\ln W^2 - 4.4 < \ln M_X^2 < \ln W^2 - 2.2$. The vertical lines indicate the maximum M_X value up to which diffractive cross sections are determined.

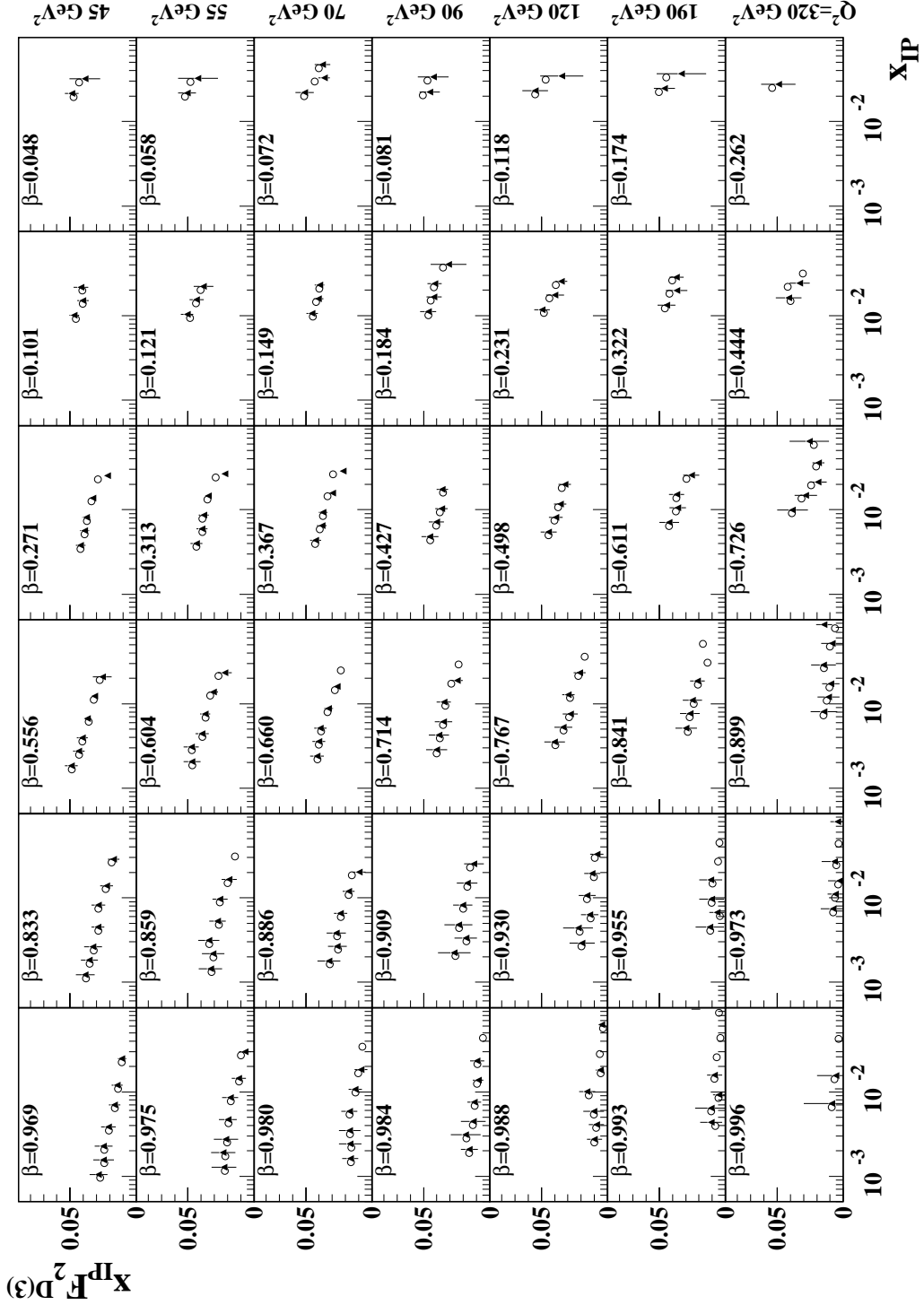


Figure 6: The diffractive structure function of the proton multiplied by x_P , $x_P F_2^{D(3)}$, as a function of x_P for different regions of β and Q^2 : comparison of the MC generated values (open points) with the MC measured values (solid triangles) as determined via the fit to the $\ln M_X^2$ distributions. The $x_P F_2^{D(3)}$ values for MC measured are shown at values of x_P increased by 10%.

ZEUS

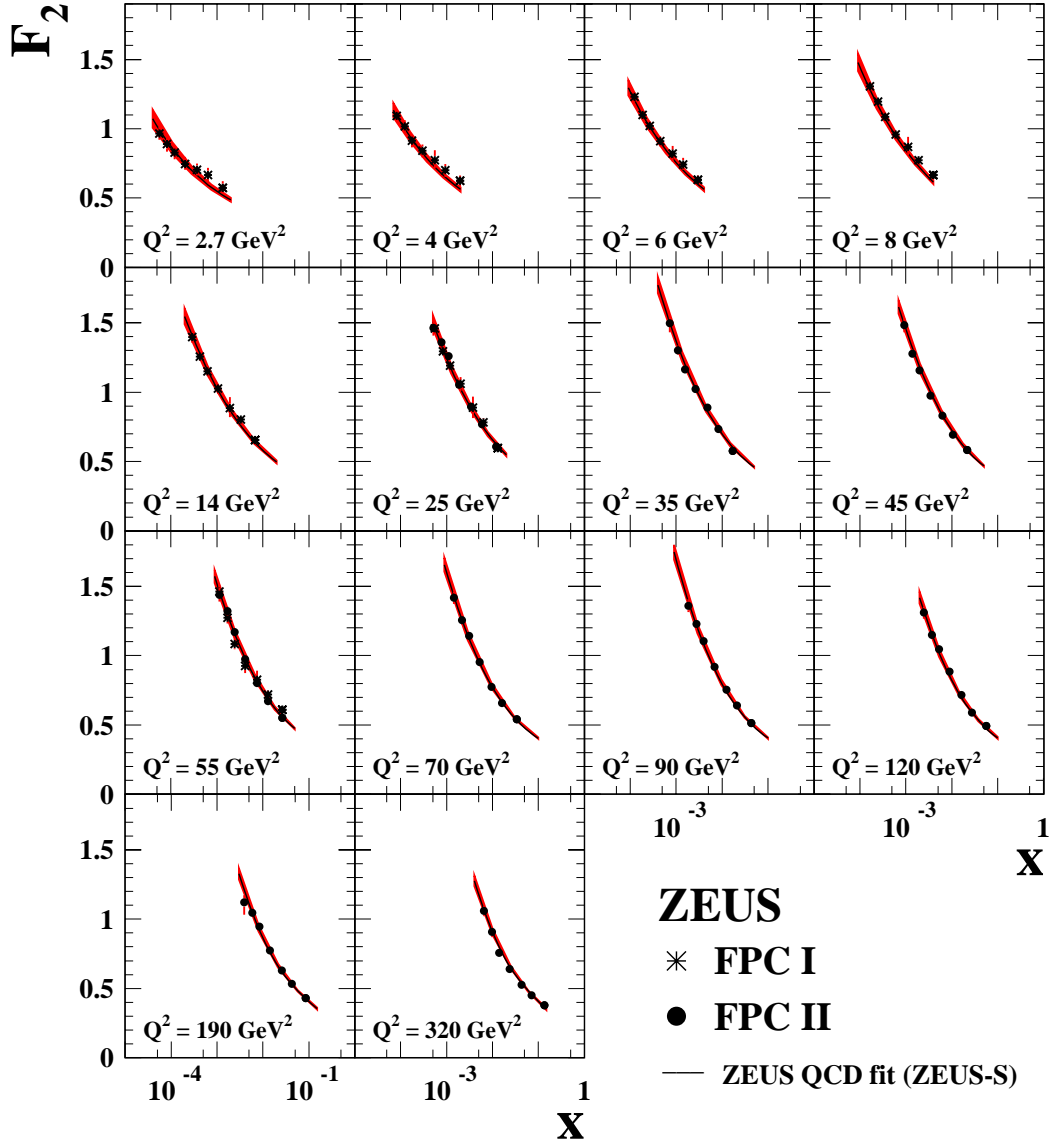


Figure 7: The proton structure function F_2 versus x for the Q^2 values indicated. The results from this analysis, FPC II, are shown together with those from the FPC I analysis. The inner error bars show the statistical uncertainties and the full bars the statistical and systematic uncertainties added in quadrature. The line shows the result of ZEUS-S NLO QCD fit with its uncertainty band.

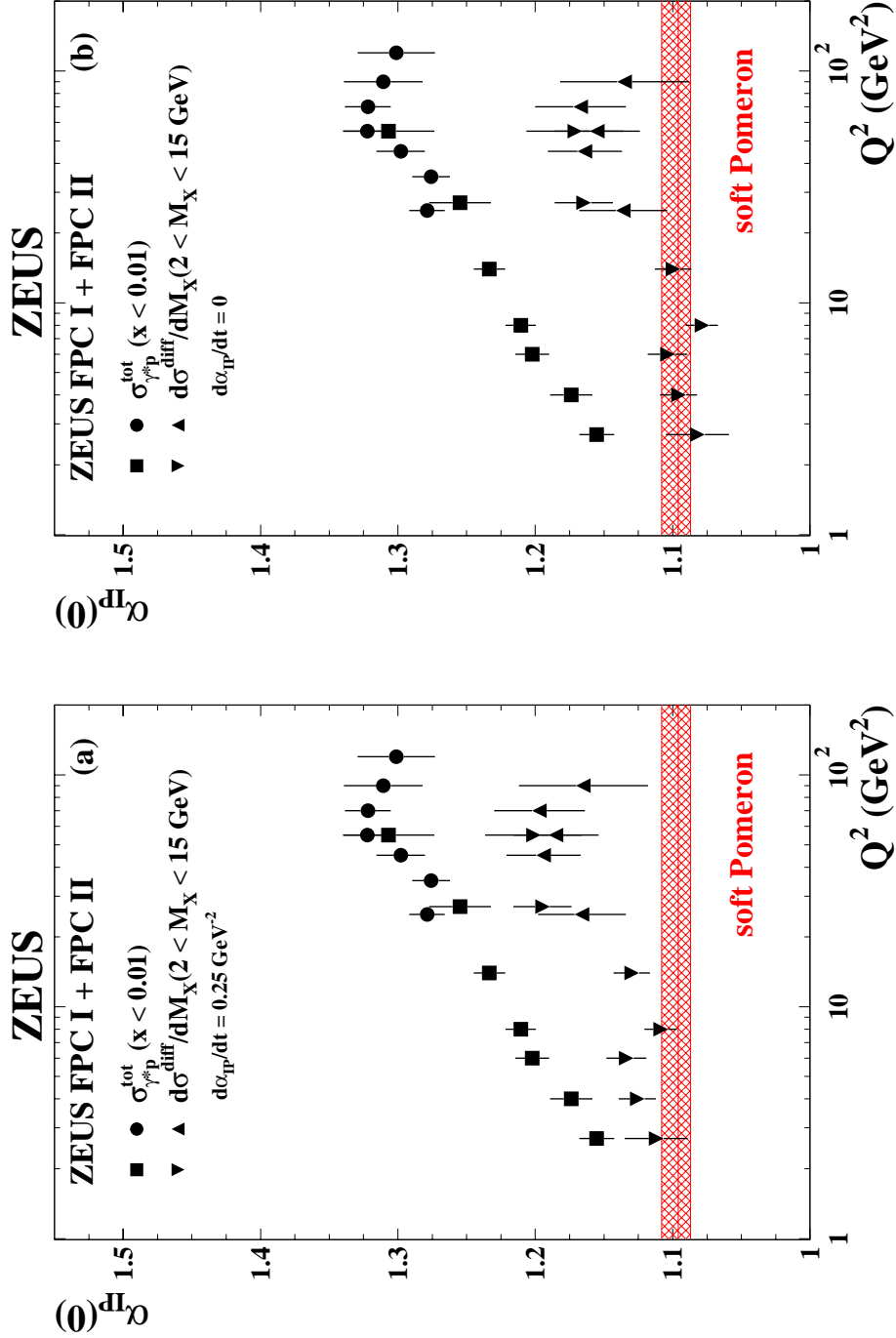


Figure 8: The intercepts of the Pomeron trajectory, $\alpha_P^{\text{tot}}(0)$ and $\alpha_P^{\text{diff}}(0)$, as a function of Q^2 , obtained from the W dependences of the total γ^*p cross section and of the diffractive cross section, $d\sigma_{\gamma^*p \rightarrow XN}^{\text{diff}}/dM_X$ for $2 < M_X < 15 \text{ GeV}$, from the FPC I and FPC II analyses, for (a) $\alpha'_P = 0.25 \text{ GeV}^{-2}$ and (b) $\alpha'_P = 0$. The error bars show the sum of the statistical and systematic uncertainties added in quadrature. The shaded bands show the expectation for the soft Pomeron.

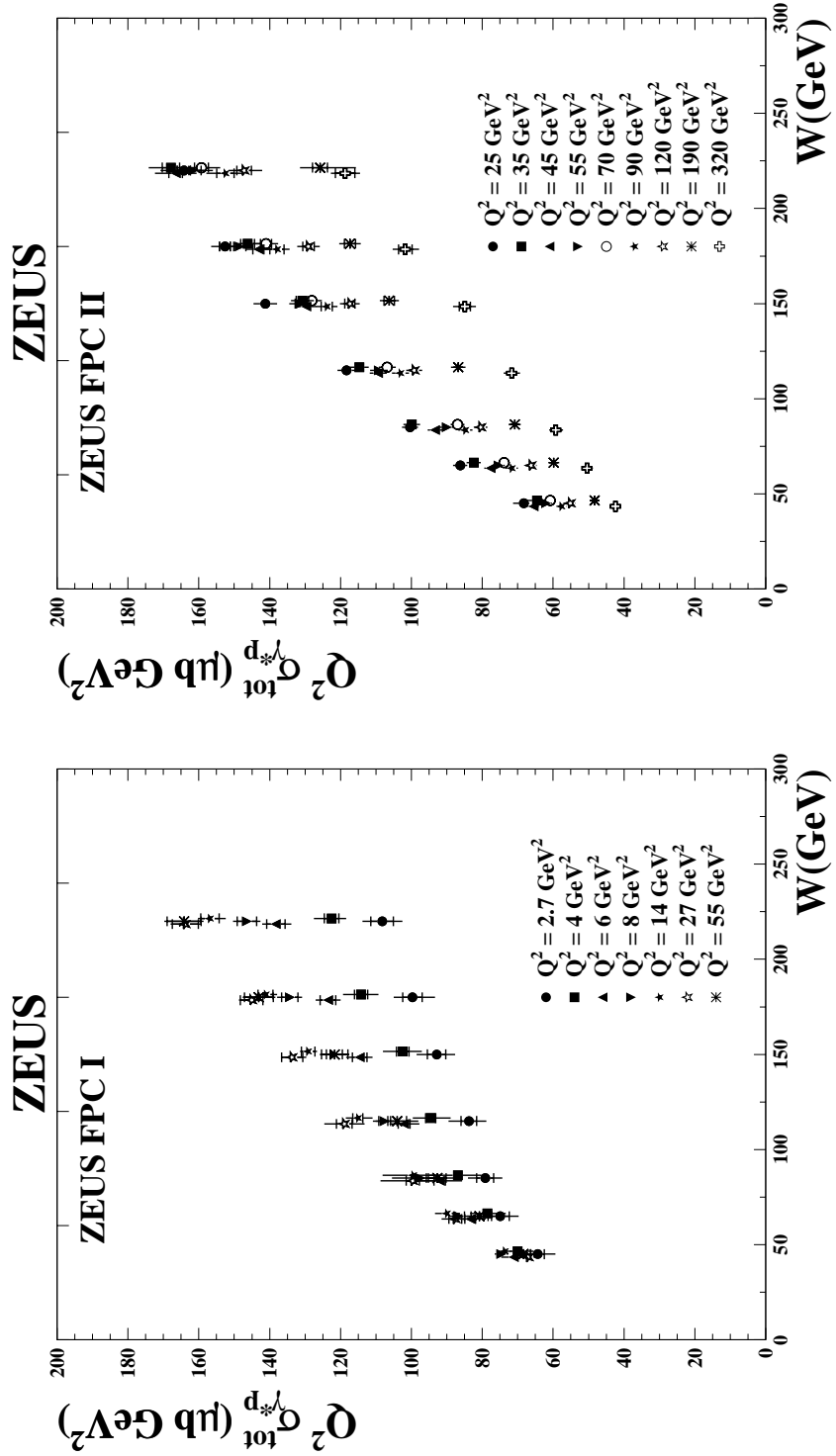


Figure 9: The total virtual photon-proton cross section, $\sigma_{\gamma^*p}^{\text{tot}}$, multiplied by Q^2 , as a function of W , for the Q^2 intervals indicated. The inner error bars show the statistical uncertainties and the full bars the statistical and systematic uncertainties added in quadrature. For better visibility, the points for adjacent values of Q^2 were shifted in W by zero, +1.5 GeV or -1.5 GeV. Data are shown (a): from the FPC I analysis; (b) from the FPC II analysis.

ZEUS

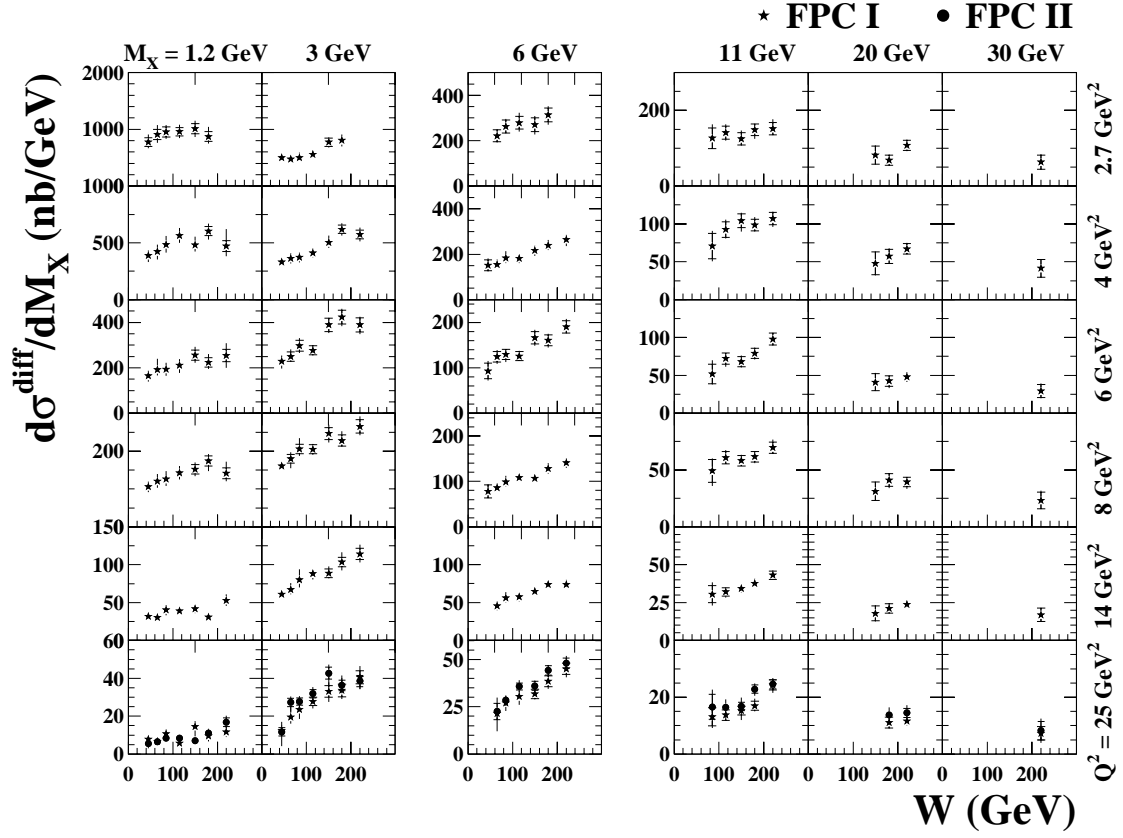


Figure 10: The differential cross sections, $d\sigma^{\text{diff}}_{\gamma^*p \rightarrow XN}/dM_X$, $M_N < 2.3$ GeV, as a function of W for bins of Q^2 and of M_X , for FPC I data (stars) and FPC II data (dots), for Q^2 between 2.7 and 25 GeV². The inner error bars show the statistical uncertainties and the full bars the statistical and systematic uncertainties added in quadrature.

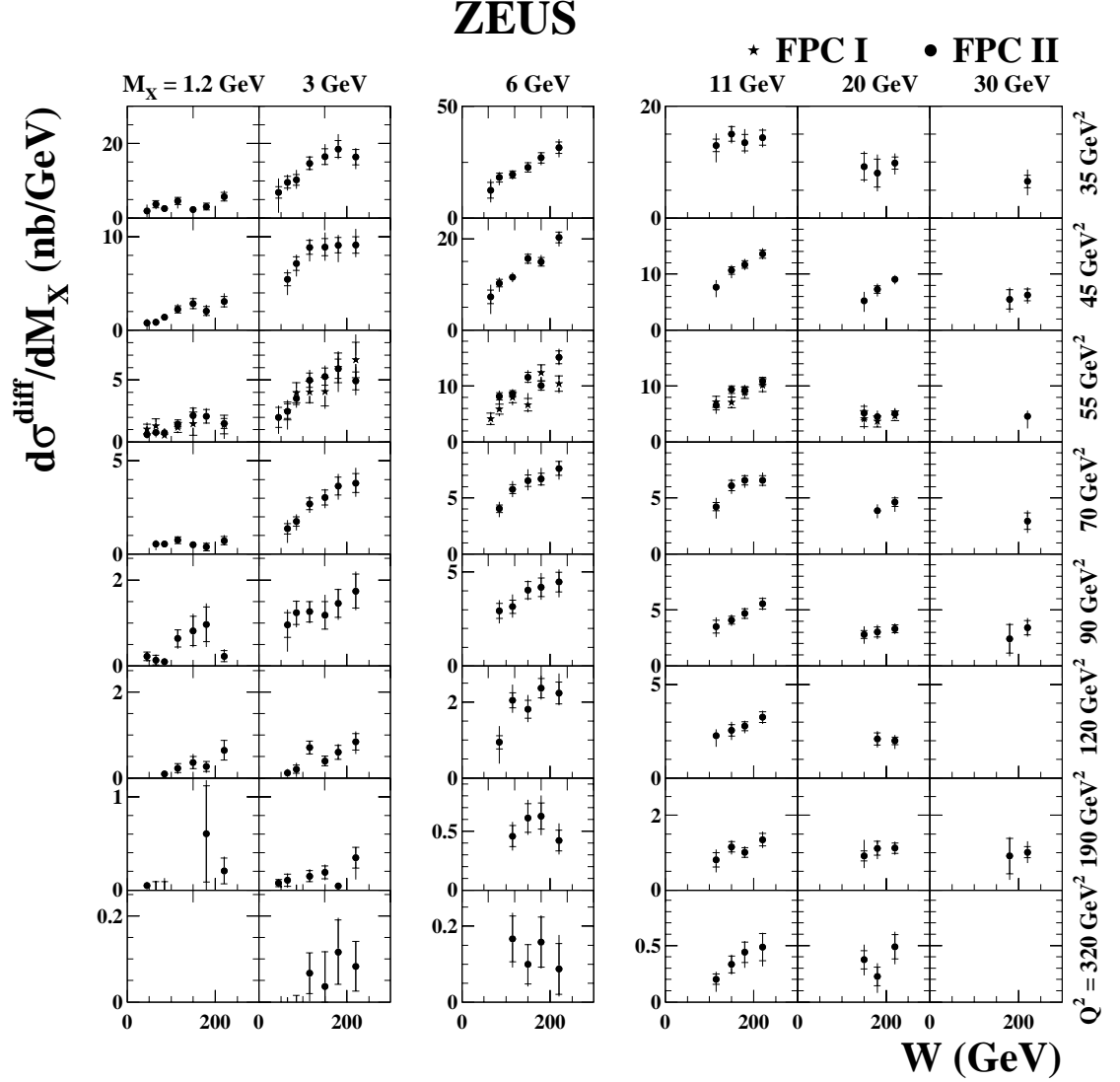


Figure 11: The differential cross sections, $d\sigma_{\gamma^*p \rightarrow XN}^{\text{diff}}/dM_X$, $M_N < 2.3 \text{ GeV}$, as a function of W for bins of Q^2 and of M_X , for FPC I data (stars) and FPC II data (dots), for Q^2 between 35 and 320 GeV^2 . The inner error bars show the statistical uncertainties and the full bars the statistical and systematic uncertainties added in quadrature. For display purposes, some of the cross section values at $Q^2 = 320 \text{ GeV}^2$ are not shown but given in Tables 7 – 12.

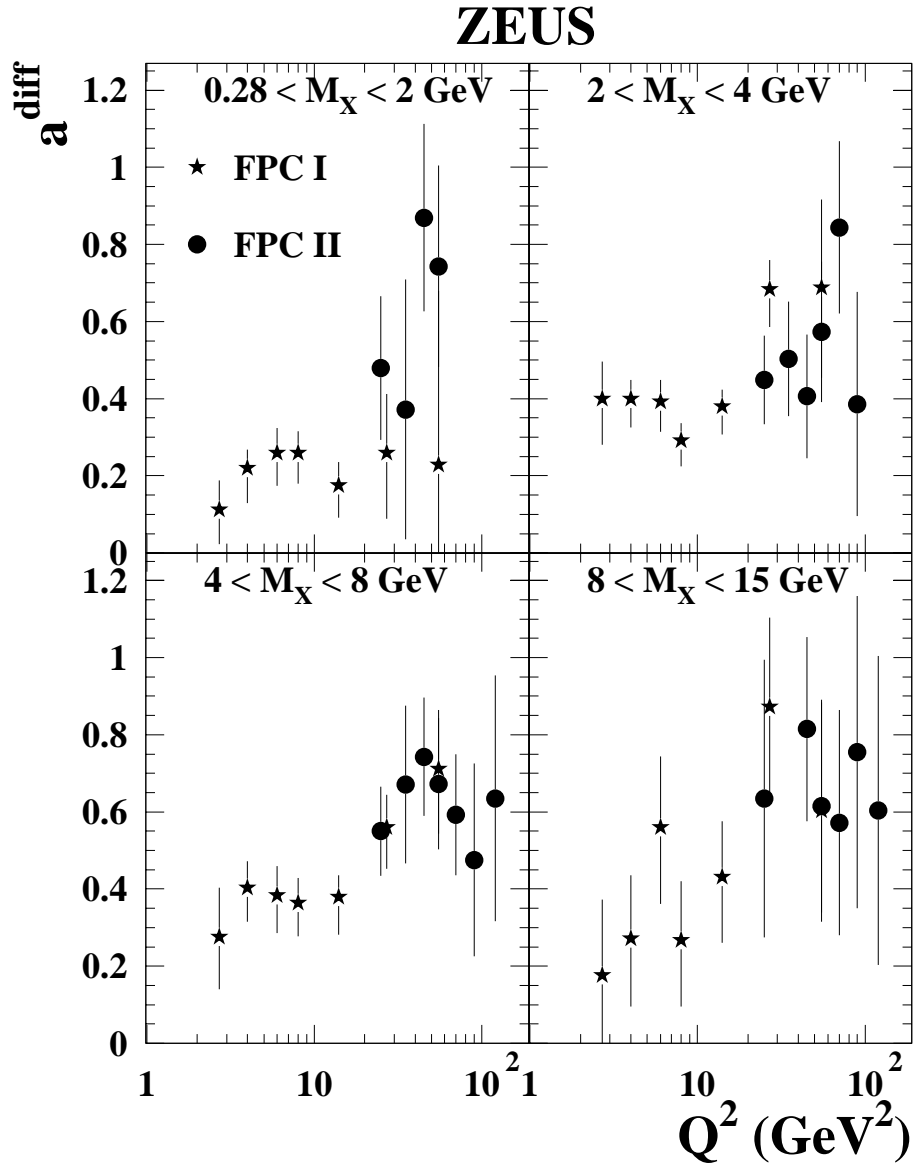


Figure 12: The power a^{diff} , obtained from fitting the diffractive cross section to the form $d\sigma_{\gamma^*p \rightarrow XN}^{\text{diff}}(M_X, W, Q^2)/dM_X \propto (W/W_0)^{a^{\text{diff}}}$, $W_0 = 1$ GeV, as a function of Q^2 for the different M_X bins indicated, for FPC I data (stars) and FPC II data (dots). The error bars show the statistical and systematic uncertainties added in quadrature.

ZEUS

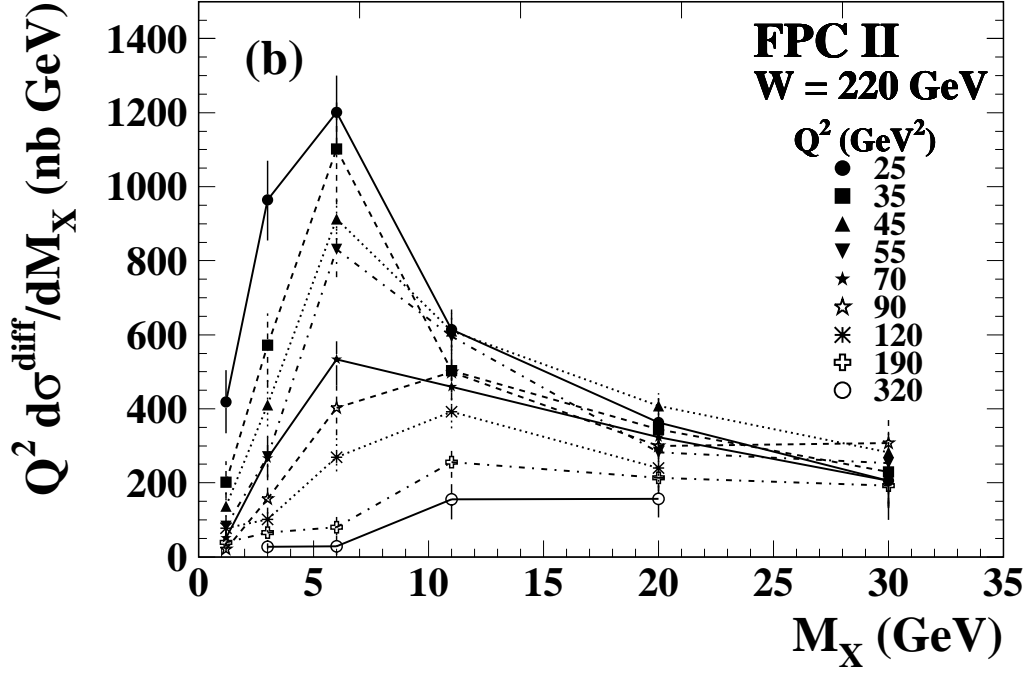
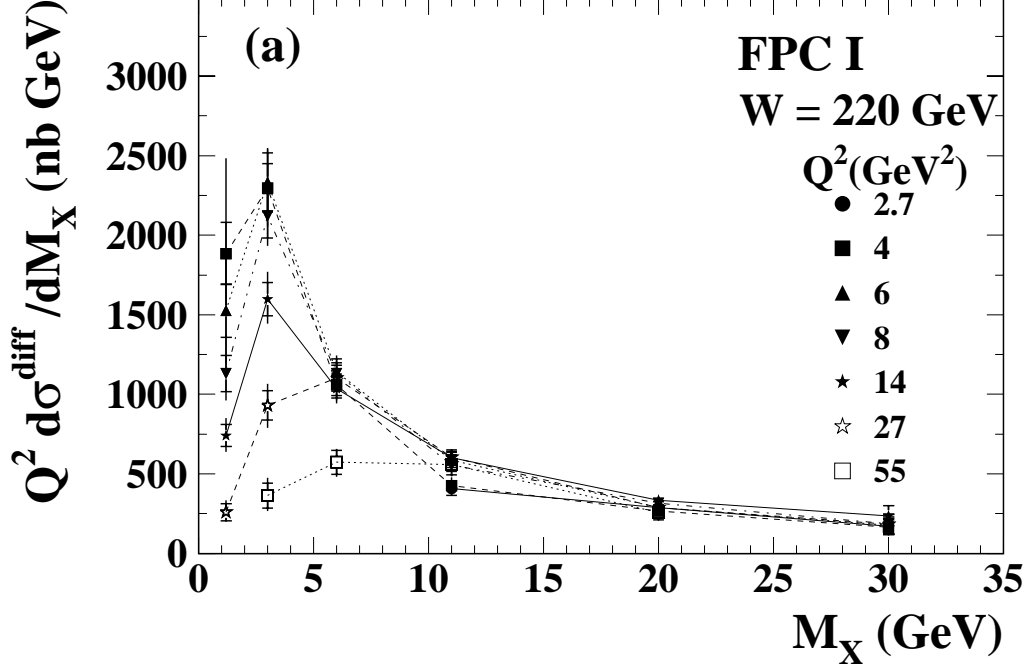


Figure 13: The diffractive cross section multiplied by Q^2 , $Q^2 d\sigma_{\gamma^*p \rightarrow XN}^{\text{diff}}/dM_X$, $M_N < 2.3 \text{ GeV}$, $W = 220 \text{ GeV}$ as a function of M_X for the Q^2 values indicated, for (a) FPC I data and (b) FPC II data. The inner error bars show the statistical uncertainties and the full bars the statistical and systematic uncertainties added in quadrature.

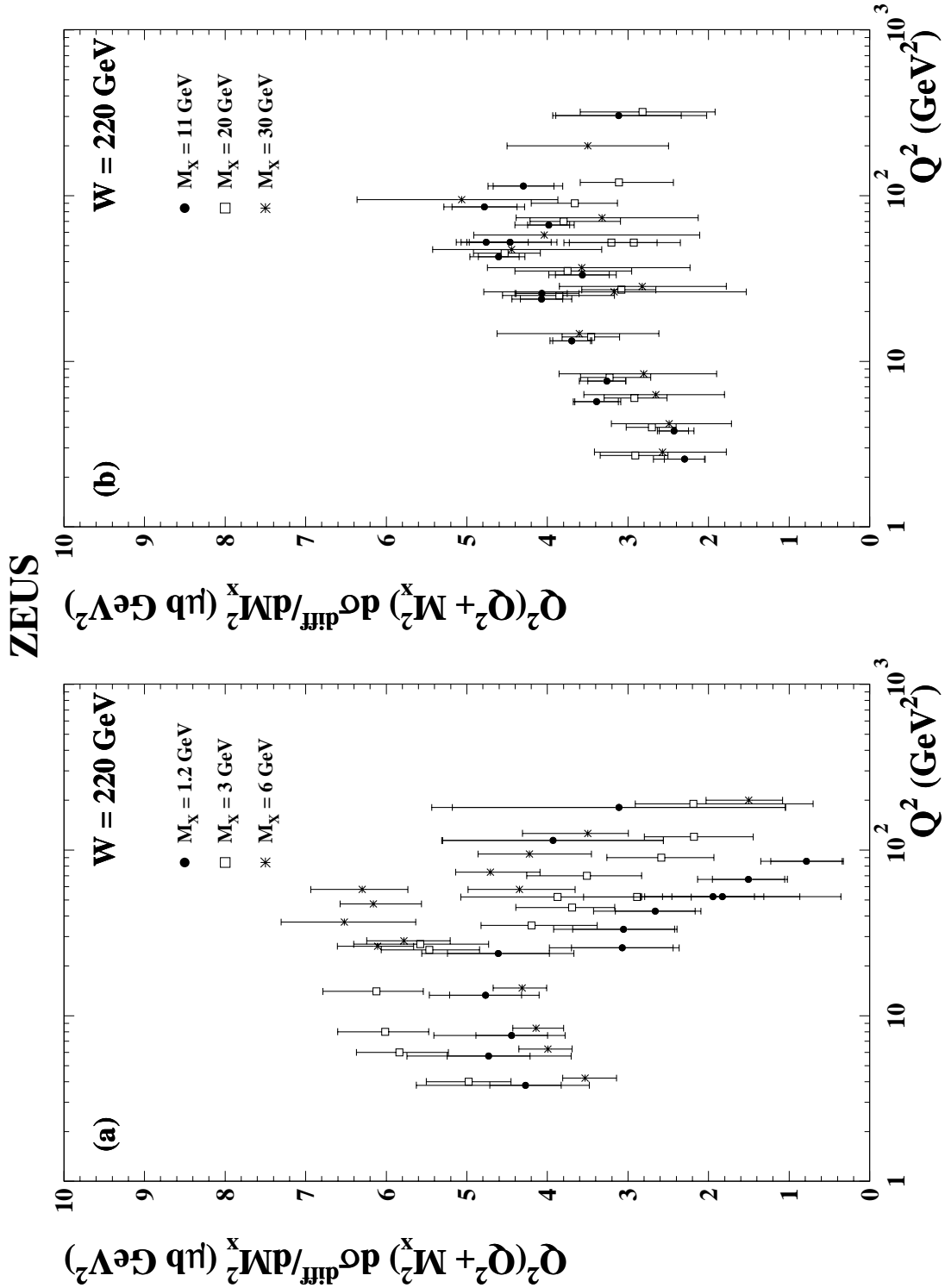


Figure 14: The diffractive cross section multiplied by $Q^2(Q^2 + M_X^2)$, $Q^2(Q^2 + M_X^2)d\sigma^{\text{diff}}_{\gamma^*p \rightarrow XN}/dM_X^2$, $M_N < 2.3 \text{ GeV}$, for $W = 220 \text{ GeV}$ as a function of Q^2 for (a) $M_X = 1.2, 3, 6 \text{ GeV}$ and (b) $M_X = 11, 20, 30 \text{ GeV}$. Shown are the combined results from the FPC I data and FPC II data. The inner error bars show the statistical uncertainties and the full bars the statistical and systematic uncertainties added in quadrature. For better visibility, in each figure the x-axis values of the data points with the lowest (highest) value of M_X have been decreased (increased) by a factor of 1.05.

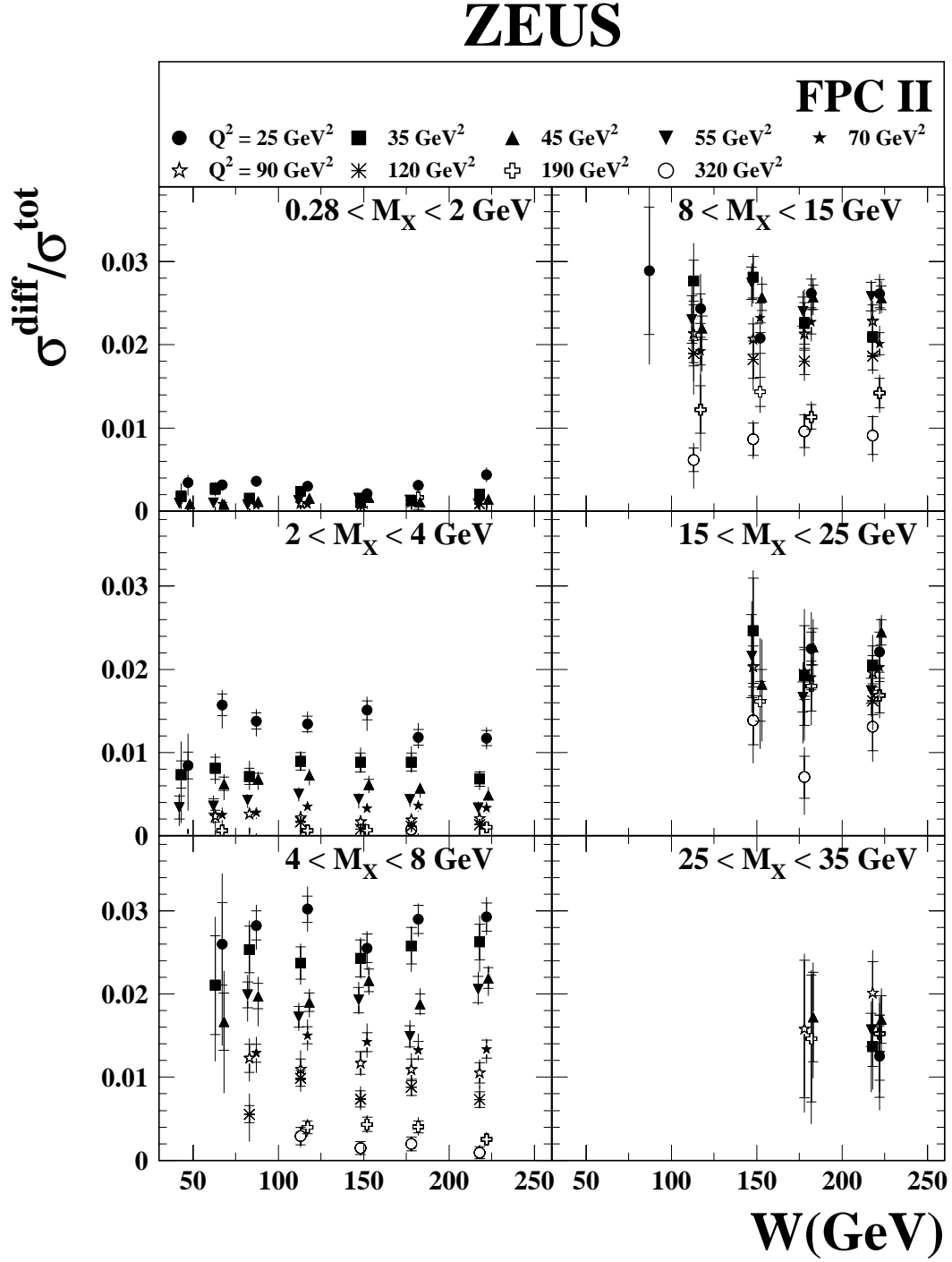


Figure 15: The ratio of the diffractive cross section, integrated over the M_X intervals indicated, $\int_{M_a}^{M_b} dM_X d\sigma_{\gamma^*p \rightarrow XN, M_N < 2.3 \text{ GeV}}^{\text{diff}}/dM_X$, to the total γ^*p cross section, $r_{\text{tot}}^{\text{diff}} = \sigma^{\text{diff}}/\sigma_{\gamma^*p}^{\text{tot}}$, as a function of W for the Q^2 values indicated, for the FPC II data. The inner error bars show the statistical uncertainties and the full bars the statistical and systematic uncertainties added in quadrature.

ZEUS

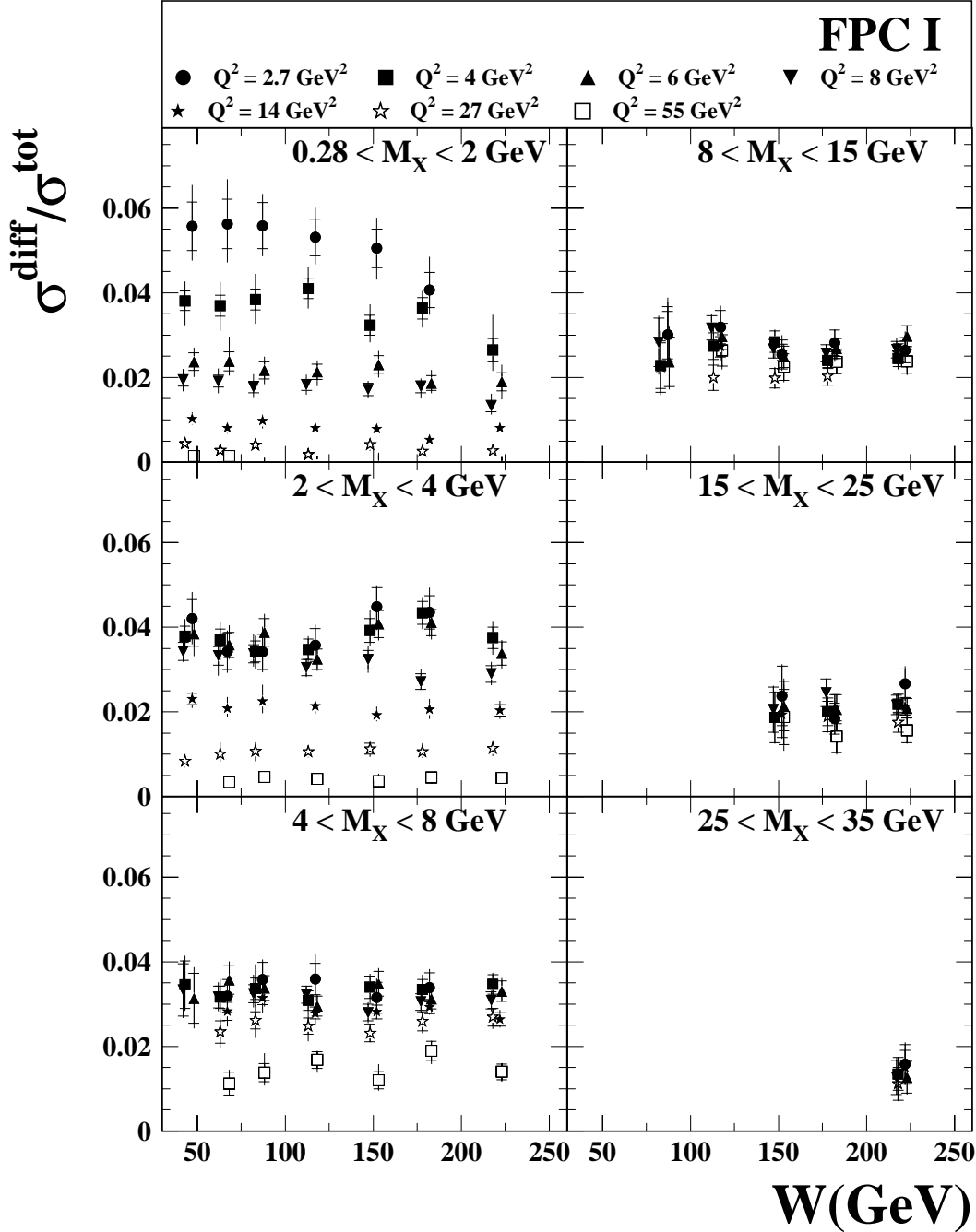


Figure 16: The ratio of the diffractive cross section, integrated over the M_X intervals indicated, $\int_{M_a}^{M_b} dM_X d\sigma_{\gamma^*p \rightarrow XN, M_N < 2.3 \text{ GeV}}^{\text{diff}}/dM_X$, to the total γ^*p cross section, $r_{\text{tot}}^{\text{diff}} = \sigma^{\text{diff}}/\sigma_{\gamma^*p}^{\text{tot}}$, as a function of W for the Q^2 intervals indicated. The inner error bars show the statistical uncertainties and the full bars the statistical and systematic uncertainties added in quadrature. The plot shown is taken directly from the FPC I paper.

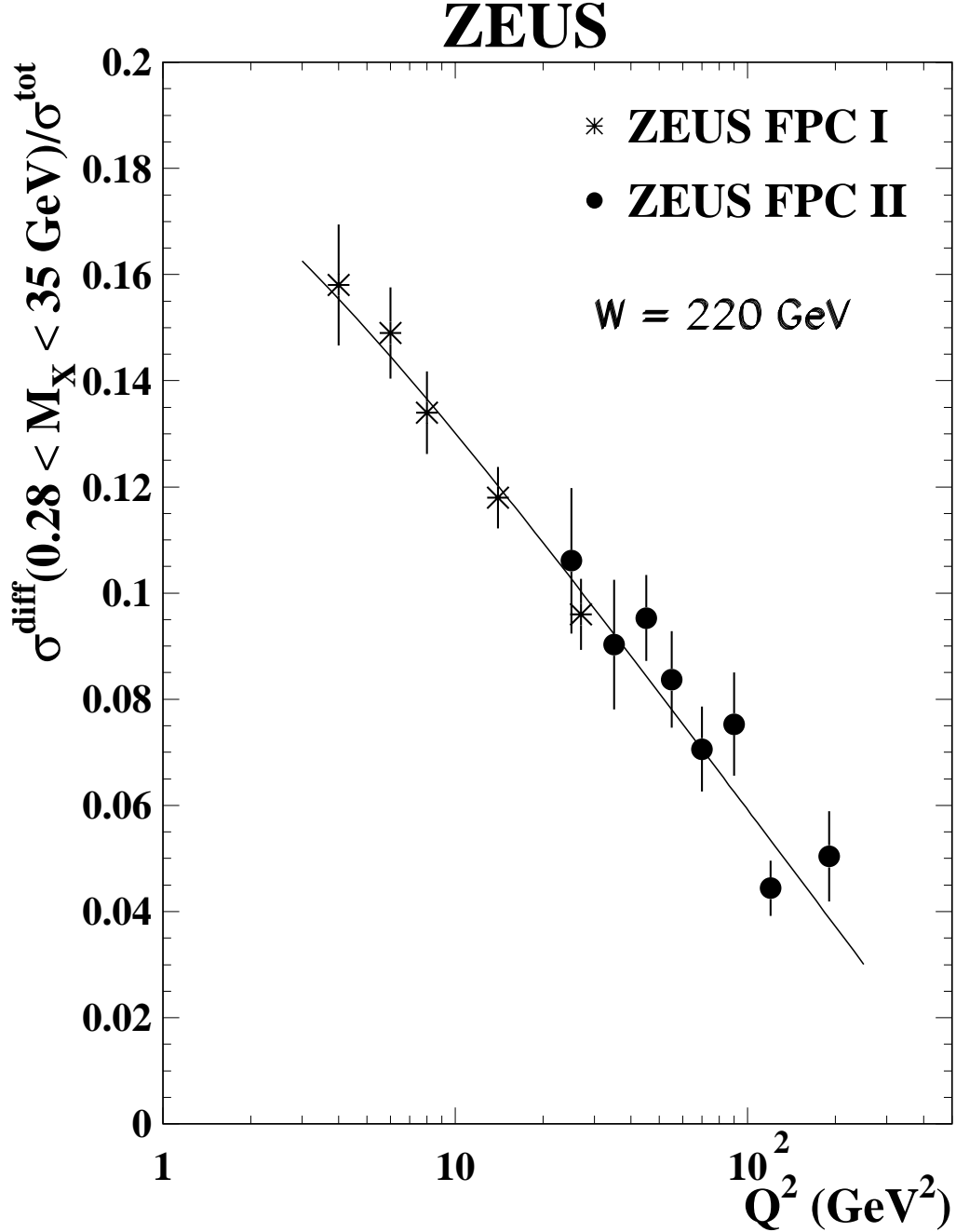


Figure 17: The ratio of the diffractive cross section, integrated over $0.28 < M_X < 35 \text{ GeV}$, to the total γ^*p cross section, at $W = 220 \text{ GeV}$ as a function of Q^2 . The error bars represent the statistical and systematic uncertainties added in quadrature. Shown are the combined data from FPC I (stars) and FPC II (dots). The line shows the result of fitting the data to the form $r = a - b \cdot \ln(1 + Q^2)$, see text.

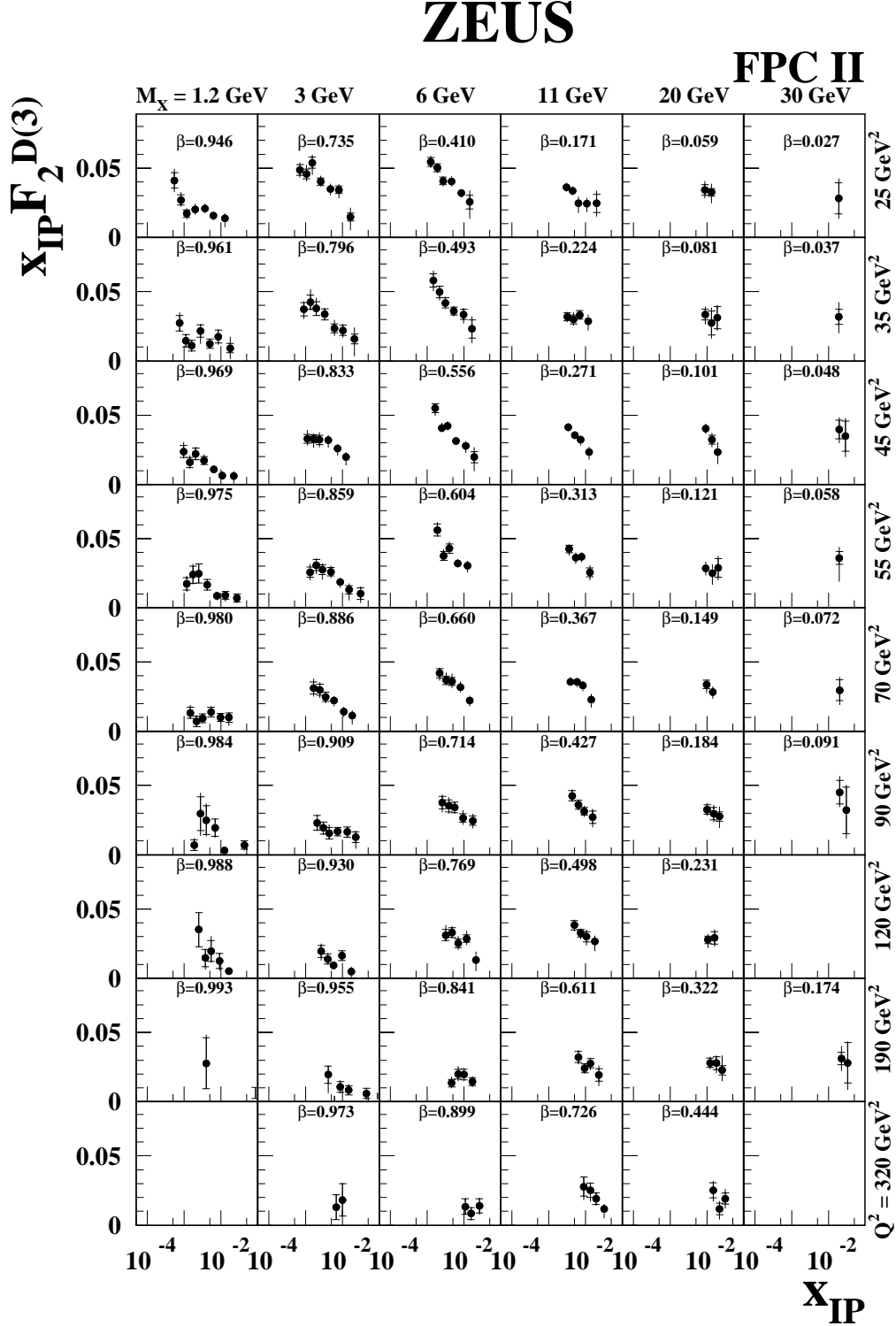


Figure 18: The diffractive structure function of the proton multiplied by x_p , $x_p F_2^{D(3)}$, for $\gamma^* p \rightarrow XN$, $M_N < 2.3$ GeV as a function of x_p for different regions of β and Q^2 , for the FPC II data. The inner error bars show the statistical uncertainties and the full bars the statistical and systematic uncertainties added in quadrature. For display purposes, some of the $x_p F_2^{D(3)}$ values at $Q^2 = 90, 120, 190$ and 320 GeV² with large uncertainties are not shown but given in Tables 25 – 29.

ZEUS

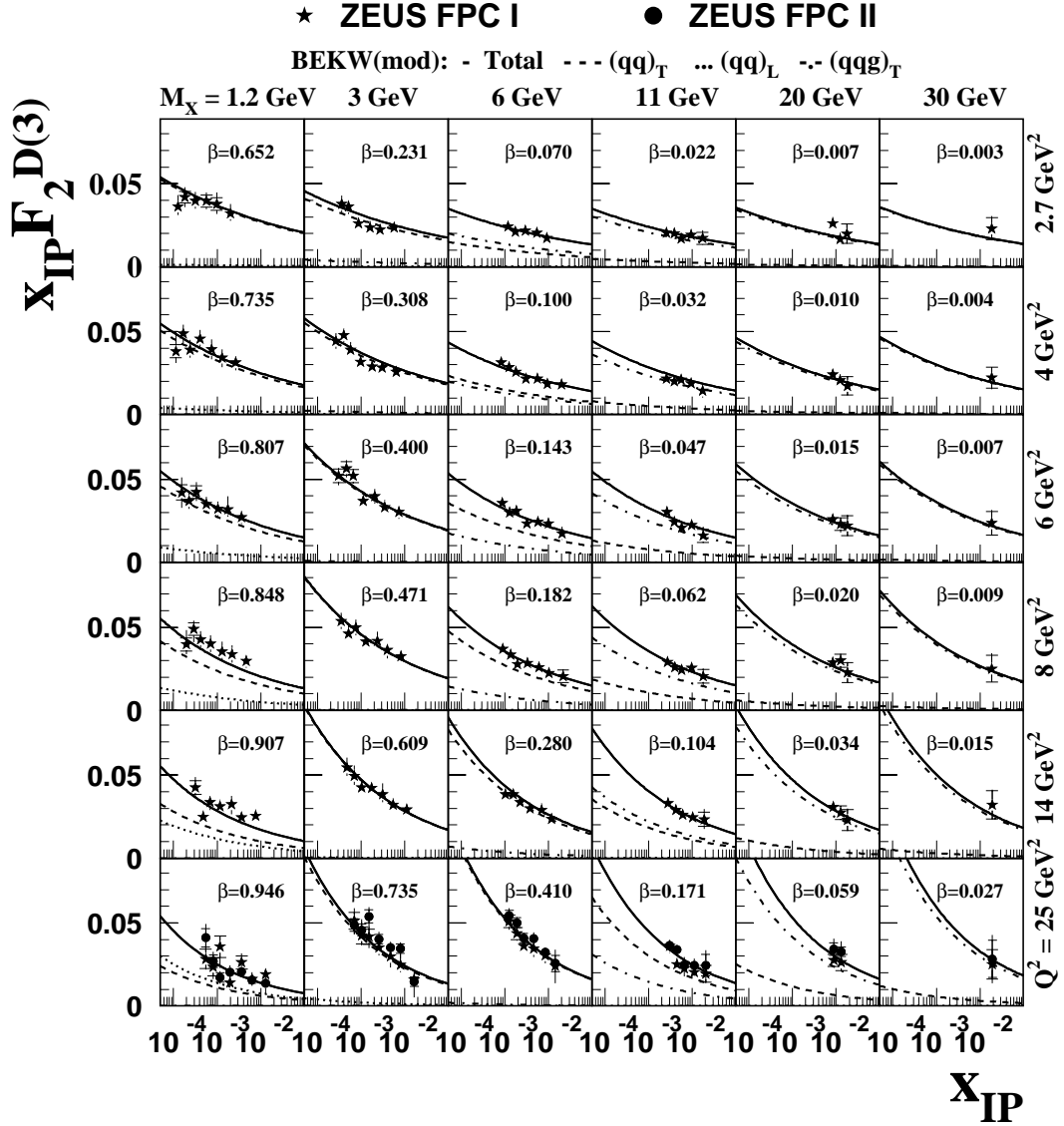


Figure 19: The diffractive structure function of the proton multiplied by x_p , $x_p F_2^{D(3)}$, for $\gamma^* p \rightarrow XN$, $M_N < 2.3 \text{ GeV}$ as a function of x_p for different regions of β and $Q^2 \leq 25 \text{ GeV}^2$: both FPC I data (stars) and FPC II data (dots) are shown. The inner error bars show the statistical uncertainties and the full bars the statistical and systematic uncertainties added in quadrature. The curves show the results of the BEKW(mod) fit for the contributions from $(q\bar{q})$ for transverse (dashed) and longitudinal photons (dotted) and for the $(q\bar{q}g)$ contribution for transverse photons (dashed-dotted) together with the sum of all contributions (solid).

ZEUS

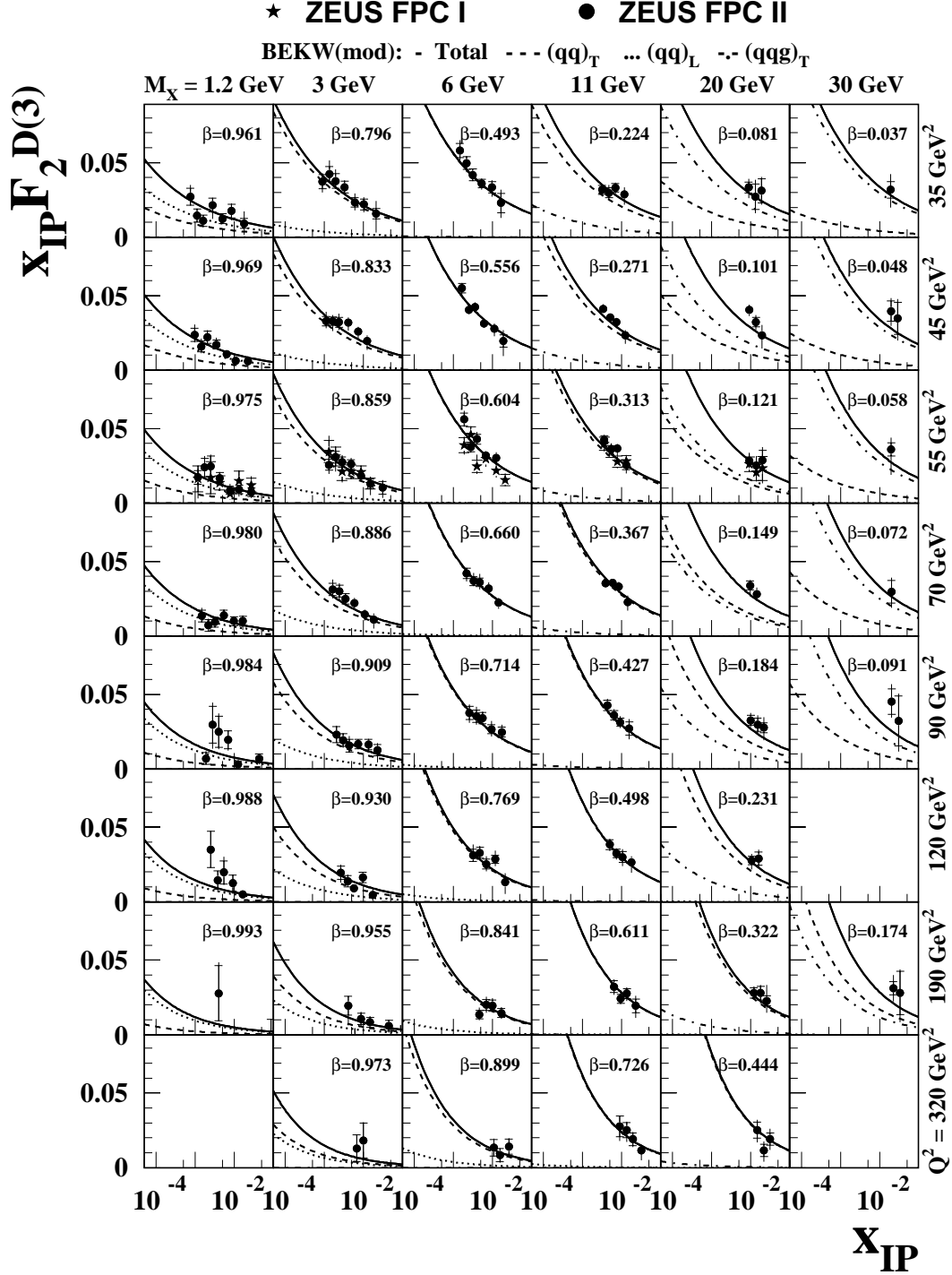


Figure 20: The diffractive structure function of the proton multiplied by x_p , $x_p F_2^{D(3)}$, for $\gamma^* p \rightarrow XN$, $M_N < 2.3 \text{ GeV}$ as a function of x_p for different regions of β and $Q^2 \geq 35 \text{ GeV}^2$: both FPC I data (stars) and FPC II data (dots) are shown. The inner error bars show the statistical uncertainties and the full bars the statistical and systematic uncertainties added in quadrature. The curves show the results of the BEKW(mod) fit for the contributions from $(q\bar{q})$ for transverse (dashed) and longitudinal photons (dotted) and for the $(q\bar{q}g)$ contribution for transverse photons (dashed-dotted) together with the sum of all contributions (solid). For display purposes, some of the $x_p F_2^{D(3)}$ values at $Q^2 = 90, 120, 190$ and 320 GeV^2 with large uncertainties are not shown but given in Tables 27 – 29.

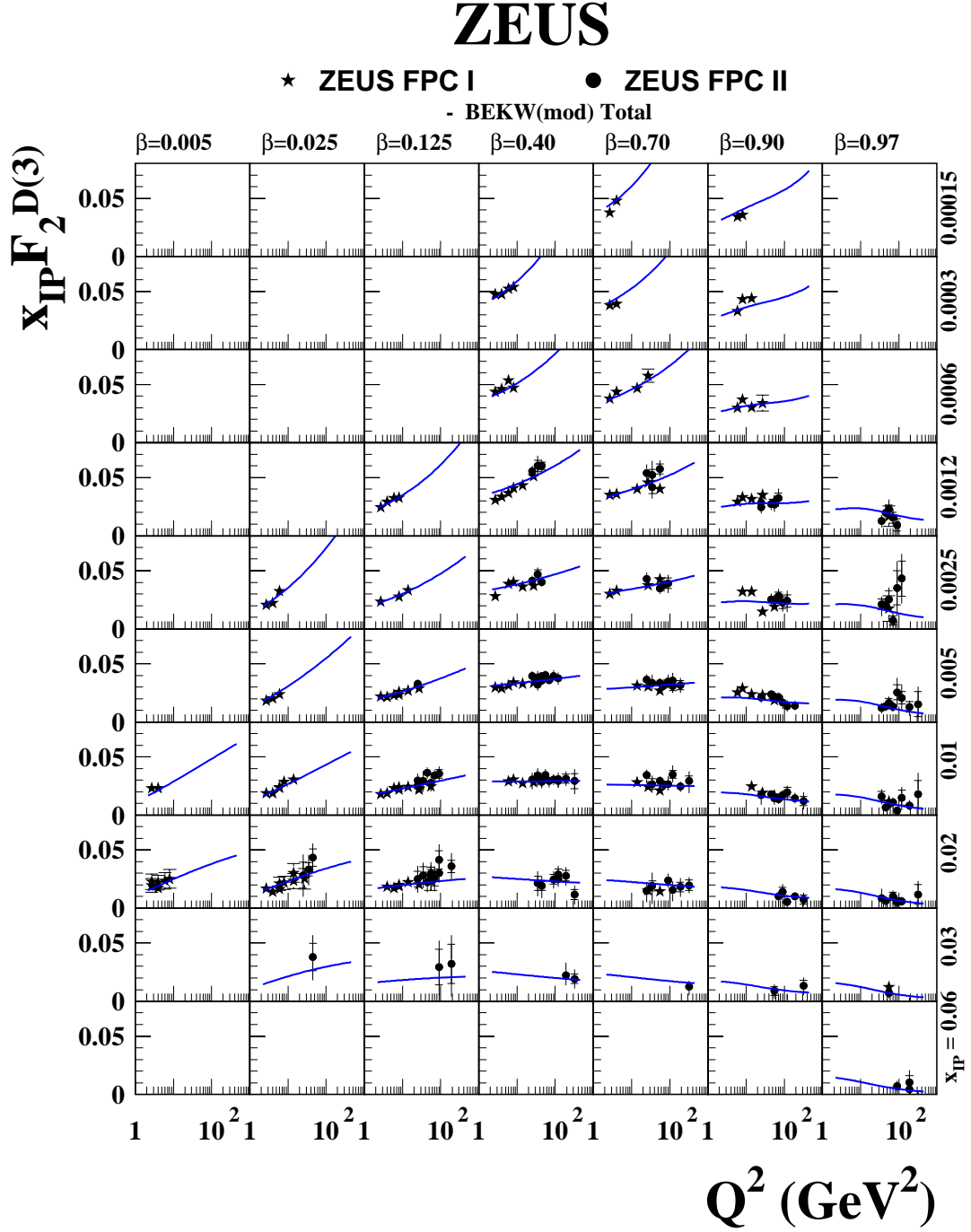


Figure 21: The diffractive structure function of the proton multiplied by x_p , $x_p F_2^{D(3)}$, as a function of Q^2 for different regions of β and x_p from the FPC I data (stars) and FPC II data (dots). The inner error bars show the statistical uncertainties and the full bars the statistical and systematic uncertainties added in quadrature. The curves show the result of the BEKW(mod) fit to the data.

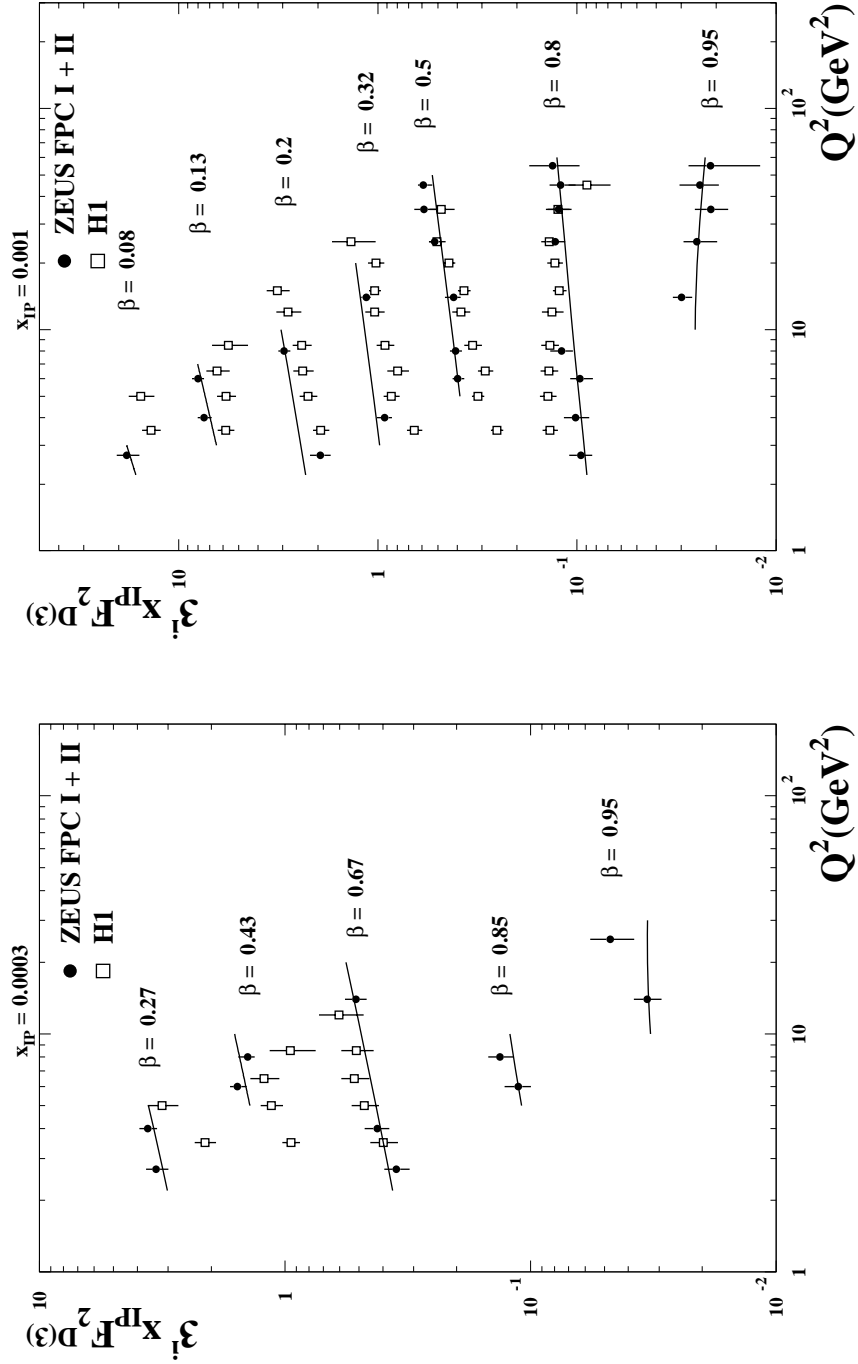


Figure 22: The diffractive structure function of the proton multiplied by x_P , $x_P F_2^{D(3)}$, as a function of Q^2 for fixed $x_P = 0.0003$ and $x_P = 0.001$ as indicated, for different values of β . The results of the FPC I and FPC II data are compared with those of H1. The data are multiplied by a factor of 3^i for better visibility with $i = 0$ for the highest value of β , $i = 1$ for the next highest β , and so on. The curves show the result of the BEKW(mod) fit to the FPC I and FPC II data.

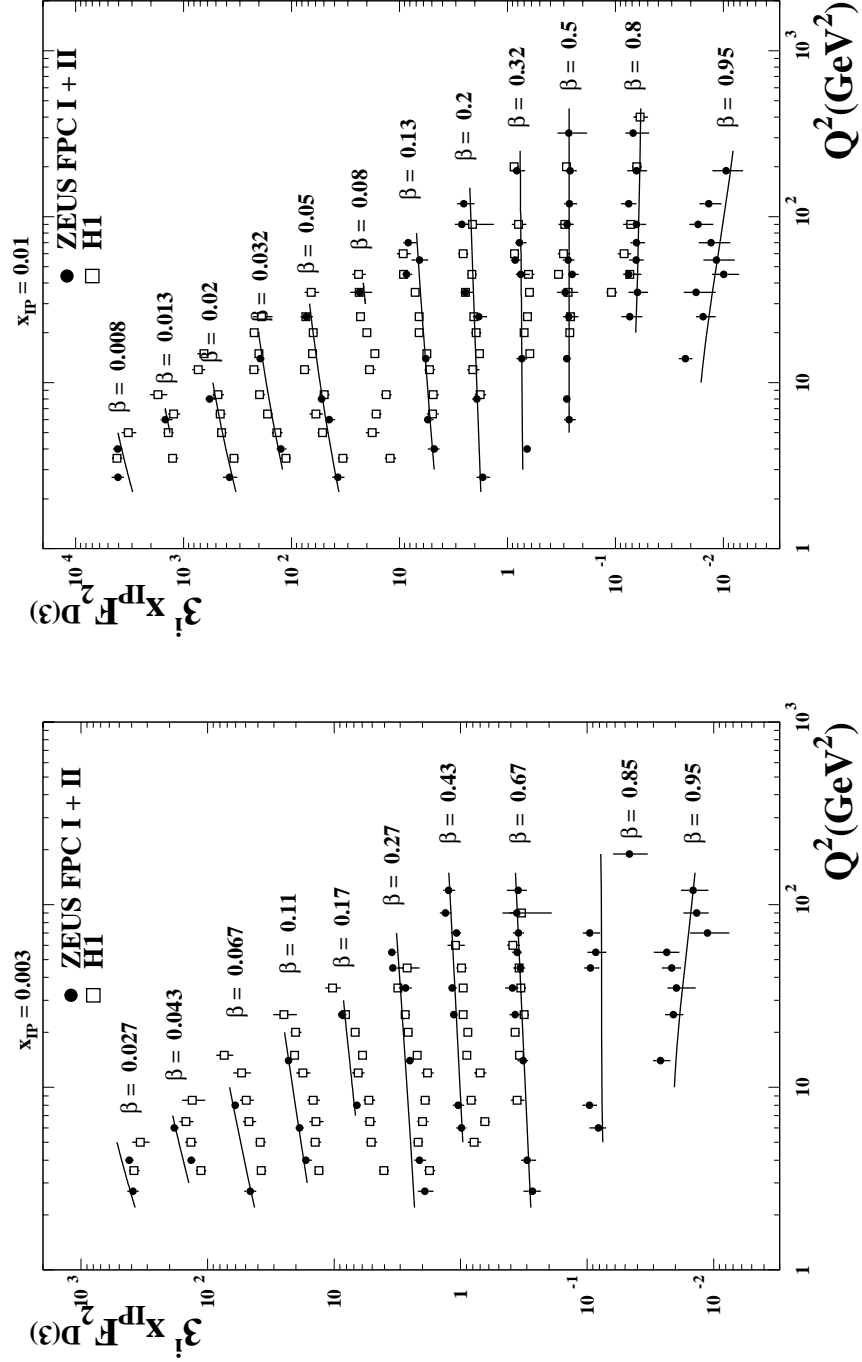


Figure 23: The diffractive structure function of the proton multiplied by x_{P} , $x_{\text{P}} F_2^{D(3)}$, as a function of Q^2 for fixed $x_{\text{P}} = 0.003$ and $x_{\text{P}} = 0.01$, as indicated, for different values of β . The results of the FPC I data and FPC II data are compared with those of H1. The data are multiplied by a factor of 3^i for better visibility with $i = 0$ for the highest value of β , $i = 1$ for the next highest β , and so on. The curves show the result of the BEKW(mod) fit to the FPC I and FPC II data.

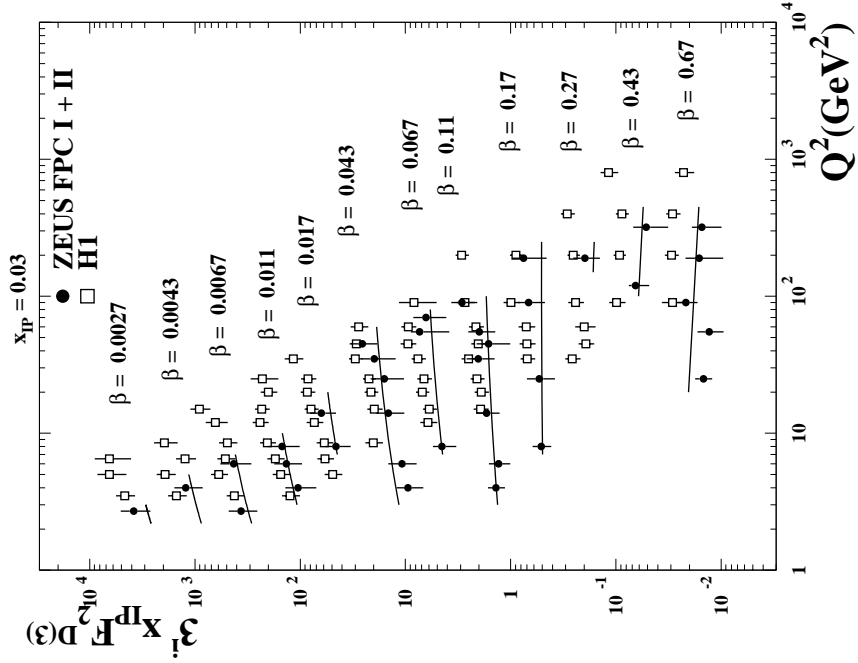


Figure 24: The diffractive structure function of the proton multiplied by x_p , $x_p F_2^{D(3)}$, as a function of Q^2 for fixed $x_p = 0.03$, for different values of β . The results of the FPC I and FPC II data are compared with those of H1. The data are multiplied by a factor of 3^i for better visibility with $i = 0$ for the highest value of β , $i = 1$ for the next highest β , and so on. The curves show the result of the BEKW(mod) fit to the FPC I and FPC II data.

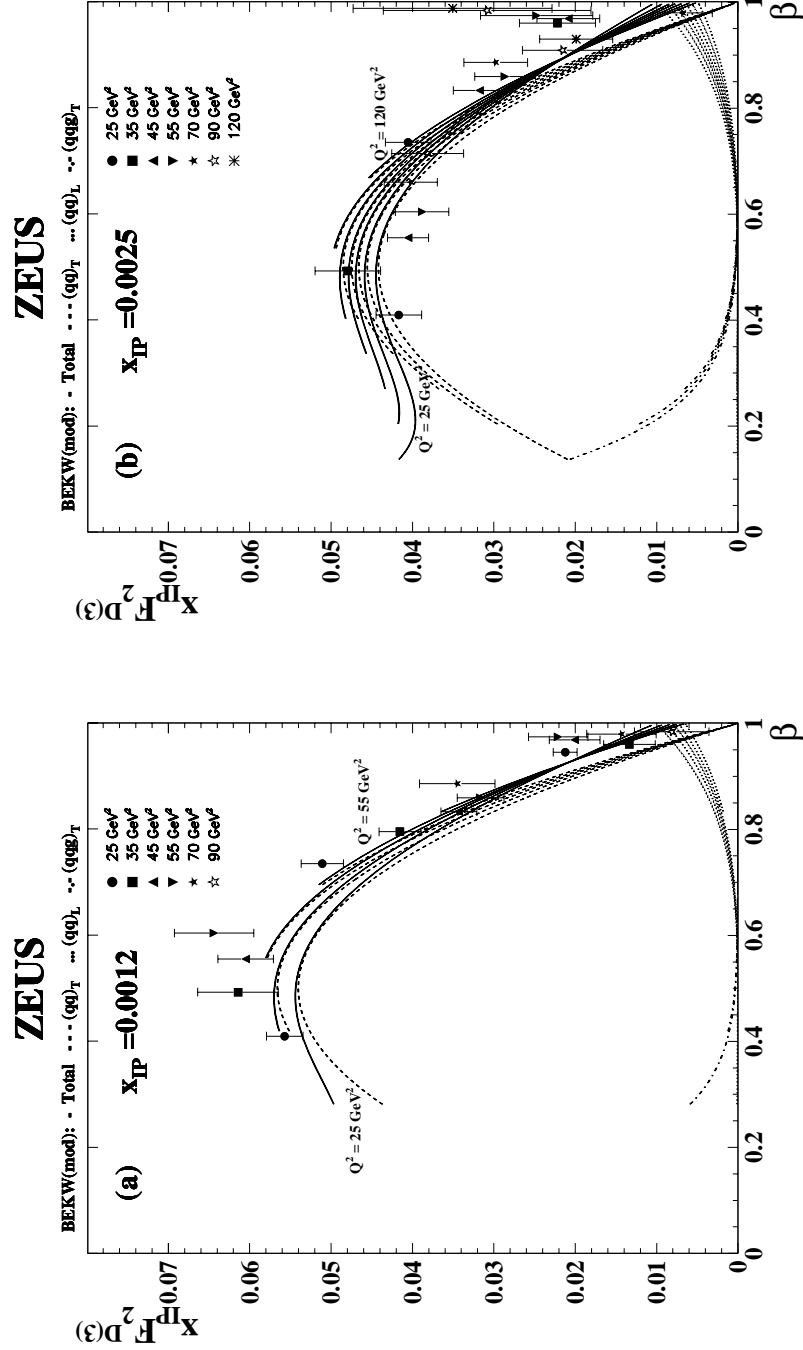


Figure 25: The diffractive structure function of the proton multiplied by x_p , $x_p F_2^{D(3)}$, as a function of β for the Q^2 values indicated, at fixed (a) $x_p = 0.0012$ and (b) $x_p = 0.0025$, for the FPC I and FPC II data. The curves show the results of the BEKW(mod) fit for the contributions from $(q\bar{q})$ for transverse (dashed) and longitudinal photons (dotted) and for the $(q\bar{q}g)$ contribution for transverse photons (dashed-dotted) together with the sum of all contributions (solid), for the β -region studied for diffractive scattering.

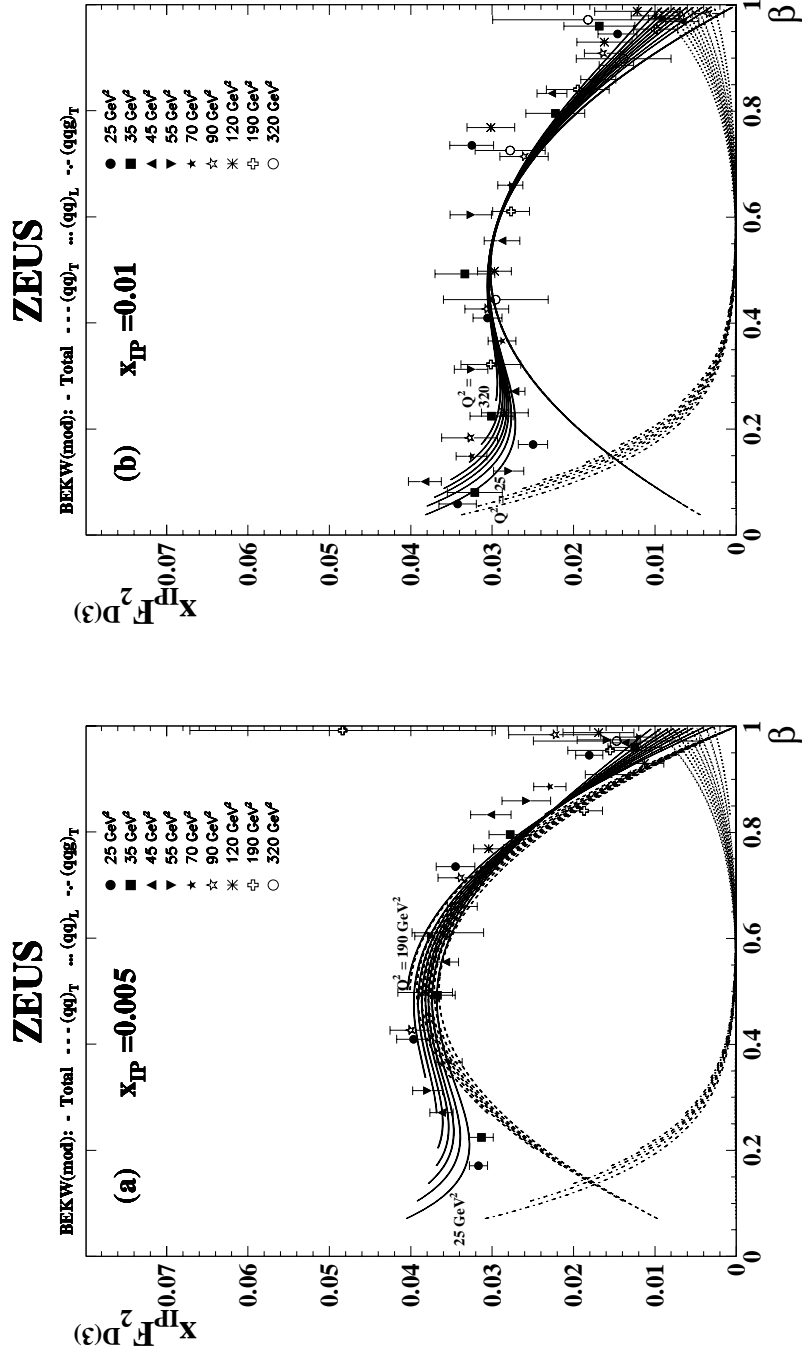


Figure 26: The diffractive structure function of the proton multiplied by x_P , $x_P F_2^{D(3)}$, as a function of β for the Q^2 values indicated, at fixed (a) $x_P = 0.005$ and (b) $x_P = 0.01$, for the FPC I and FPC II data. The curves show the results of the BEKW(mod) fit for the contributions from $(q\bar{q})$ for transverse (dashed) and longitudinal photons (dotted) and for the $(q\bar{q}g)$ contribution for transverse photons (dashed-dotted) together with the sum of all contributions (solid), for the β -region studied for diffractive scattering.

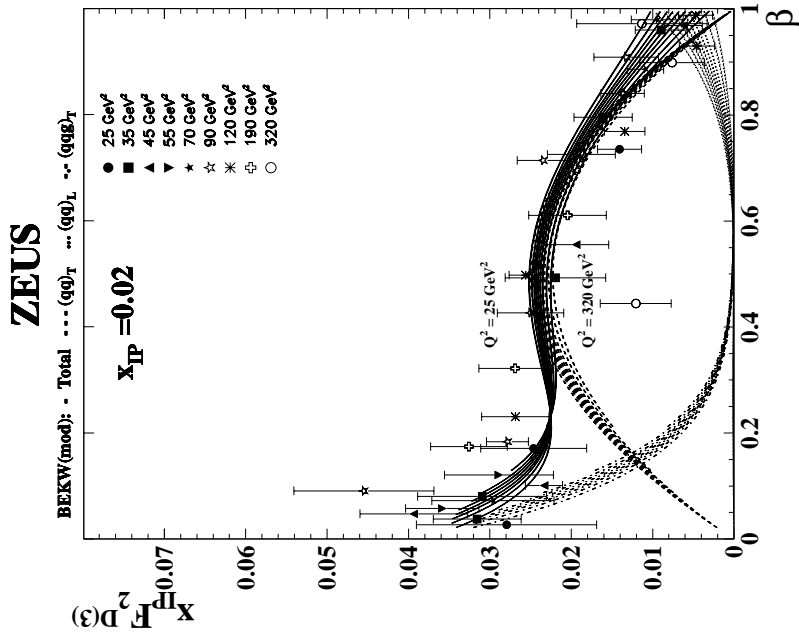


Figure 27: The diffractive structure function of the proton multiplied by x_P , $x_P F_2^{D(3)}$, as a function of β for the Q^2 values indicated at fixed $x_P = 0.02$, for the FPC I and FPC II data. The curves show the results of the BEKW(mod) fit for the contributions from $(q\bar{q})$ for transverse (dashed) and longitudinal photons (dotted) and for the $(q\bar{q}g)$ contribution for transverse photons (dashed-dotted) together with the sum of all contributions (solid), for the β -region studied for diffractive scattering.